AD-A094 470 ITT GILFILLAN VAN NUYS CA F/G 17/9
COMMUTATING FEED ASSEMBLY.(U)
JUN 80 R I WOLFSON F19628-79-C-0034
UNCLASSIFIED RADC-TR-80-180 NL

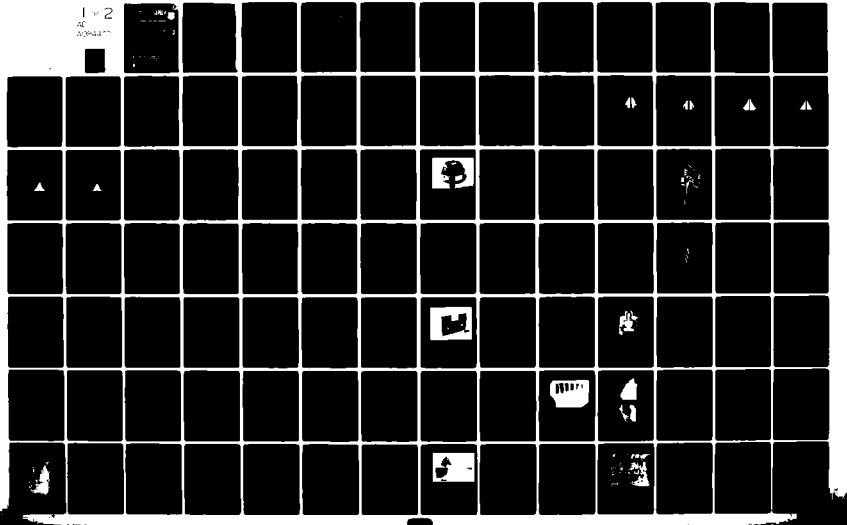

COMMUTATING [illegible]

[illegible] Gilfillan

Ronald Wolfson

ROME AIR DEVELOPMENT CENTER
Air Force Systems Command
Griffiss Air Force Base, New York 13441

This report has been reviewed by the RADC Public Affairs Office and is releasable to the National Technical Information Service (NTIS). At NTIS it will be releasable to the general public, including foreign nations.

RADC-TR-80-180 has been reviewed and is approved for publication.

APPROVED: Gregory Cruz

GREGORY CRUZ, 1Lt, USAF
Project Engineer

APPROVED: Allan C. Schell

ALLAN C. SCHELL
Chief, Electromagnetic Sciences Division

FOR THE COMMANDER: John P. Huss

JOHN P. HUSS
Acting Chief, Plans Office

If your address has changed or if you wish to be removed from the mailing list, or if the addressee is no longer employed by your organization, please notify RADC (EEA) Hanscom AFB MA 01731. This will assist us in maintaining a current mailing list.

Do not return this copy. Retain or destroy.

UNCLASSIFIED

SECURITY CLASSIFICATION OF THIS PAGE (When Data Entered)

REPORT DOCUMENTATION PAGE	READ INSTRUCTIONS BEFORE COMPLETING FORM
1. REPORT NUMBER: RADC-TR-80-180	2. GOVT ACCESSION NO.: AD-A094 470
3. RECIPIENT'S CATALOG NUMBER:	
4. TITLE (and Subtitle): COMMUTATING FEED ASSEMBLY	5. TYPE OF REPORT & PERIOD COVERED: Final Technical Report, Dec 78 - Feb 80
6. PERFORMING ORG. REPORT NUMBER: N/A	
7. AUTHOR(s): Ronald I. Wolfson	8. CONTRACT OR GRANT NUMBER(s): F19628-79-C-0034
9. PERFORMING ORGANIZATION NAME AND ADDRESS: ITT Gilfillan, 7821 Orion Avenue, Van Nuys CA 91409	10. PROGRAM ELEMENT, PROJECT, TASK AREA & WORK UNIT NUMBERS: 12412F, 24480118, 01
11. CONTROLLING OFFICE NAME AND ADDRESS: Deputy for Electronic Technology (RADC/EEA), Hanscom AFB MA 01731	12. REPORT DATE: Jun 1980
	13. NUMBER OF PAGES: 182
14. MONITORING AGENCY NAME & ADDRESS (if different from Controlling Office): Same	15. SECURITY CLASS. (of this report): UNCLASSIFIED
	15a. DECLASSIFICATION/DOWNGRADING SCHEDULE: N/A

16. DISTRIBUTION STATEMENT (of this Report)

Approved for public release; distribution unlimited.

17. DISTRIBUTION STATEMENT (of the abstract entered in Block 20, if different from Report)

Same

18. SUPPLEMENTARY NOTES

RADC Project Engineer: Gregory Cruz, 1Lt, USAF (EEA)

19. KEY WORDS (Continue on reverse side if necessary and identify by block number)

Commutator
UAR - Unattended Radar

20. ABSTRACT (Continue on reverse side if necessary and identify by block number)

This Final Report describes the principal activities performed during the Commutating Feed Assembly contract. Development of a stripline feed network and non-contacting loop couplers for low-loss transfer and distribution of RF energy is described.

DD FORM 1 JAN 73 1473 EDITION OF 1 NOV 65 IS OBSOLETE

UNCLASSIFIED

SECURITY CLASSIFICATION OF THIS PAGE (When Data Entered)

Preface

This Final Report covers the activities conducted in the development of a Commutating Feed Assembly on Contract No. F19628-79-C-0034. In addition to this development, a study was conducted on the costs, reliability and fabrication techniques of a production version of this commutator with 200 output ports.

The commutator described not only has superior electrical performance over that of an electronic system, but also offers improvements in reliability and life-cycle cost (LCC). It can be accessibly located where maintenance actions are more easily carried out than in an electronically-scanned system or a conventional rotating antenna. Non-contacting loop couplers achieve low-loss transfer and distribution of RF energy, with precise control of amplitude and phase that is needed to realize low sidelobe levels. This method of coupling is preferable to the capacitive coupling used in existing electromechanical commutating feeds, where illumination flutter results in unacceptable MTI performance. To obtain multiple beam groups in elevation, two or more commutators may be stacked on a common drive shaft.

TABLE OF CONTENTS

LIST OF ILLUSTRATIONS

LIST OF TABLES

SECTION 1

INTRODUCTION

An electronically scanned circular array antenna is advantageous for applications where 360-degree azimuth scan is required, and where the characteristics of the beam must remain unchanged for every azimuth angle. Electronically scanning a set of three or more planar phased arrays can provide the required 360 degrees of coverage, but results in beam distortion as the angle varies. Mechanically rotating antennas provide the required beam characteristics but usually do not have the required data rate.

Existing all-electronic circular arrays also have disadvantages. In a practical configuration, they require many active subassemblies with an unacceptably large amount of loss, and they require frequent maintenance. In addition, variations in subassembly characteristics due to component differences may cause small variations in the beam characteristics with azimuth scan angle, as well as high sidelobes. The existing Wullenweber electro-mechanical commutating feed has the desirable low drive power and high reliability as it uses a low-inertia mechanically rotating feed. In that device, the power is capacitively coupled from a rotating to a stationary transmission line that connects to the large circular array elements. However, the capacitive coupling used causes unacceptable loss and flutter, or fluctuations in the radiated beam with rotational angle.

Large-scale parallel-plate combiner/dividers have been developed by ITT Gilfillan that make use of a magnetic loop coupler. This device derives its properties from both the waveguide loop coupler and the -3dB quarter-wave

directional coupler. In the waveguide version, matched coupling to the dominant mode is obtained by proper quarter-wave transformation of the waveguide impedance to that of the coaxial input. Wide bandwidth is insured by coupling to the fields in a manner that minimizes impedance change, thereby reducing the Q of the network. The use of magnetic loop couplers in a commutating feed provides low RF loss and inertia while limiting flutter to the narrow range of angles where the rotor loops pass over small gaps between adjacent stator loops.

SECTION 2

COMMUTATING FEED ASSEMBLY REQUIREMENTS

The overall objectives are to develop, construct and test a power divider and commutator to feed an electronically rotating 90^{o} sector of an Unattended Radar (UAR) circular array, and to study the costs, reliability and fabrication costs of production versions of the device.

Table 2-1 presents a summary of the requirements for the Commutating Feed Assembly. Significant mechanical requirements include a drive power of below 50 watts and the ability to stack two or more commutators for systems with multiple beams. In addition, the system concept should be readily extendable to a circular array with approximately 200 outputs, with as many as one-third of these excited at one time. Other important considerations are the environmental conditions encountered in the Arctic, as well as the extremely high MTBF required for unattended operation. For high-performance radar operation, low phase and amplitude variations are required for good MTI performance. In addition, electrical contact noise often encountered in electro-mechanical assemblies must be minimized.

TABLE 2-1. COMMUTATING FEED ASSEMBLY REQUIREMENTS

Frequency Band	1.2 to 1.4 GHz
Number of Output Ports	100
Number of Excited Ports	26
Excited Sector	90^{o}
Aperture Illumination	Consistent with -20 dB Sidelobes
VSWR	
Input Port	1.3:1 maximum
Output Ports	1.3:1 maximum
Insertion Loss	1.0 dB maximum
Power Capacity	
Peak	10 kW
Average	500 W
Rotation Rate	15 rpm
Drive Power	50 Watts maximum
Environment	-35^{o}F to $+100^{o}$F minimum (as encountered in Arctic)
Reliability	Consistent with Unattended Radar operation
Stacking	2 or more Commutators
Growth	200 Outputs
	68 Excited

SECTION 3

TECHNICAL ISSUES

Increasing emphasis is being placed on minimizing the total Life Cycle Cost of new radar programs. At the same time, more stringent mission requirements call for increased operational availability, A_o, and reduced repair times. These goals are perhaps best exemplified in the U.S. Air Force SEEK FROST program. This program is examining the replacement of current DEW Line radars with equipments that will operate unattended for extended periods of time of up to one year. Maintenance teams located at centralized maintenance nodes will provide preventive and emergency repair services for these sites. The reduction in the total number of personnel required to operate and maintain the line is expected to reduce significantly O&M costs from that of the existing system.

For unattended operation, it is clear that very high reliability designs are required. This includes not only the designs of the individual components, but also the fundamental architectures of major subsystems. An additional consideration relating to both operating costs and reliability is the overall system efficiency and power consumption. This becomes especially important due to the rapidly escalating costs of energy, and to the costs and difficulties associated with replenishing the supply of energy at isolated sites.

One of several antenna concepts being considered for systems such as the UAR is a circular array, shown in Figure 3-1. The principal motivations for such an approach over a conventional rotating antenna are reduced drive

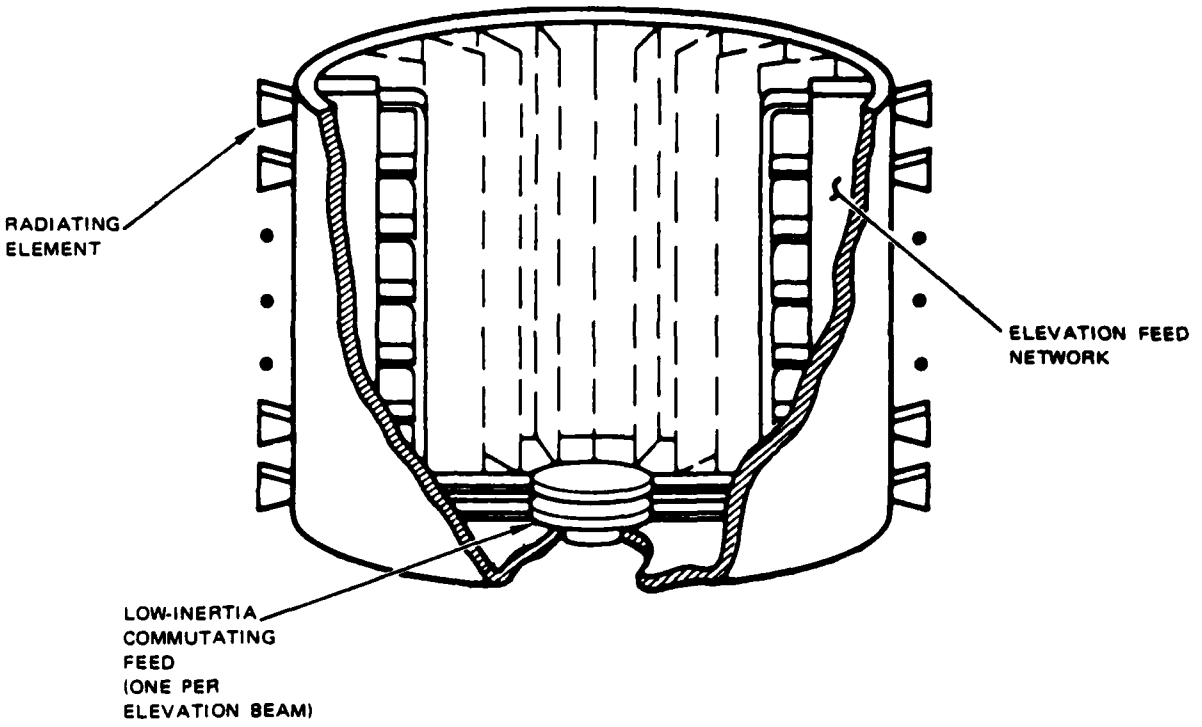

Figure 3-1. Circular array antenna concept using low-inertia commutating feed

power, improved reliability, and availability of simplified maintenance. Over the past decade, numerous purely electronic scan concepts for circular arrays have been developed. All of these approaches have been plagued by high loss and poor reliability due to the large number of components in series, and poor sidelobe performance due to large amplitude and phase errors.

To address these problems, the Department of the Air Force, Electronic Systems Division, has funded ITT Gilfillan to develop, construct and evaluate a Commutating Feed Assembly for steering the beam of a circular array. The advantages of such an approach are simplicity, low cost, and low drive power. Properly designed, such a commutator offers superior electrical performance over an electronic system and significant improvements in reliability and LCC.

3.1 System Design

3.1.1 Radius of Circular Array

The specifications given for the model circular array include 100 columns of vertical dipole radiators with an inter-element spacing of 0.62λ at the design frequency of 1.3 GHz. The diameter of such an array is nominally 180 inches. The chosen number of array elements is one-half that required for a full-sized antenna with the same inter-element spacing.

Azimuth patterns were computed for several circular array designs using two different design illumination functions, and several diameters for a fixed total number of array columns. The illumination functions

chosen are -25dB, $\bar{N}$ = 4 Taylor and -29dB, $\bar{N}$ = 4 Taylor. Array diameters of 180, 160 and 135 inches are used for the model array, and 360, 320 and 270 inches for the full-sized array. The illumination sector used is 90 degrees for all cases; in addition, a 120-sector is considered for the full-sized array.

The patterns shown in Figures 3-2 through 3-7, are computed at the upper frequency end of the band, 1.4 GHz. As expected, the designs with the largest inter-column spacing, 0.67 wavelengths at this frequency, show high grating lobes which in some cases do not meet the -20 dB sidelobe level requirement. The exact level of the grating lobe is influenced appreciably by the azimuth pattern of an individual column. All the cases shown assume a cosine element power pattern.

As the primary purpose of this development was to demonstrate the feasibility of a low-inertia commutating feed, work proceeded on the basis of a 0.62λ inter-element spacing at 1.3 GHz. However, to realize the potential low-sidelobe performance of which this commutator feed concept is capable, further analysis of the circular array antenna system is indicated.

3.1.2 Design Illumination

Three types of illumination function were considered for this application: Taylor, Chebyshev, and a modified (sin u)/u. The Taylor illumination produces a determined number of near-in sidelobe pairs at the design level, after which the sidelobe structure gradually decays to the level established by random errors. For most applications with moderate

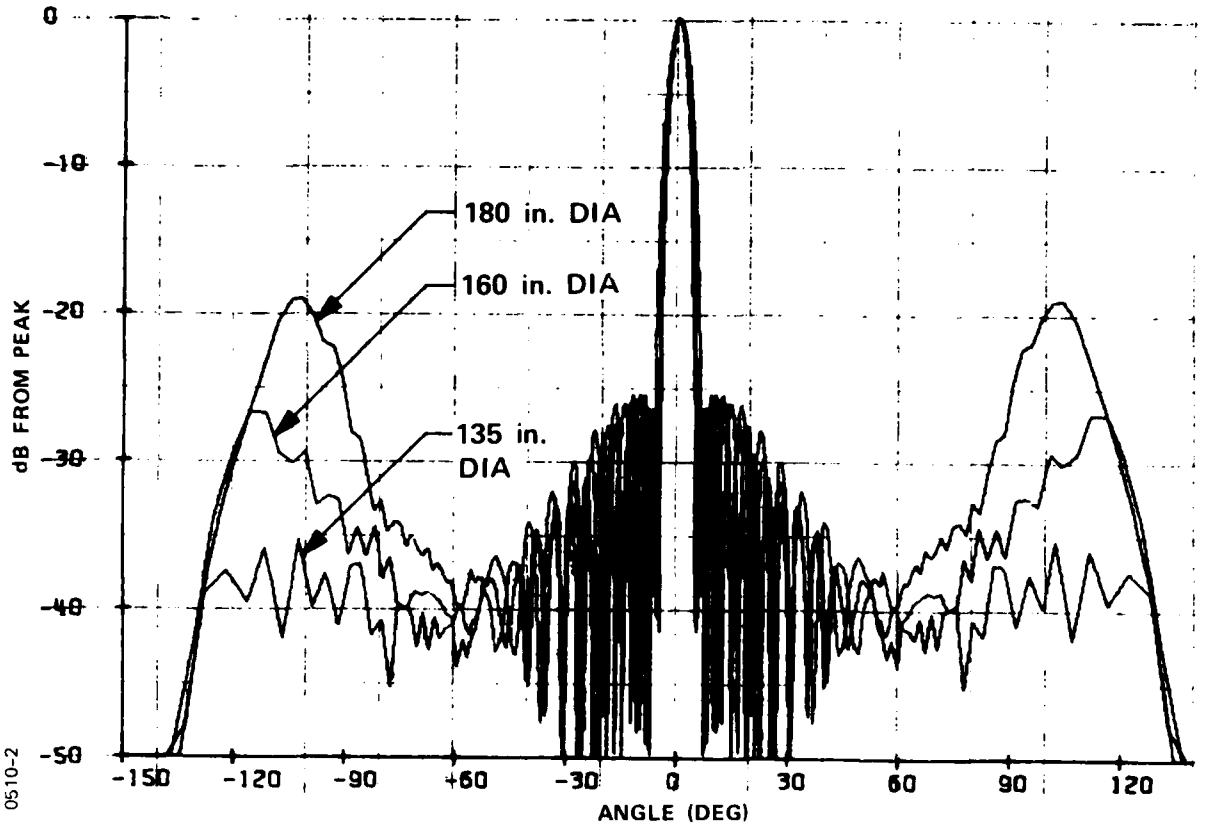

Figure 3-2. Computed azimuth patterns: 100 elements, 90° sector, -25 dB Taylor illumination

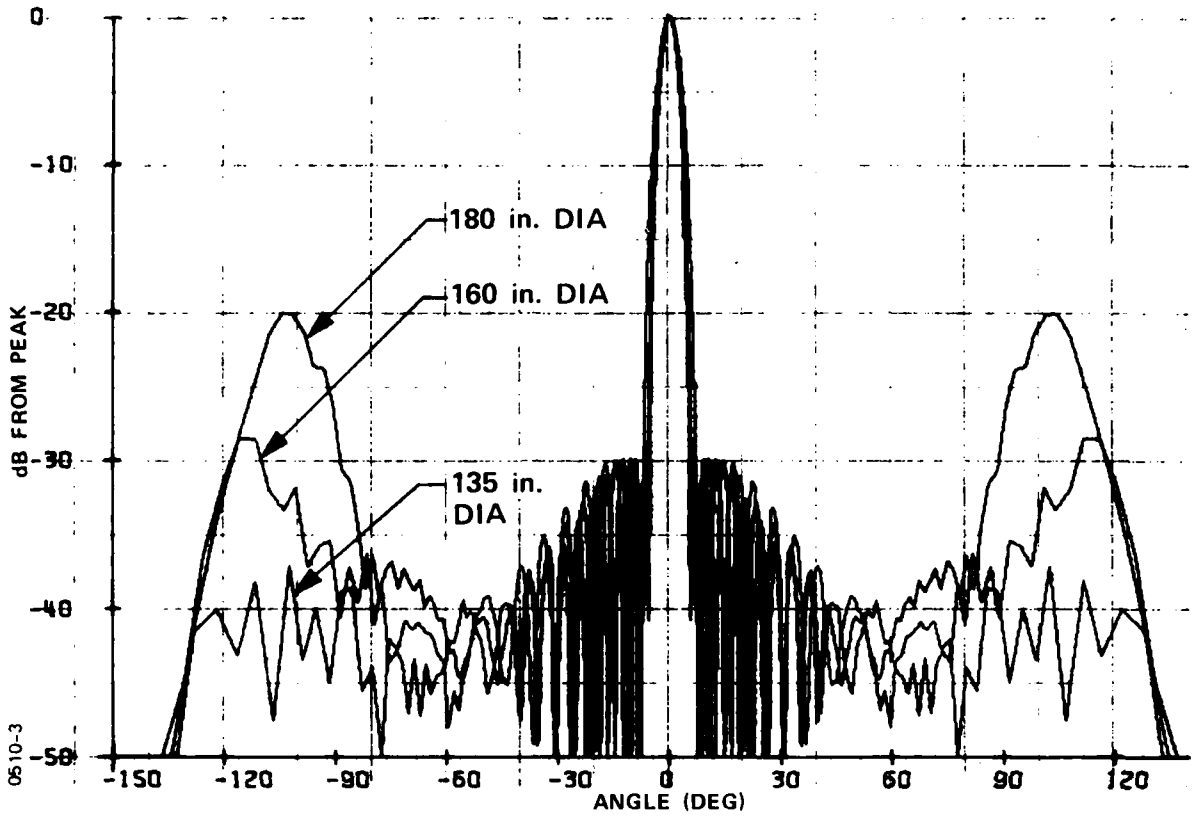

Figure 3-3. Computed azimuth patterns: 100 elements, 90° sector, -29 dB Taylor illumination

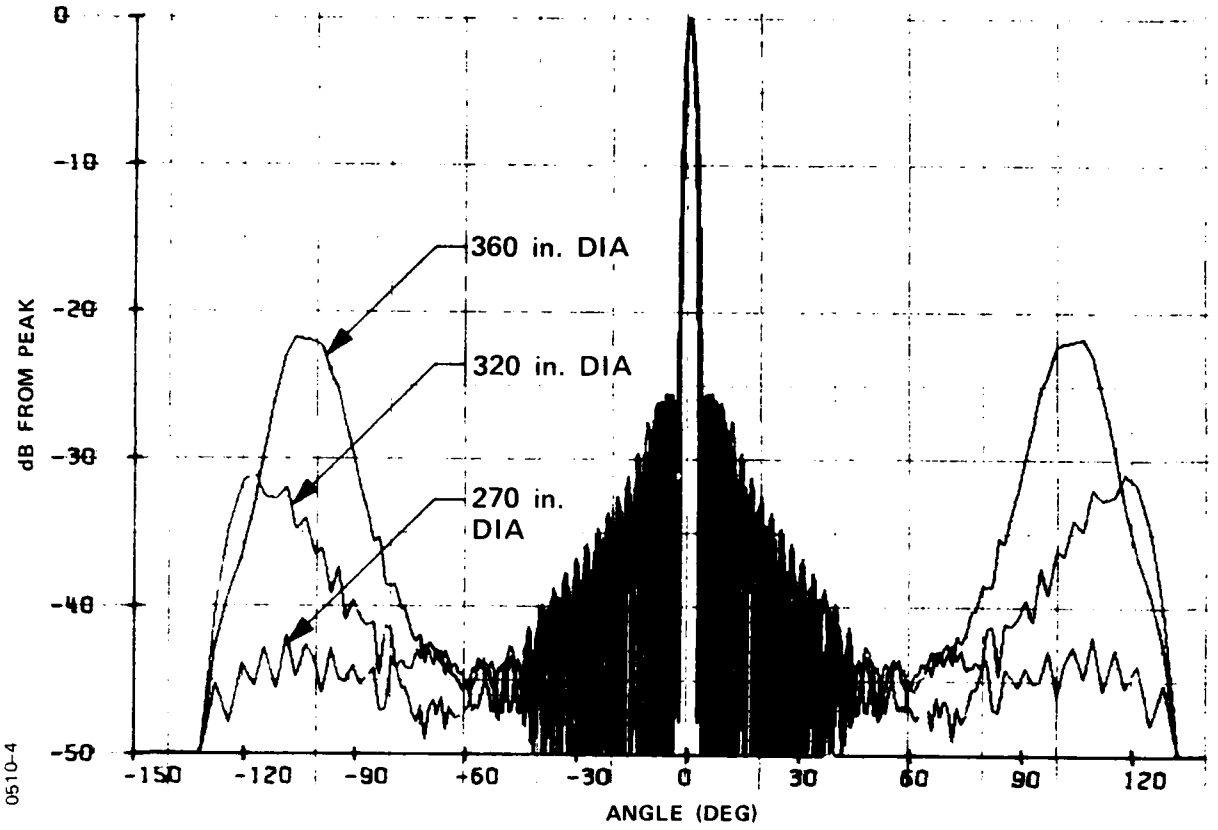

Figure 3-4. Computed azimuth patterns: 200 elements, 90° sector, -25 dB Taylor illumination

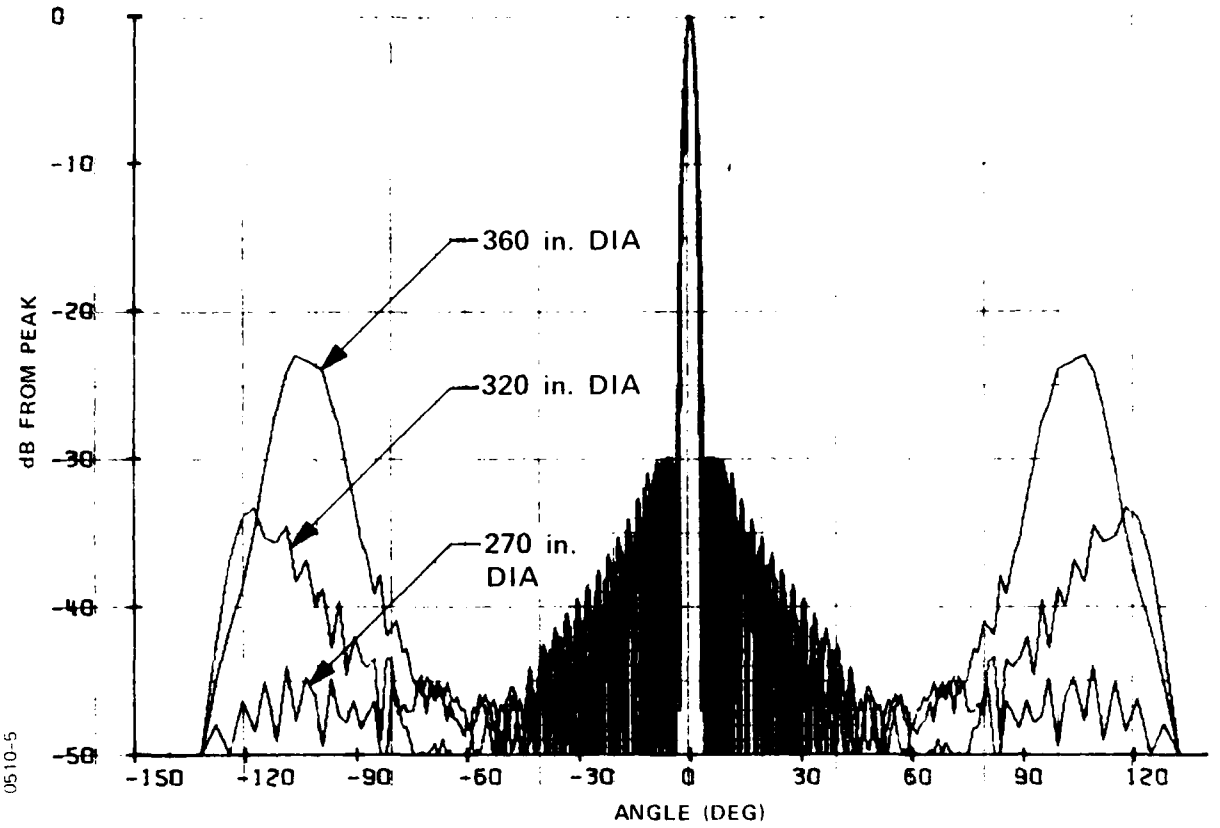

Figure 3-5. Computed azimuth patterns: 200 elements, 90° sector, -29 dB Taylor illumination

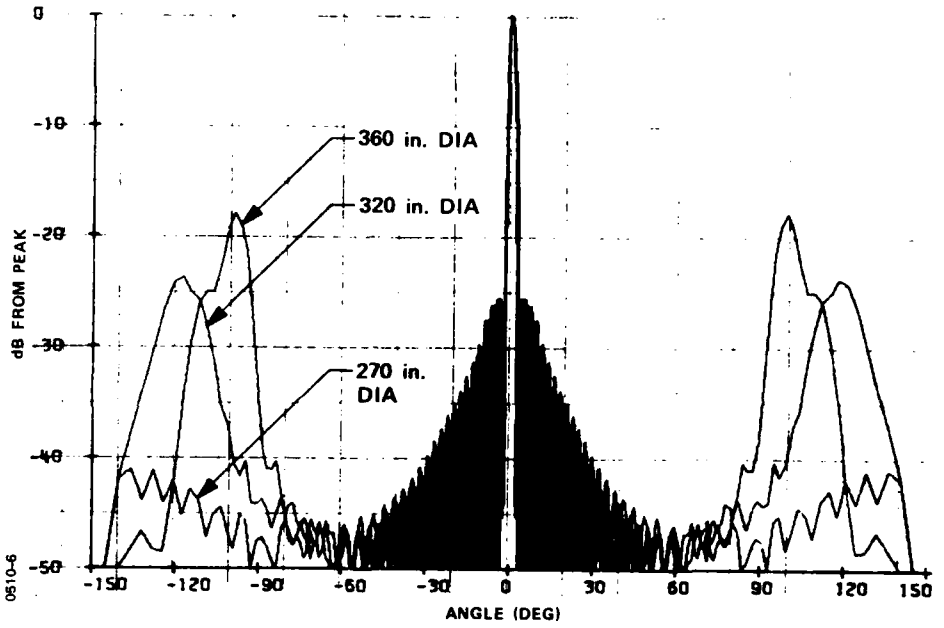

Figure 3-6. Computed azimuth patterns: 200 elements, 120° sector, -25 dB Taylor illumination

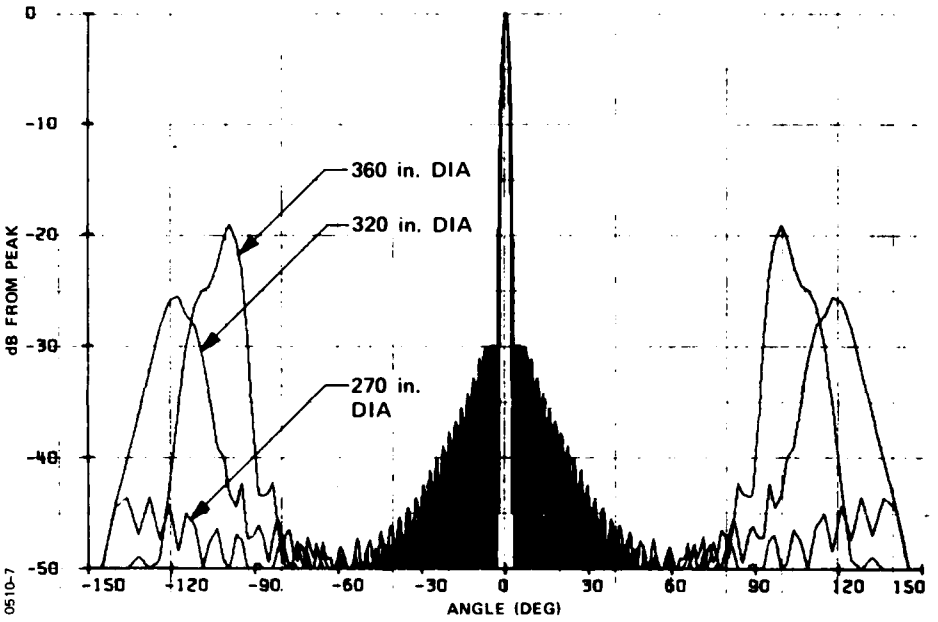

Figure 3-7. Computed azimuth patterns: 200 elements, 120° sector, -29 dB Taylor illumination

sidelobe-level requirements, this function is preferred because it results in the best compromise between sidelobe level and aperture efficiency, and in practice the element-coupling values are readily achievable. The Chebyshev illumination results in all sidelobes at essentially the same level; very low first sidelobes can be obtained at the expense of foregoing further reduction in the level of far-out sidelobes. This illumination function is the most efficient of the three types mentioned but can be difficult to realize because of the precise amplitude control required at the edge elements. The (sin u)/u function, which is the least efficient of these, gives a gradual reduction in sidelobe level after the first pair until the random-error level is reached.

As shown in the computed patterns of Figure 3-2, a -25dB, $\bar{N}$ = 4 Taylor distribution readily fulfills the sidelobe level specification of -20dB with adequate margin, except for the grating lobes at 1.4 GHz in the 180-inch diameter circular array. However, a -29dB, $\bar{N}$ = 4 Taylor distribution will be used for the model Commutating Feed Assembly in order to demonstrate the potential low-sidelobe performance more convincingly. The penalty in aperture efficiency for chosing a -29dB rather than -25dB Taylor excitation is about 0.25dB.

3.1.3 Elevation Scan Angle for Zero Phase Error

In order to obtain a planar wavefront from a circular array of radiating elements, it is necessary to compensate for unequal pathlengths that occur in space due to curvature of the array. The geometry for this

situation is illustrated in Figure 3-8. The differential pathlengths relative to the edge elements that are required for a planar wavefront are given by the equation

$$\Delta \ell_n = \frac{R\ (\cos\phi_n - \cos\phi_{max})\ \cos\ \theta}{\sqrt{\varepsilon_r}}$$

where:

R = radius of circular array,
ϕ_{max} = one-half of sector angle,
ϕ_n = angle of n^{th} element relative to center of sector,
θ = desired elevation scan angle for zero phase error, and
ε_r = relative dielectric constant of stripline feed.

Note that the differential pathlengths, $\Delta \ell_n$, required for a planar wavefront are a function of elevation scan angle, θ. Thus, the circular array can be compensated exactly only at one preselected value of elevation scan angle. A value of 15 degrees is assumed, as this angle is the maximum value of θ for which there is essentially no degradation in beamwidth and sidelobe performance at the horizon. As $\Delta \ell_n$ is independent of frequency, this configuration is inherently broadband.

3.1.4 RF Loss Budget

Total pathlength in stripline between input and rotor loop averages about 60 inches; thus, the insertion loss of the stripline feed network is about 0.7dB. The overall Commutating Feed Assembly loss budget is given in Table 3-1.

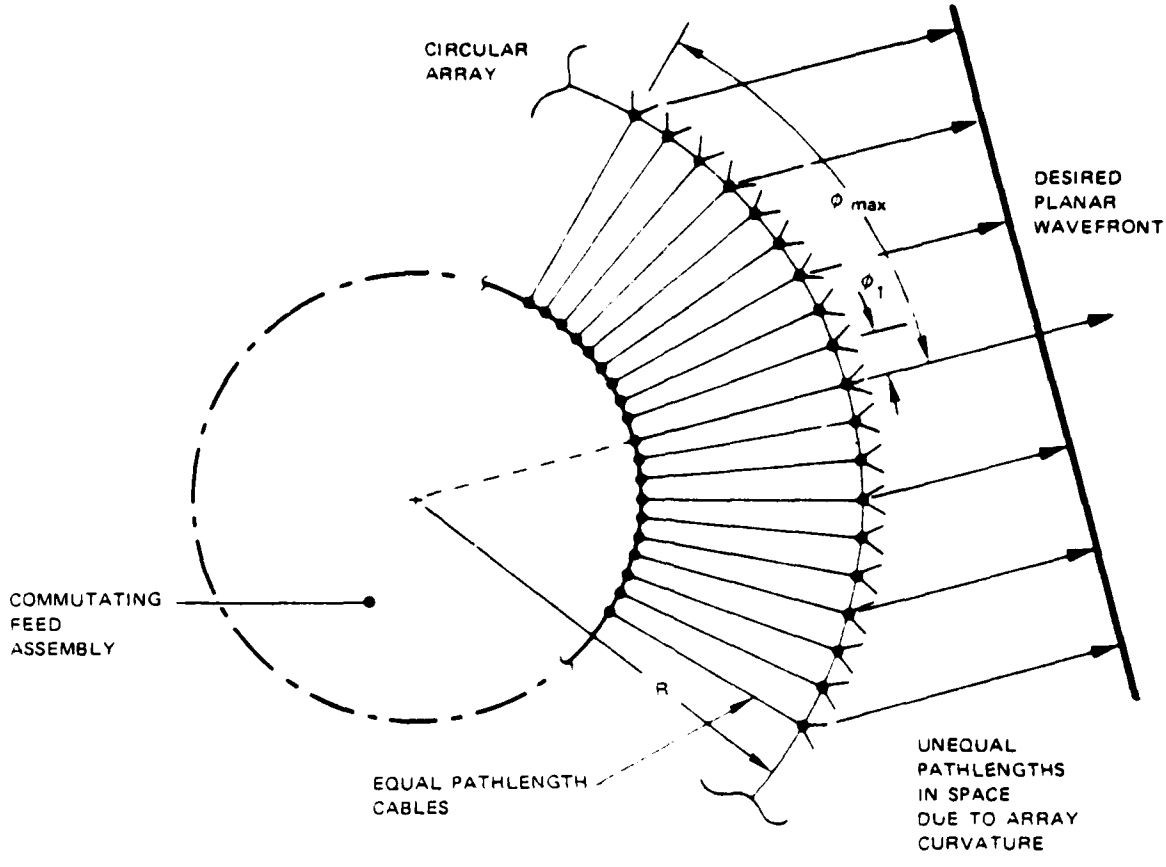

Figure 3-8. Pathlength variations in circular array

TABLE 3-1. LOSS BUDGET OF COMMUTATING FEED ASSEMBLY	
Component	Loss
Rotary Joint	0.2
Stripline Feed	0.7
Loop Couplers (including mismatches)	0.2
Coax and Connectors	0.1
Total Loss	1.2 dB

3.2 Rotator Pedestal Assembly

3.2.1 Drive Train

The function of the drive train is to rotate the stripline feed assembly at a constant rate of 15 rpm with high efficiency and high reliability. Although both ac and dc torque motors were considered for this application, the latter type was chosen for the following reasons:

(a) A dc torque motor contains only one moving part, the rotor, whereas an ac motor must also have a gear-reduction train that requires lubrication. As a consequence of having fewer moving parts, the dc torque motor is more reliable.

(b) The bearing life of the dc torque motor is longer for two reasons. First, the dc torque motor selected has only two bearings, both large, whereas the ac motor and associated gear train have several bearings, all small. Large bearings result in less loading, which is a significant factor in bearing life. A second important key to bearing life is shaft speed, which is at least two orders of magnitude less

for the dc torque motor than for the ac motor.

(c) The dc torque motor provides high starting torque. This feature is particularly important for failsafe starting of the Commutating Feed Assembly in sub-zero climate during periods of routine maintenance.

(d) The dc torque motor is more efficient than an ac motor, primarily because the need for a gear-reduction train is eliminated.

Figure 3-9 is a photograph of the rotator pedestal assembly. The drive motor is a seven ft-lb dc torque motor, which is accessible through a cover plate in the bottom side of the housing casting. For future designs, it would be more convenient to provide an access door in the side of the pedestal. This would facilitate maintenance, such as replacement of motor brushes.

Figure 3-10 shows calculated drive power required, both for start-up and for continuous rotation at 15 rpm, as a function of stripline rotor diameter. It is seen that for both conditions, considerably less drive power would be required than the maximum 50 watts specified.

Figure 3-11 similarly shows estimated drive power required for a number of 3-foot diameter stripline rotors stacked on a common shaft. It is seen that up to five commutators can be driven within the 50-watt drive power limitation.

3.2.2 Support Structure

The support structure of the Commutating Feed Assembly is shown in

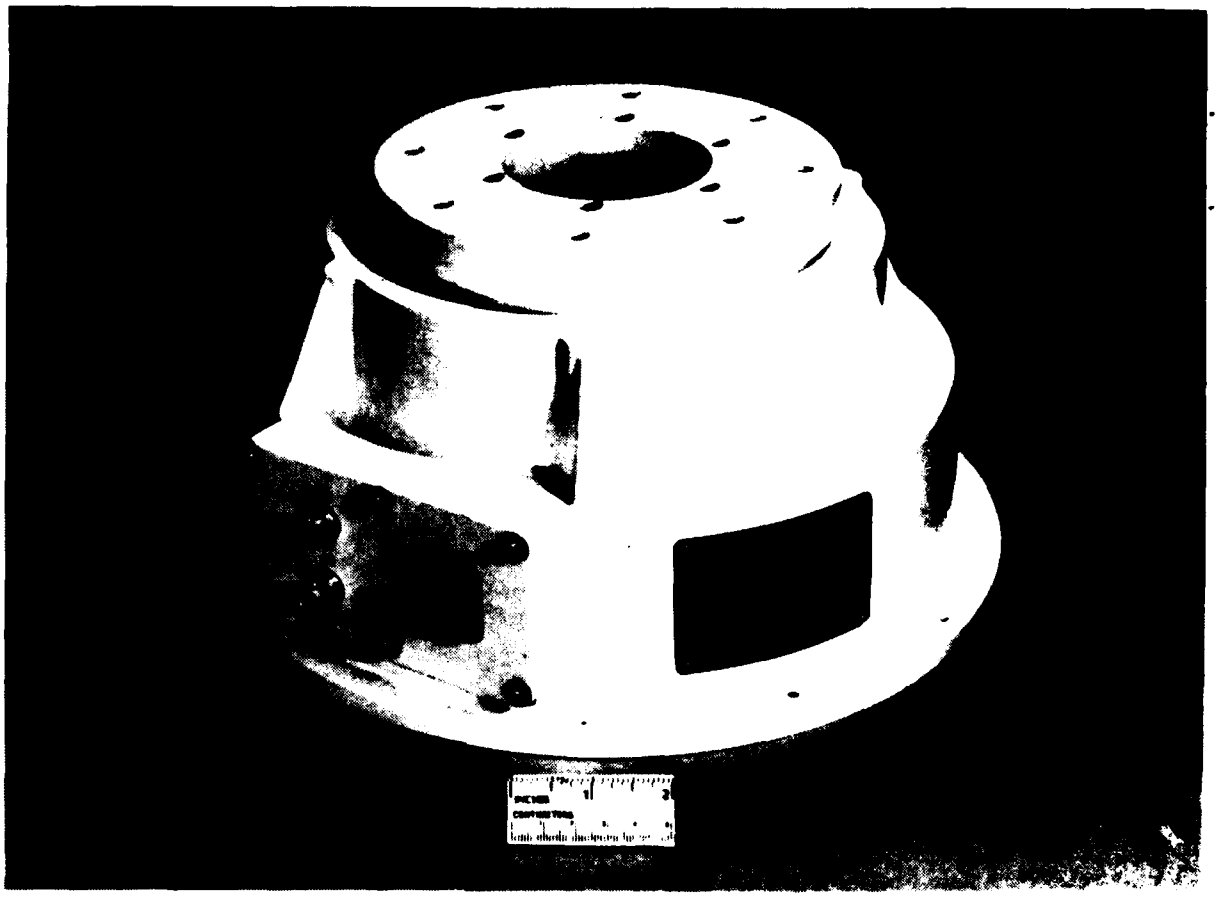

Figure 3-9. Rotator pedestal assembly

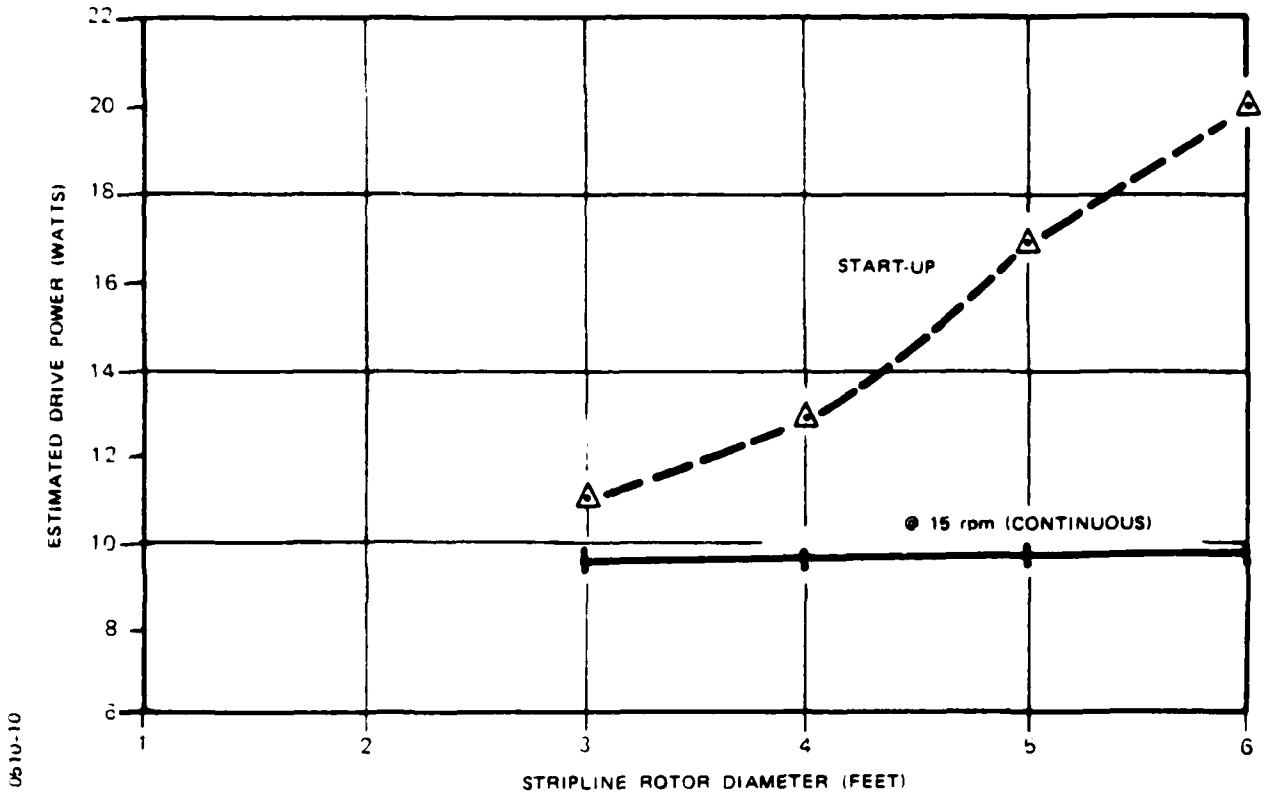

Figure 3-10. Drive power required as a function of stripline rotor diameter

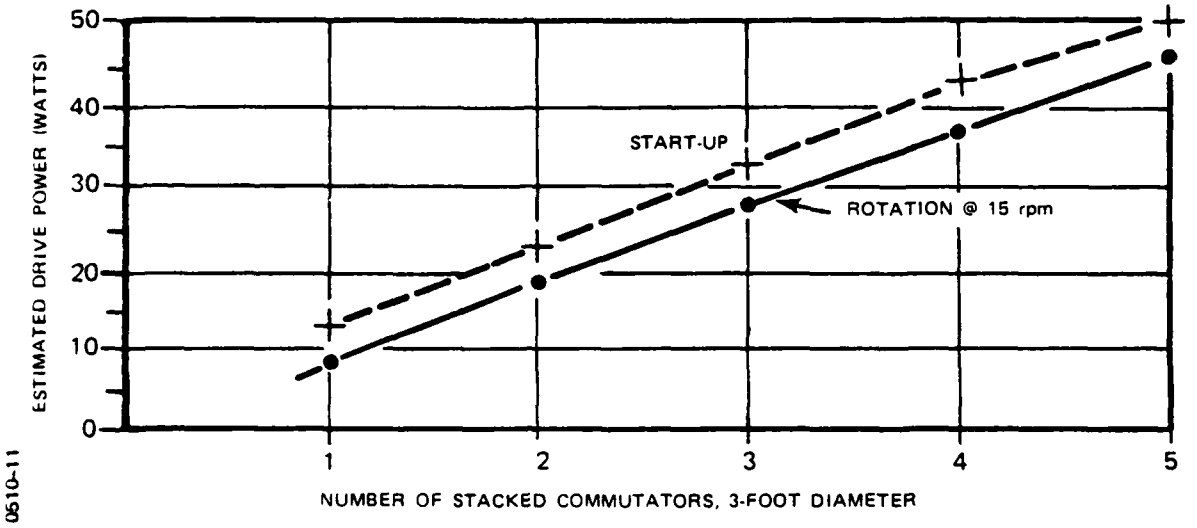

Figure 3-11. Drive power required as a function of number of stacked 3-foot diameter commutators

Figure 3-12. Brace supports are bolted between the pedestal drive assembly housing and the stripline feed housing to form a rigid, lightweight structure.

3.3 Annular Rotary Coupler

Power is fed to the rotating feed network through a rotary joint from the input line. In order to stack two or more commutators on a common drive shaft, an annular rotary coupler with access hole through the center is required. A trade off exists between annular rotary coupler insertion loss and VSWR on one hand, and hole diameter on the other. Typical parameters for two different size units over the 1.2 to 1.4 GHz frequency band are given in Table 3-2.

TABLE 3-2. TYPICAL PARAMETERS FOR ANNULAR ROTARY COUPLERS

Hole Diameter, Inches	Insertion Loss, dB	VSWR
0.406	0.2	1.20:1
1.000	0.5	1.50:1

For the experimental model commutator, an annular rotary coupler with a 0.406-inch diameter hole was selected in order to take advantage of the superior electrical characteristics. This allows the use of a 3/8-inch diameter drive shaft, which is adequate for a single or two stacked commutators. For multiple stacked units, excessive torsion may cause this size shaft to twist, and result in loss of synchronization among the several commutators. Analysis can be used to determine the magnitude of the problem, and to find the optimum annular rotary coupler hole diameter.

3.4 Stripline Feed Network

Figure 3-13 is a schematic of the rotating stripline feed network. A

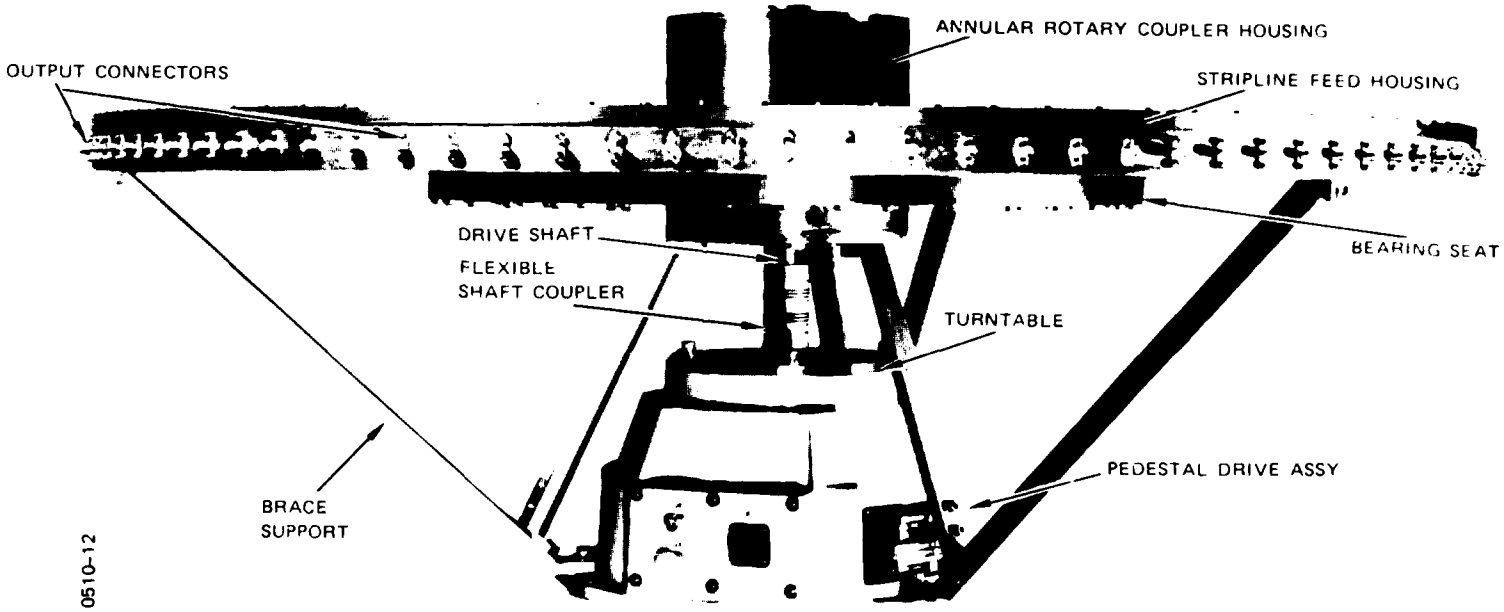

Figure 3-12. Support structure of the commutating feed assembly

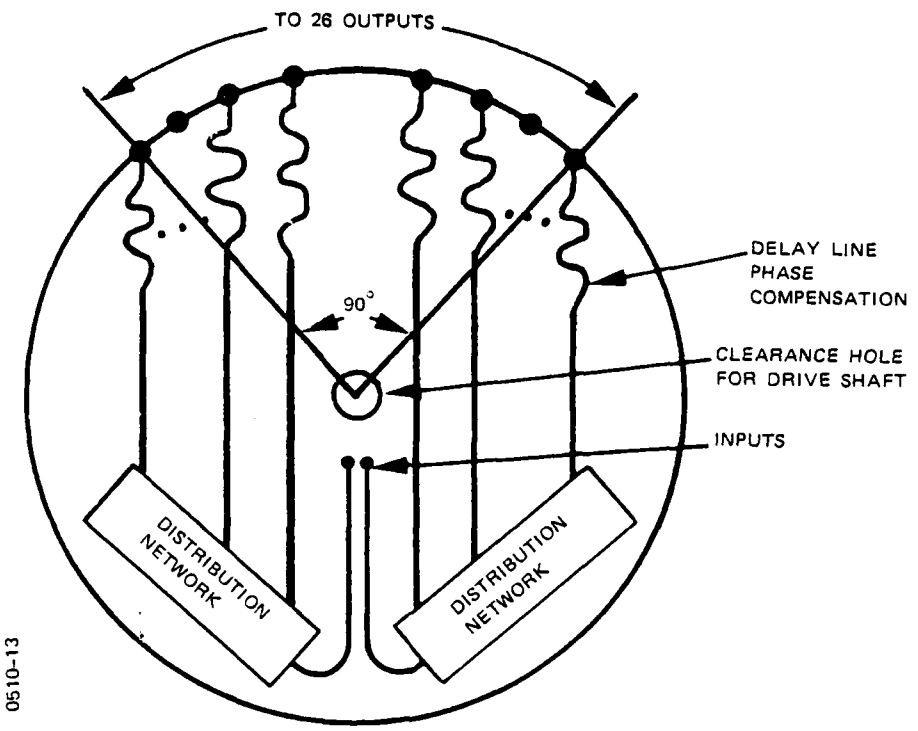

Figure 3-13. Schematic of stripline feed network

diameter of approximately three feet is required to allow sufficient space for the amplitude distribution networks and delay lines that provide the circular-array phase compensation. TEM delay lines produce the correct phase, independent of frequency. The amplitude distribution networks consist of stripline couplers that provide the cylindrical-array illumination amplitudes required for -30 dB sidelobes.

Several types of array feed networks were considered for this application. Parallel or corporate-feed approaches were rejected because of high sensitivity to coupling errors, difficulty in realizing the required illumination with a reasonable range of coupling values, and excessive size. A center-fed, phase-compensated, series array feed was selected for low loss, wide bandwidth, relative insensitivity to coupling errors, and compact form factor.

3.4.1 Range of Coupling Values vs. Percent Power into Load

A trade-off exists in the design of a series feed network between the range of element coupling factors and the amount of power dissipated in the main-line load termination. This is illustrated in Figure 3-14 for a 13-element series feed with -29 dB, $\bar{N}$ = 4 Taylor illumination. It can be seen that with no power into the end load, a wide range of coupling factors is required: 0 dB to -7.47 dB. With three percent power into the end load, which represents an additional insertion loss penalty of only 0.13 dB, a more viable range of design coupling factors is obtained: -5.56 dB to -7.60 dB. Another advantage to using nearly equal coupling factors is better element-to-element amplitude and phase tracking, so that degradation in array performance at the operating band edges is minimized.

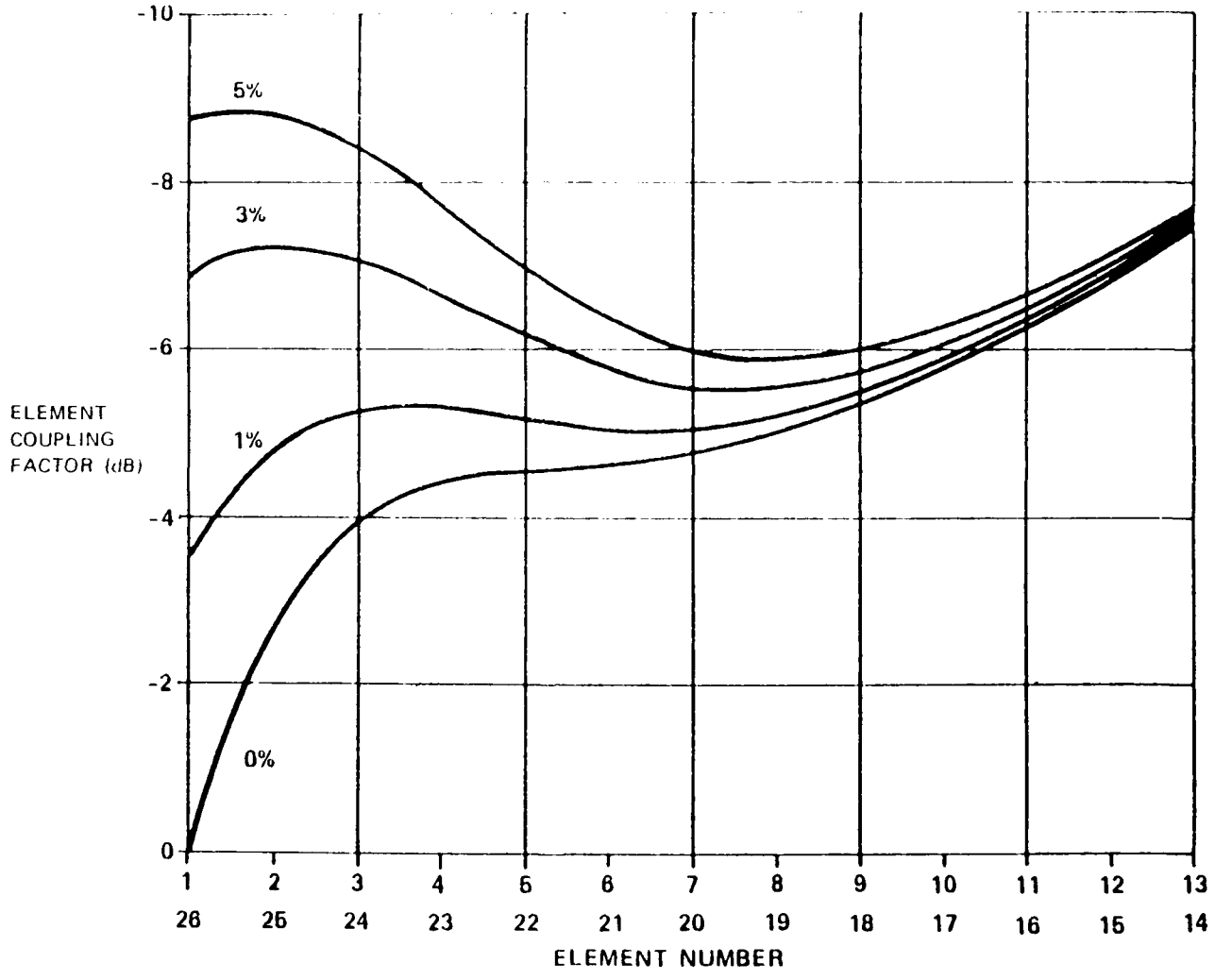

Figure 3-14. Element coupling factor vs element number with percent power into end load as parameter

3.4.2 Coupler Configuration Trade-Off

In order to select the best type stripline coupler for this application, a trade-off study of key parameters was made for several commonly used coupler configurations. A nominal coupling factor of -6 dB was assumed, with performance at first considered over the 1.2 to 1.4 GHz radar band alone, and then over the extended band of 1.03 to 1.4 GHz to include IFF operation. The results of this trade-off study are summarized in Table 3-3. The single-section branchline coupler was rejected due to high VSWR, low isolation, and excessive phase runout. While the hybrid-ring coupler is acceptable electrically, it is too large, with the ports awkwardly located for a series feed. The compensated in-line divider has excellent electrical characteristics, but is long, and requires an internal isolating resistor that is usually not easily accessible for test or replacement. Best electrical performance is obtained with the two types of quarter-wave coupler. Where coupling tighter than -10 dB is needed, the $\lambda/4$ sidewall coupler becomes impractical to reproduce because of the small, accurate, etched gap required. This problem is avoided with the $\lambda/4$ overlap coupler, where the through and coupled lines are etched on opposite sides of a thin dielectric board. This type of coupler does, however, require a three-layer construction with accurate front-to-backside registration. Although somewhat more expensive to manufacture than other types, the $\lambda/4$ overlap coupler has been chosen for the commutator stripline feed networks because it excels in all the parameters important to this application.

TABLE 3-3. COMPARISON OF -6 dB STRIPLINE COUPLERS

PARAMETER	BRANCHLINE COUPLER	HYBRID RING COUPLER	COMPENSATED IN LINE DIVIDER	λ/4 SIDEWALL COUPLER	λ/4 OVERLAP COUPLER	REQUIRED VALUE
Operating Band						
Required (GHz)	1.2 1.4	1.2 - 1.4	1.2 1.4	1.2 - 1.4	1.2 - 1.4	1.2 - 1.4
Other (GHz)	1.03 - 1.09	1.03 - 1.09	1.03 1.09	1.03 - 1.09	1.03 - 1.09	
Board Size (ϵ_r = 2.5)	1.7" X 1.7"	3.0" X 3.0"	0.8" X 4.5"	0.5" X 1.7"	0.4" X 1.7"	Approx. 2" X 2" max.
Coupling Values						
Required (dB)						-5 to -8
Practical (dB)	3 to 9	3 to - 9	- 3 to - 10	Weaker than -10	-3 to - 30	
Coupling Flatness						
(dB)	0.05 0.25	0.20 0.60	0.10 0.20	0.02 0.08	0.02 0.08	<0.2/0.6*
VSWR	1.12:1 1.26:1	1.06:1 1.18:1	1.05:1 1.12:1	<1.05:1	<1.05:1	<1.05:1/1.20:1*
Isolation (dB)	14 8	27 20	32 25	>30	>30	>25/16*
Phase Runout	14° 19°	2° 4°	0° ≤0°	≤0°	≤0°	<2°/5°*
Special Features	Thru & coupled ports are adjacent	Thru & coupled ports are separated by input port	Requires internal isolating resistor	Requires small gap for tighter then -10 dB coupling	Requires 3-layer construction with accurate registration	
Estimated relative production cost	0.7	0.8	0.5	0.6	1.0	

*Values given are for sidelobe levels of -30dB and -20 dB respectively; required SLL is -20 dB.

3.4.3 Choice of Stripline Material

Four stripline configurations were considered for this application: air-strip, foam dielectric, honeycomb, and the conventional solid-dielectric sandwich type. Of these, air-strip has the least insertion loss per unit length, with foam, honeycomb and then solid dielectric following.

A solid Teflon-fiberglass dielectric medium was selected for the following features: moderate cost, good mechanical properties, low-loss characteristics, and reduction of wavelength in the medium, with correspondingly smaller size. A summary of the Teflon-fiberglass properties is given in Table 3-4.

TABLE 3-4. PROPERTIES OF TEFLON-FIBERGLASS

Dielectric Constant	2.5
Loss Tangent	0.0012
Usable Temperature Range	$-40^{\circ}C$ to $+200^{\circ}C$
Tensile Strength	15 kg/mm^2
Flexural Strength	10 kg/mm^2
Thermal Conductivity	2.6×10^{-4} $cal/sec/cm^2/^{\circ}C/cm$
Coefficient of Thermal Expansion	10×10^{-6} $(cm/cm)/^{\circ}C$
Thickness range available	0.20 to 0.125 inches
Specific Gravity	2.2

Because of the three-layer construction required for overlap couplers, the stripline configuration shown in Figure 3-15 was chosen. A total ground-plane spacing of 0.270 inch provides a reasonable compromise between the theoretical insertion loss of 0.0141 dB/inch, and the line width of 0.190 inch required for 50 ohms.

The center-board thickness of 0.020 inch represents a trade-off between two undesirable effects. As the center board becomes thinner, the coupling factor accuracy becomes increasingly more sensitive to the degree of overlap in the couplers. For example, a $\pm$ 0.001 inch error

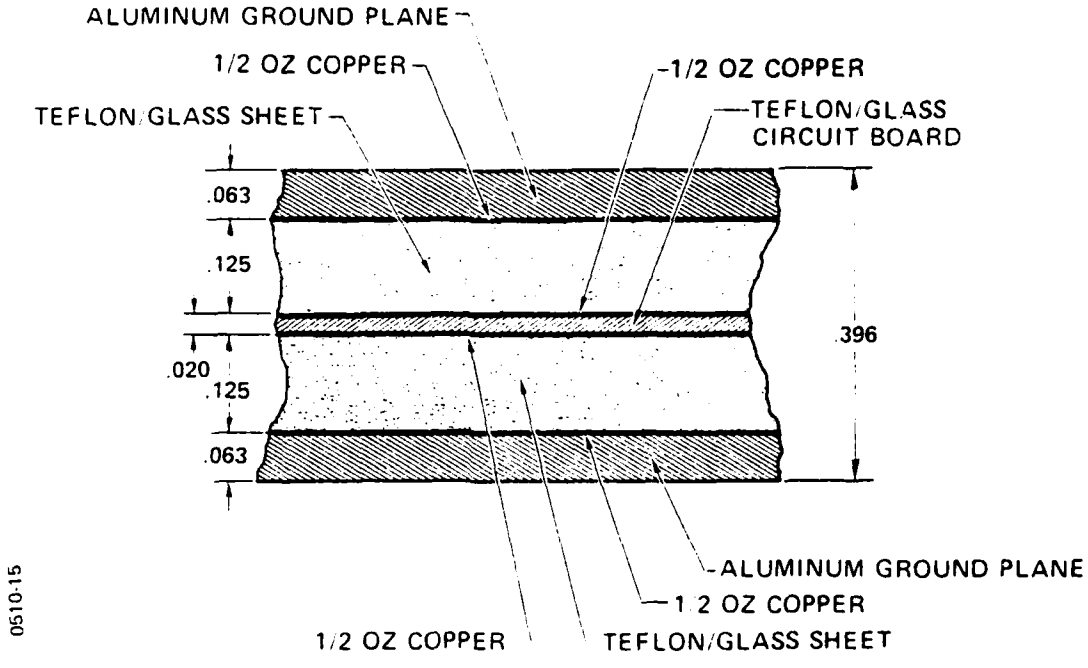

Figure 3-15. Three-layer stripline configuration

in overlap results in a ± 0.2 dB error in coupling factor for 0.020-inch thick material, and ± 0.3 dB error for 0.010-inch thick material. On the other hand, if the center board is made thick with respect to the outer dielectric sheets, the center conductor does not lie on the centerline between ground planes. If this unbalance is too great, serious moding problems can result.

½-ounce copper was chosen for cladding the center board rather than the usual 1-ounce or 2-ounce copper. This provides greater etched-line definition in the critical overlap region, but does not appreciably affect insertion loss or average power-handling capability.

3.4.4 Delay Phase Compensation

The feed network uses delay lines of appropriate length, as shown in Figure 3-16, to provide the exact phase correction required at each element. For an antenna 180 inches in diameter with an illumination sector of 90°, the pathlength in dielectric to the center element must be 16.077 inches longer than to the edge element. The additional insertion loss of as much as 0.23 dB due to the differential pathlengths must be considered in determining the coupling factors of the series line feed.

3.4.5 Phase Trimmers

In order to realize first sidelobes of -30 dB, the element-to-element phase error must be held to about 2° or less. However, accumulated phase errors in a stripline package of this kind could run as large as 10° due to various tolerances and uncontrolled factors. Some of these sources of error are the thickness and dielectric constant of the boards, etched line widths, line lengths, miters, impedance mismatches,

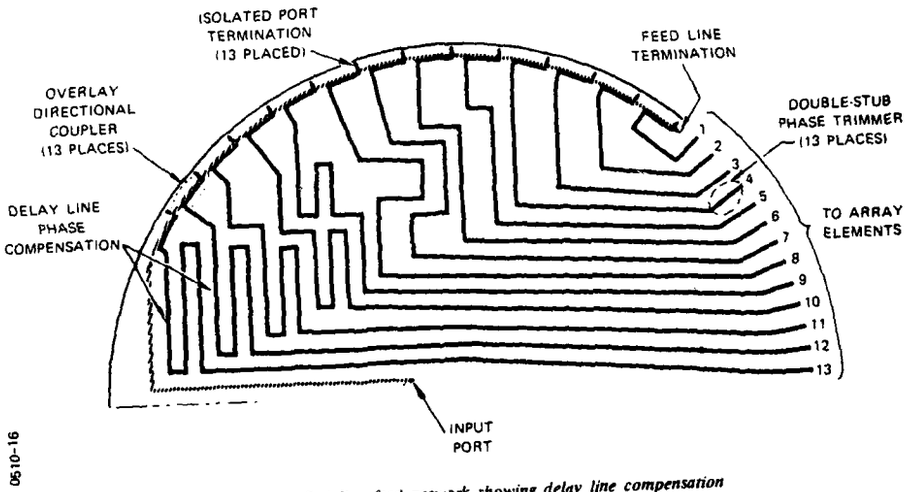

Figure 3-16. Stripline feed network showing delay line compensation

solder connections and connectors. Double-stub phase trimmers with approximately 15° of adjustment range, similar to Figure 3-17, are placed in each of the 26 coupled lines so that accumulated phase errors in the rotating stripline feed assembly can be corrected to an acceptably low value.

3.5 Loop Couplers

Operation of the magnetic loop couplers can be explained by referring to Figure 3-18. The device shown schematically on the left is a conventional quarter-wavelength directional coupler in TEM transmission line. If the normal through and coupled ports are short-circuited as shown on the right, and the line impedances and coupling factor are properly adjusted, all of the input power, minus losses, can be routed to the indicated port. The 0-dB coupler exhibits many of the fine performance traits of the conventional $\lambda/4$ coupler, namely low insertion and wideband operation.

3.5.1 Loop-Coupling Region

A plan view of the loop-coupling region of the Commutating Feed Assembly is shown in Figure 3-19, and in perspective in Figure 3-20. The coupling performance is expected to vary somewhat as the rotor loops pass over the stator loops. These variations are minimized in magnitude and duration by using magnetic coupling with narrow rotor loops and much wider stator loops. Of course, during the interval when the rotor loop is over the gap region between adjacent stator loops, the effect is most noticeable. This situation can be avoided either by staggering the relative location of rotor and stator loops, or by transmitting and receiving only when the loops are overlapping.

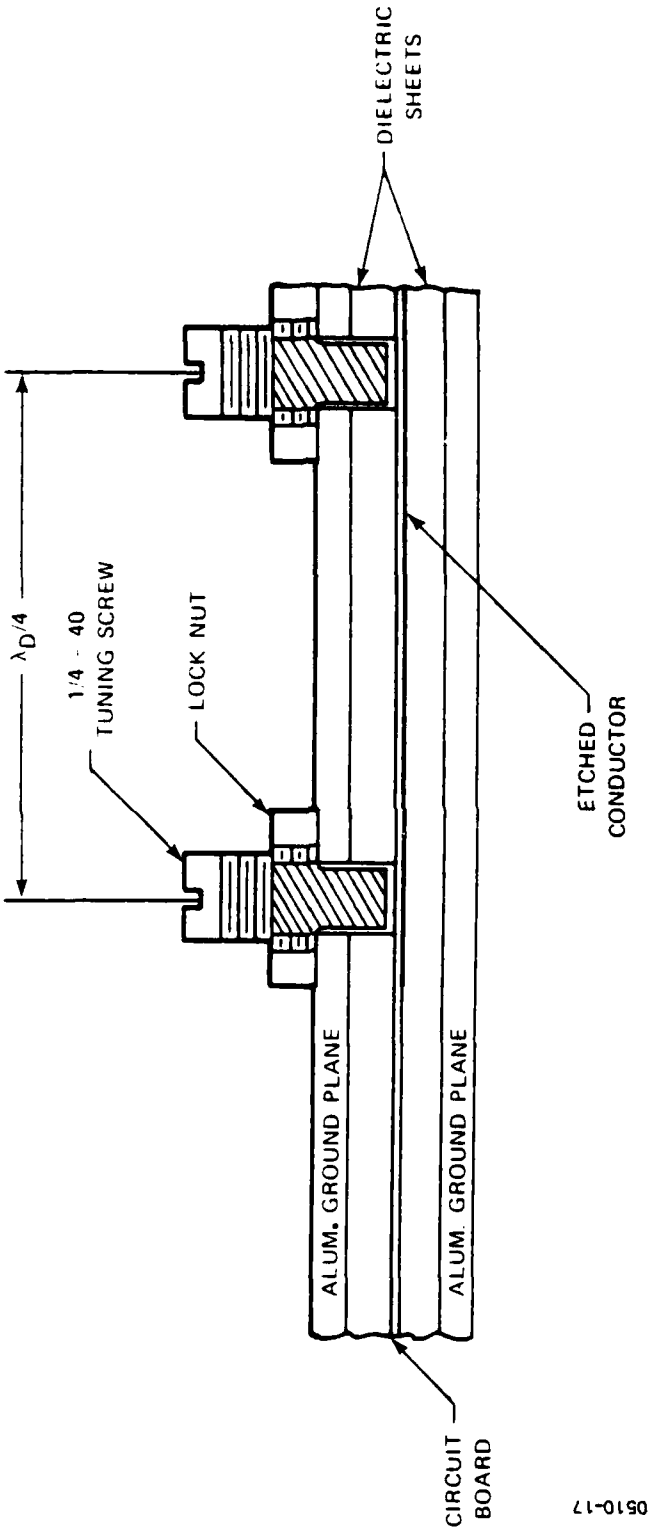

Figure 3-17. Double-stub phase trimmer

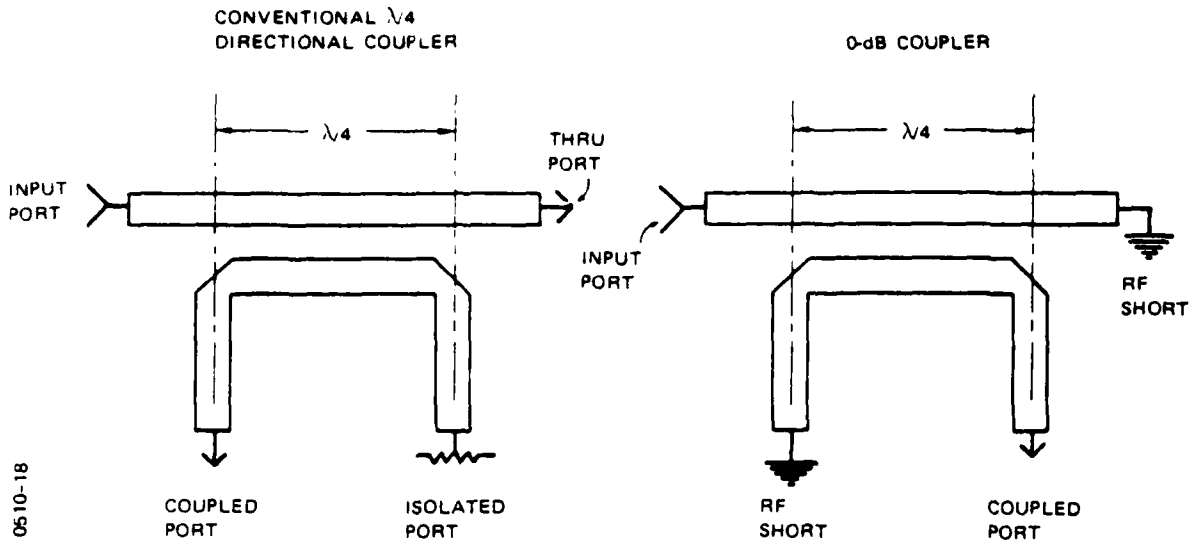

Figure 3-18. Modification of conventional λ/4 directional coupler to obtain 0 dB coupler

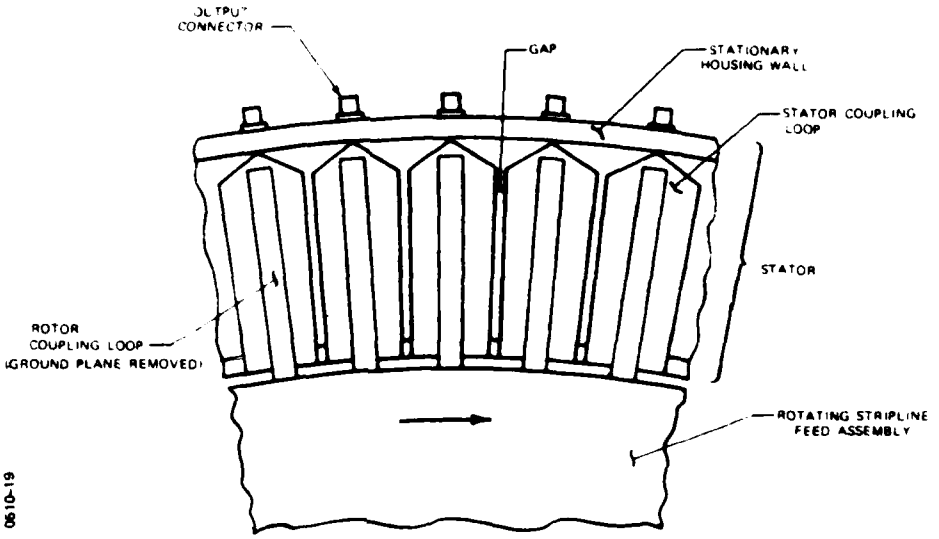

Figure 3-19. Plan view of loop coupling region

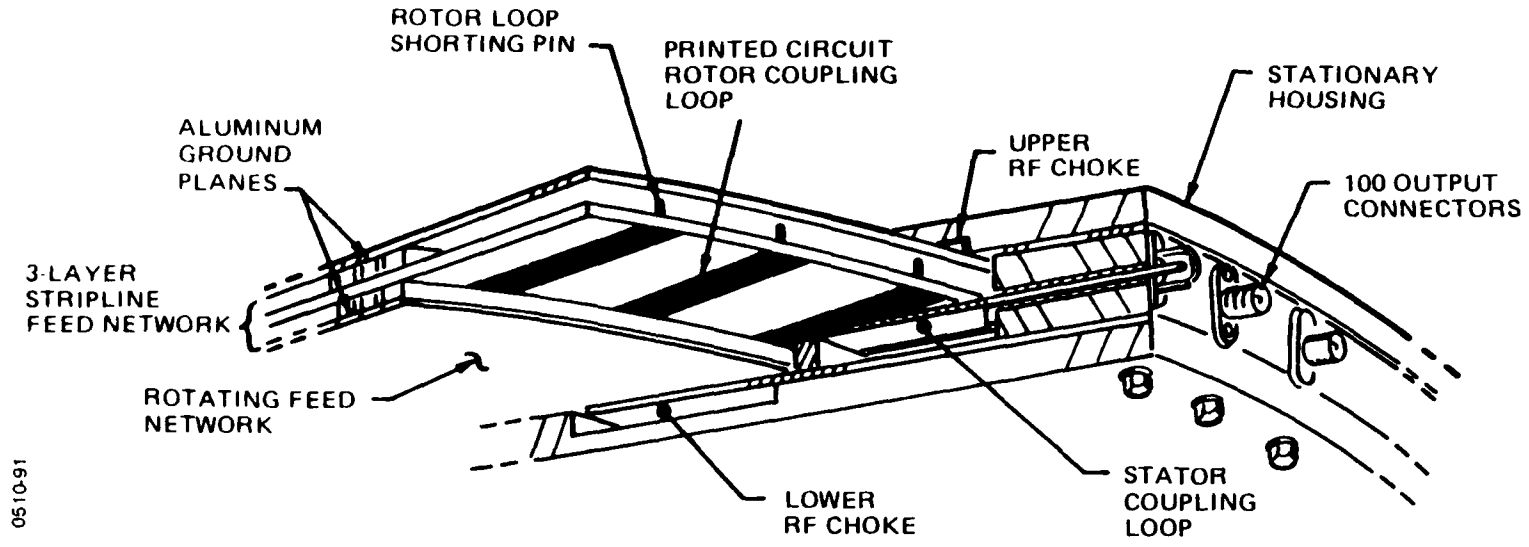

Figure 3-20. Rotating feed network mounted in stationary housing

Rotor loop fabrication and assembly can be improved significantly by etching them directly on the stripline circuit board. This solves the problem of how to attach the rotor loops both mechanically and electrically to the stripline feed network in an inexpensive and reliable fashion.

3.5.2 RF Chokes

Proper operation of the magnetic loop couplers requires that the quarter-wavelength loops are terminated in a reliable, low-loss RF short. This is easily accomplished for the stator loops by means of the aluminum shorting bar that is used to support the grounded end of each loop. The problem is more complicated for the rotor loops, which continually move relative to the commutator housing. A contacting short is undesirable from the standpoint of loss, reliability, wear, and the generation of electrical contact noise. Therefore, RF chokes of the standard double quarter-wavelength design are used to provide non-contacting RF shorts for the rotor loops. Two RF chokes are required: one in the lower housing surface that produces an RF short in the plane where the stripline ground planes end and the rotor coupling loop begins; and a second RF choke in the upper housing surface that produces an RF short in the plane of the grounded end of the rotor loop.

The choke cavities are made by machining an annular groove in the housing surface, and then using a washer-shaped ring to form the folded quarter-wavelength sections.

SECTION 4

GENERAL METHODOLOGY AND PROPOSED SOLUTIONS

A simplified block diagram of the commutator is shown in Figure 4-1. The annular rotary coupler is a special design that provides the power-splitting function with two equal-amplitude, in-phase outputs. The rotating stripline feed network consists of a center-fed array of directional couplers, delay lines for phase compensation, phase trimmers, and printed-circuit rotor coupling loops. The stationary housing includes the support structure, pedestal drive assembly, bearings, RF chokes, stator coupling loops, and output connectors.

A flow chart of the general methodology for development of the commutator is shown in Figure 4-2. This development requires a combination of analysis, synthesis and empirical validation of results at well defined checkpoints during the development cycle. Initially, overall system requirements are allocated at the subsystem or component level. Tradeoffs are then conducted at these levels to realize a design that is capable of meeting performance and operational requirements, while minimizing production cost and risk. These tradeoffs must be made with caution, however, as results depend to a large degree on the selection criteria that are used.

The commutator development can be divided into three major design tasks: the power train, the stripline feed network, and the loop couplers. The design methodology and proposed solutions for each of these is discussed below.

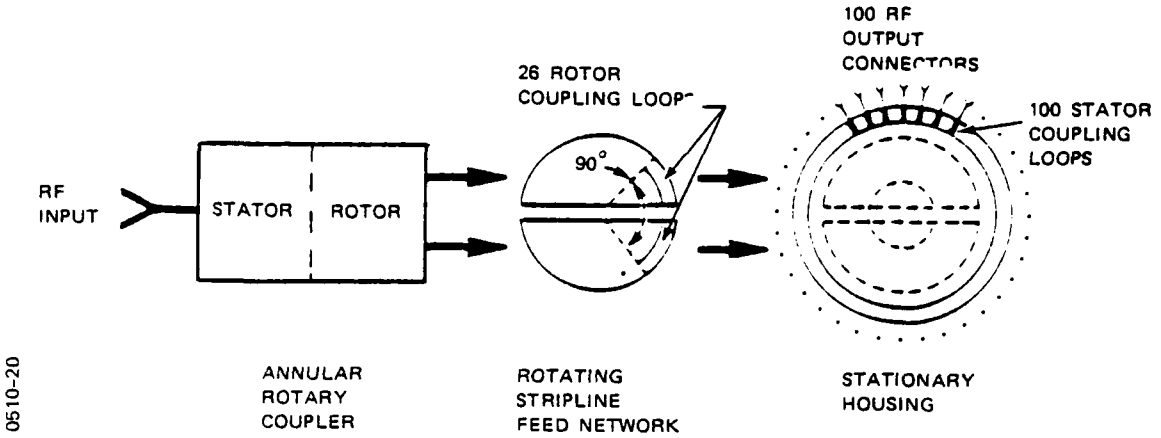

Figure 4-1. Block diagram of commutating feed assembly

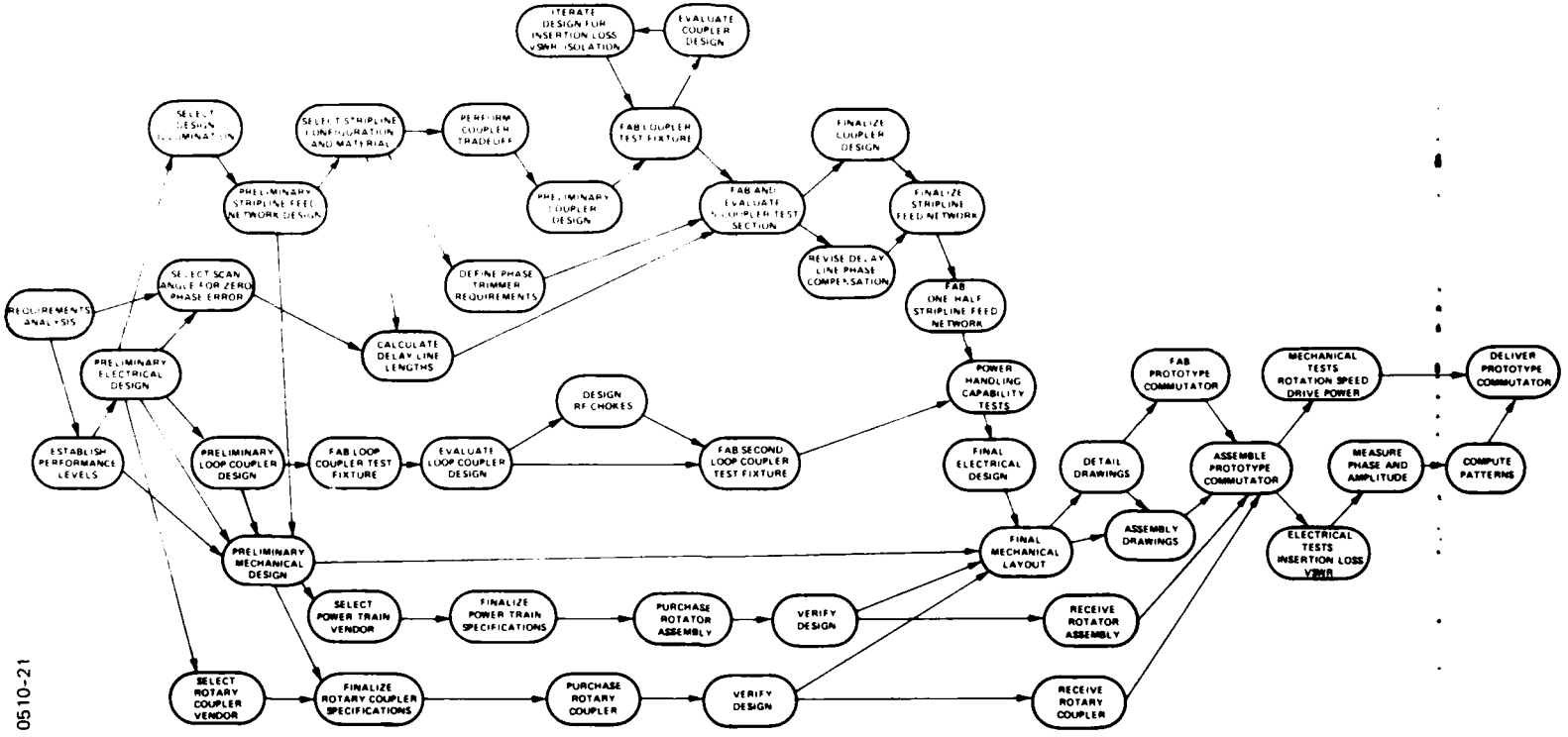

Figure 4-2. General methodology for development of commutating feed assembly

4.1 Power Train

The design of the power train is straightforward. The size estimate of the rotating section, 36 inches diameter by 0.4 inch thick, is adequate for determining bearing requirements and motor size. The rotator/pedestal drive assembly required for this rotating load is purchased from a company that specializes in the design and manufacture of torque-motor driven pedestals. The model selected is a modification of an existing rotator design; thus, little risk is involved.

4.2 Stripline Feed Network

This part of the development demands the largest effort; however, the technology required is well known and readily available. Basic design information for the overlap directional couplers is described in the literature[1]; however, a modified configuration with the load arm crossing over the through line requires additional experimental data.

In order to establish a performance baseline, the tabulated design information[1] is used to make three overlap directional couplers of the conventional configuration, with nominal coupling values of -5.0, -6.5, and -8.0 dB. This step is essential to reconcile small yet significant differences between tabulated parameters and those actually used, such as relative dielectric constant, ground-plane spacing, center-board thickness, and copper thickness. Next, a -6.5 dB coupler with the load arm "flipped" is built, and the coupling, VSWR and isolation as a function of frequency are compared to the baseline design. Dimensional changes are made to compensate for the additional capacitive loading at the load-port crossover, and matching is improved until acceptable values of coupling flatness, VSWR, and isolation are obtained. After several iterations, the design is optimized for several coupling values

over the desired range: -5.0, -6.5, and -8.0dB. Thus, an accurate design curve of coupling value versus overlap is derived for the particular coupler geometry to be used. To double-check the accuracy of this design information, a test fixture consisting of a portion of the 13-element series feed is built and evaluated. The last five couplers, for elements 9 through 13, are chosen as these cover nearly the entire range of coupling values, and require the least area when the proper delay line phase compensations are included. In addition to demonstrating the performance of several couplers connected in series, this stripline test fixture also allows design verification of delay lines, phase trimmers, flange-mounted load terminations, and line losses in the stripline medium. Next a complete 13-element series feed network, excluding the rotor loop couplers, is built and evaluated. This provides a final opportunity for minor design changes, such as to optimize coupling values in the series feed networks, and to adjust line lengths in the delay lines that compensate phase in order to produce a planar wave front from the circular array aperture. Screw fasteners provide quick access to inspect or modify breadboard stripline assemblies.

4.3 Loop Couplers

The non-contacting magnetic loop-coupler configuration proposed is basically a new concept; however, much of the technology used is available: $\lambda/4$ directional couplers, parallel-plate balun loop-couplers, and double quarter-wavelength RF chokes.

The approximate performance of the loop couplers can be surmised by modifying analytical expressions that describe broadside coupled lines[2]. This derivation is given in Appendix A.

To achieve highly-efficient, wideband, power transfer there exist a multitude of parameters that require optimization: the length, width and ground-plane spacing of both the rotor and stator loops, the gap between adjacent stator loops, and most critically, the separation between rotor and stator loops.

An excellent starting point for the stator loop-coupler design is a balun loop-coupler developed by ITT Gilfillan for a 110-way parallel-plate radial line combiner that operates over the 1.2 to 1.4 GHz band. The length, ground-plane spacing, and gap between adjacent loop couplers remains unchanged, while the width is reduced by 12.7% to account for differences between combiner and commutator in diameter and number of loop couplers, 110 versus 100.

Once the stator loop-coupler design is fixed, a relatively simple test fixture is built that allows the width and ground-plane spacing of the rotor loop-coupler, as well as the gap between rotor and stator, to be varied. In order to limit the number of variables to be optimized at one time, the rotor loop-coupler RF grounds are made using beryllium-copper spring contacts, rather than non-contacting RF chokes. After the optimum rotor loop coupler width and ground-plane spacing are found, a second test fixture with RF chokes incorporated is built to determine precisely the optimum rotor-to-stator gap setting.

Although the preceding optimizations are carried out with the rotor loops stationary, centered over the stator loops, the entire stripline section can be slowly moved by hand so that insertion loss and phase versus rotational angle can be observed.

References:

1. H. Howe, Jr., "Stripline Circuit Design," Artech House, Inc., Dedham, Ma., 1974, pp. 126, 132-150, 153-157.

2. Cohn, S. "Characteristic Impedance of Broad Side Coupled Strip Transmission Lines," IEEE Trans. Microwave Theory Tech., vol. MTT-8, pp. 633-637, 1960.

SECTION 5

DEVELOPMENTAL HARDWARE

5.1 Rotator Pedestal Assembly

The rotator pedestal assembly and control unit, shown in Figure 3-9 and Figure 5-1, provide rotational drive to the commutating feed assembly. A schematic diagram of the two units is shown in Figure 5-2.

Drive power for the dc torque motor, B1, is supplied through the servo power amplifier, AR1. Because the amplifier requires +24 volts, whereas the motor operates at only 4.8 volts, 80 percent of the input power is dropped in the amplifier. The motor winding and amplifier were selected for off-the-shelf availability, although more efficient combinations are possible. Table 5-1 shows power consumption information for other winding options of the T5730 motor. Note that total power required is only 12 watts for the G winding with the amplifier operating at +30 volts.

TABLE 5-1 POWER CONSUMPTION FOR VARIOUS MOTOR WINDINGS

Motor Winding	Current (A)	Motor Voltage (V)	Motor Power (W)	Total Power (W)
A	2.5	4.8	12.0	60.0
J	2.0	6.0	12.0	48.0
C	1.3	9.2	12.0	31.2
G	0.4	28.2	11.3	12.0

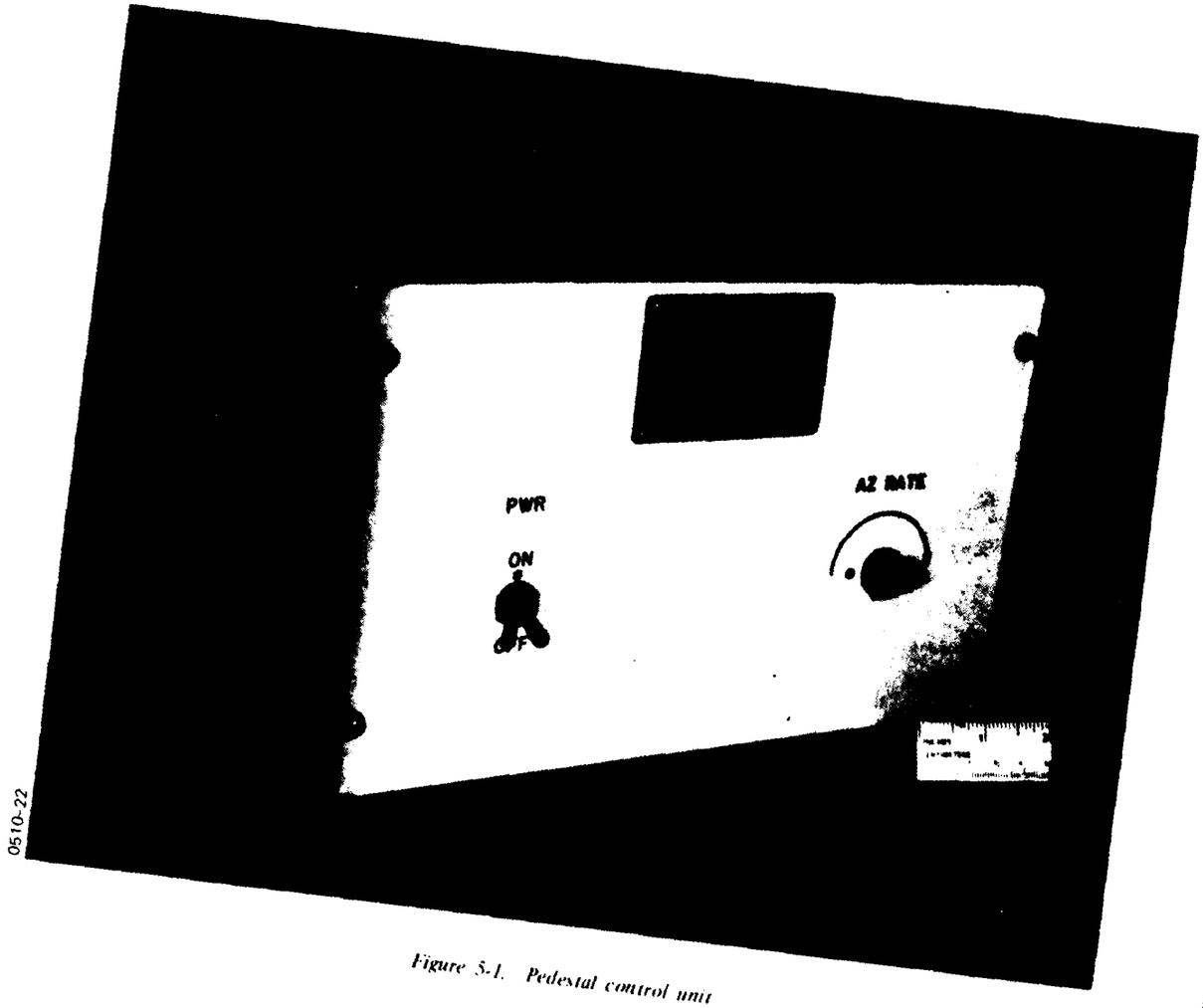

Figure 5-1. Pedestal control unit

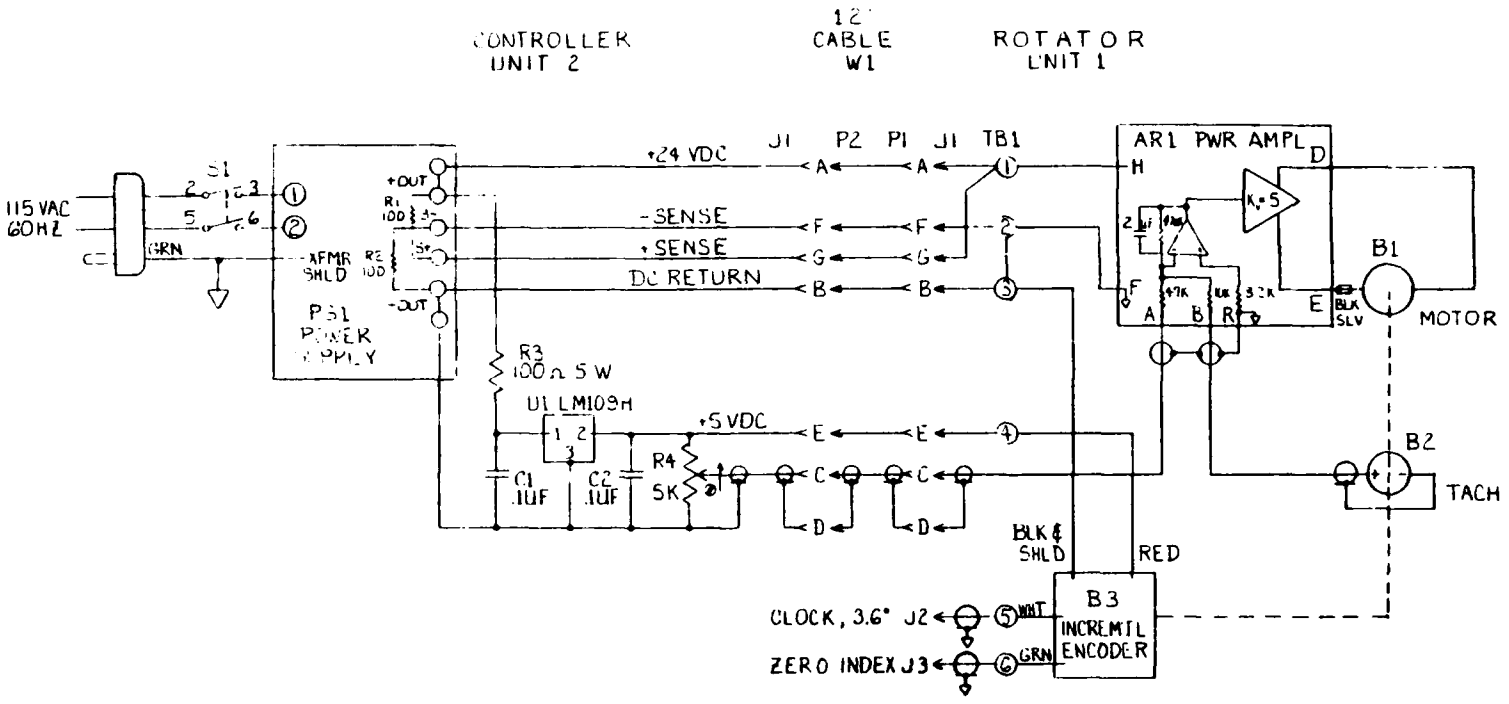

Figure 5-2. Schematic diagram of rotator controller

Speed control is accomplished by feedback from the tachometer, B2, to the servo amplifier. The present hardware uses a gear tachometer, which is accurate to about one percent. Where greater precision is desired, other types of tachometer can be used.

An optical encoder, B3, provides a TTL-compatible zero index pulse at connector J3 once every 360 degrees, and a data pulse at connector J2 every 5.6 degrees. The data pulses can be counted from the zero index pulse to determine the angular position of the rotator, hence the peak of the beam, at any given instant. These pulses can also be used to time transmit/receive sequences so that they occur during the interval when the loop couplers are well engaged.

5.2 Annular Rotary Coupler

The annular rotary coupler is a modified unit originally developed for use at the TACAN band. Changes were made to the internal corporate feeds to operate from 1.2 to 1.4 GHz, and to provide two equal-amplitude, in-phase outputs. A photograph of the unit is shown in Figure 5-3.

Measured swept-frequency insertion loss and input VSWR of the rotary coupler are shown in Figures 5-4 and 5-5. The power split between outputs is excellent: within 0.05 dB over the entire range of 1.0 to 1.5 GHz. Phase difference between output ports A and B, shown in Figure 5-6, is negligible. Note that the coupler appears to be optimized at 1.2 GHz, rather than at the operating band center, 1.3 GHz. This results in higher insertion loss and VSWR than desirable at the upper band edge. It is the opinion

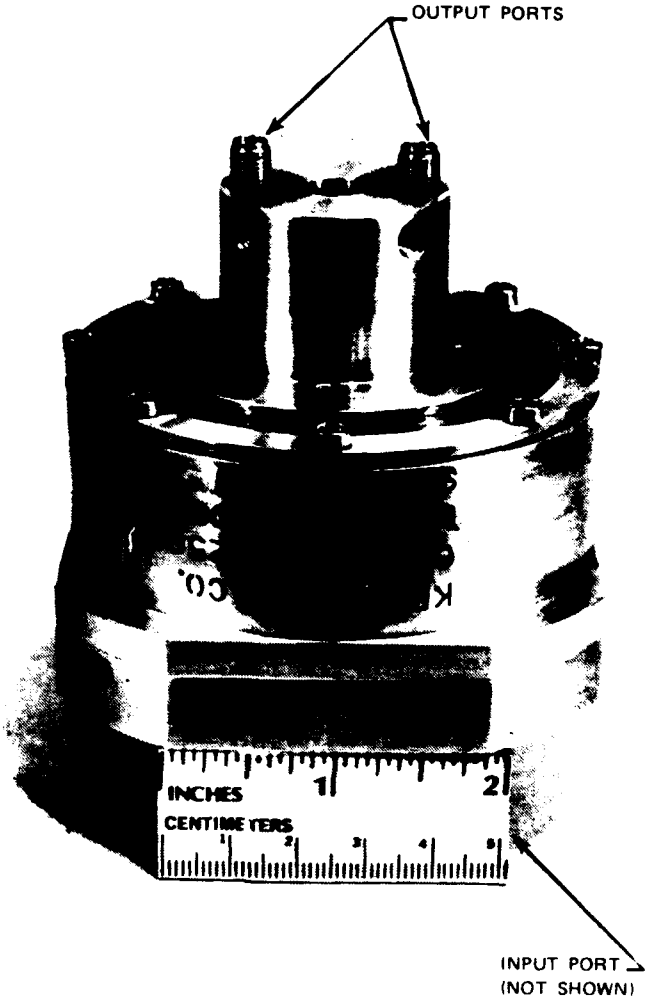

Figure 5-3. Annular rotary coupler

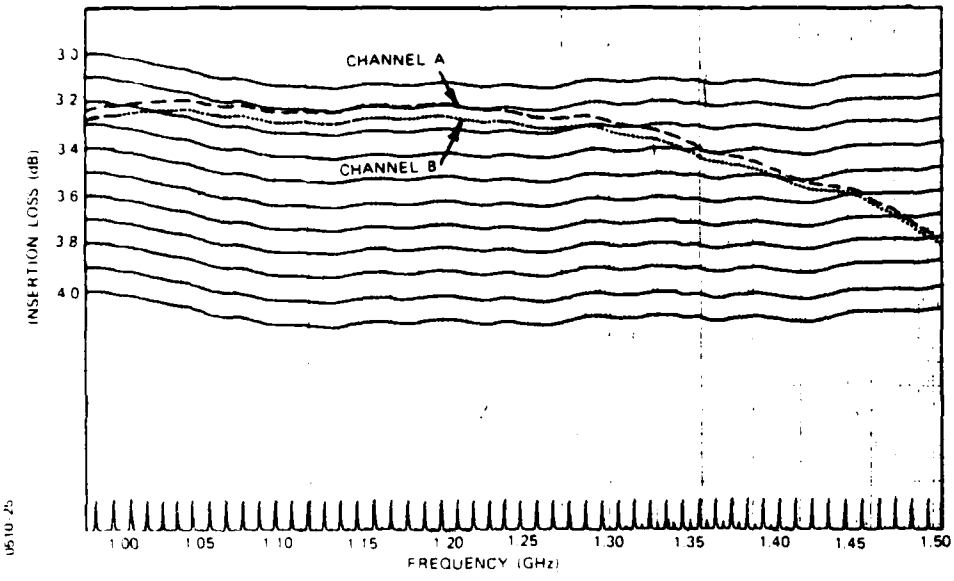

Figure 5-4. Insertion loss vs frequency of annular rotary coupler

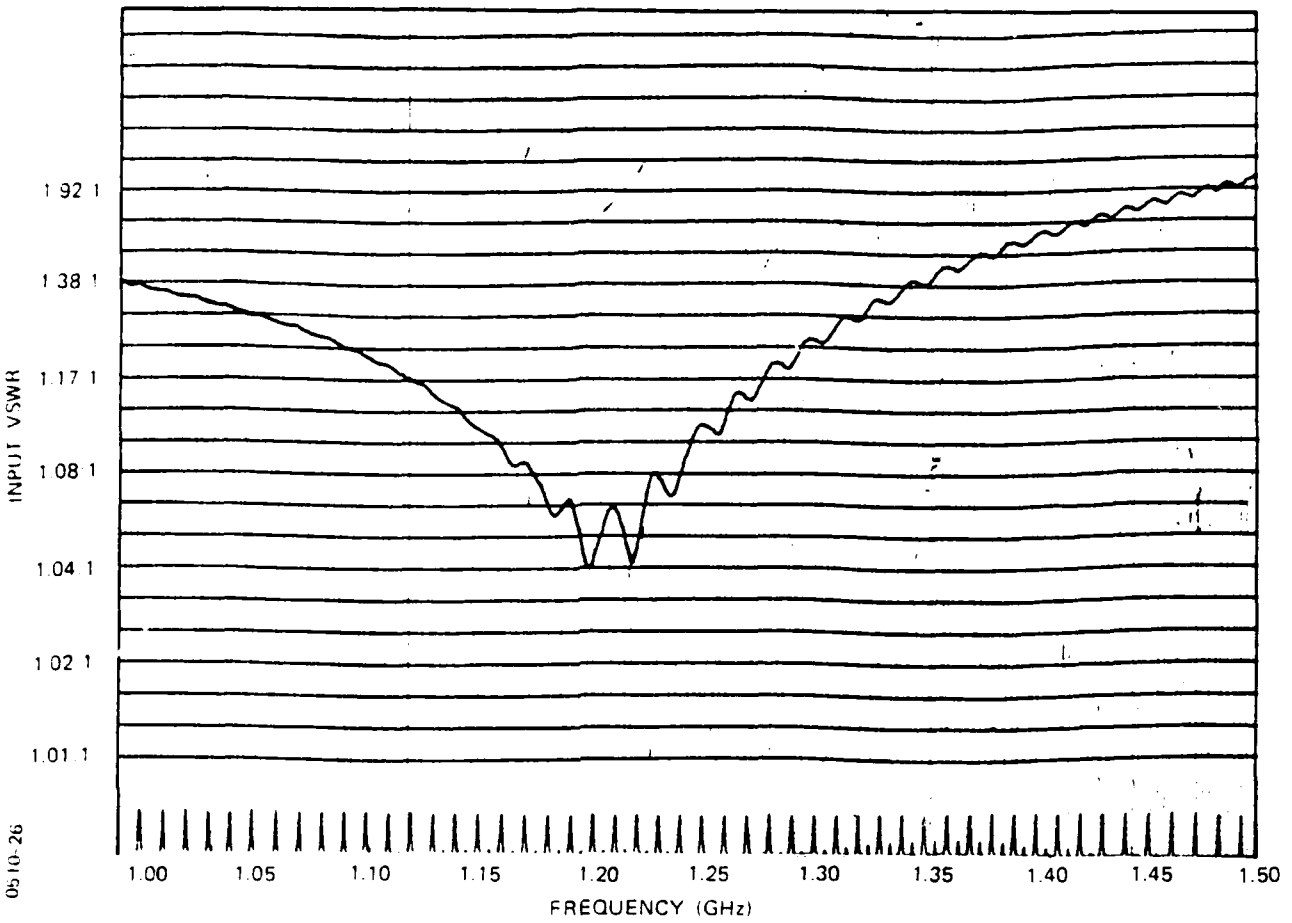

Figure 5-5. VSWR vs frequency of annular rotary coupler

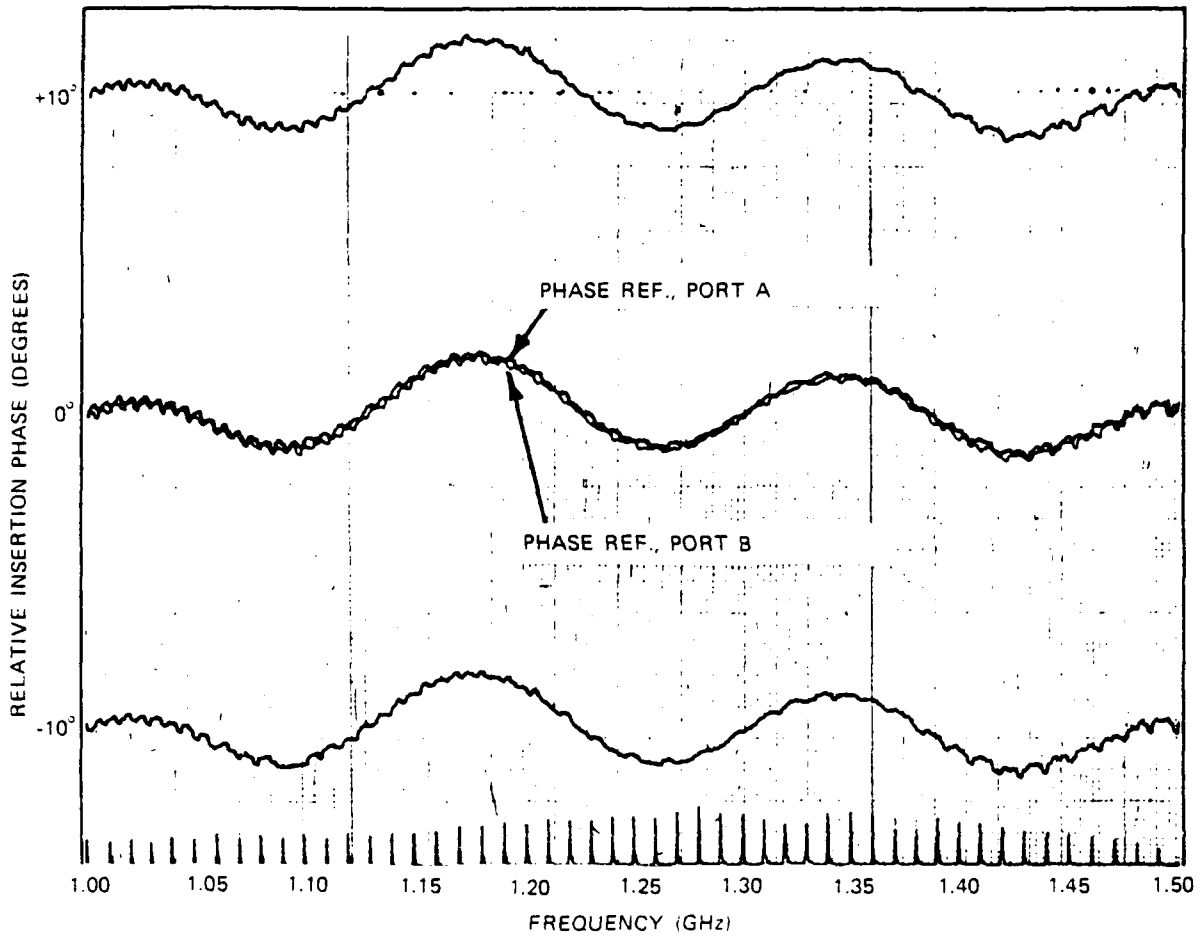

Figure 5-6. Phase difference between output ports A and B

of the vendor that no substantial improvement to this particular unit can be obtained without redesign and matching of the internal parts. Expected performance of a production version of this annular rotary coupler over the 1.2 to 1.4 GHz band is 0.15 dB excess insertion loss and 1.2:1 VSWR, with usable performance at the IFF band: 0.5 dB excess insertion loss and 2:1 VSWR.

5.3 Stripline Feed Network

5.3.1 Modified Overlap Directional Coupler

The design of the modified overlap directional coupler, with the isolated-port arm "flipped", was optimized for three coupling values over the desired range: -3.0, -6.3, and -8.0 dB. Measured data were used to generate the design curves shown in Figures 5-7 and 5-8. The measured coupling, isolation, and VSWR for the nominal -6.3 dB coupler design are shown in Figures 5-9 and 5-10. Although this coupler was intended for the 1.2 to 1.4 GHz band only, note the excellent performance of the device over the extended band, 1.0 to 1.6 GHz.

5.3.2 Flanged 50-Ohm Loads

The 50-ohm load termination selected for this application is shown in Figure 5-11. The device is rugged and compact, and can be externally mounted to the stripline assembly, where it is readily accessible. With 5% power into the main-line loads, or 7.5 watts average each, the 25-watt rating of the load provides adequate margin for this design. Swept-frequency VSWR of the load, measured in a stripline test circuit, is shown in Figure 5-12.

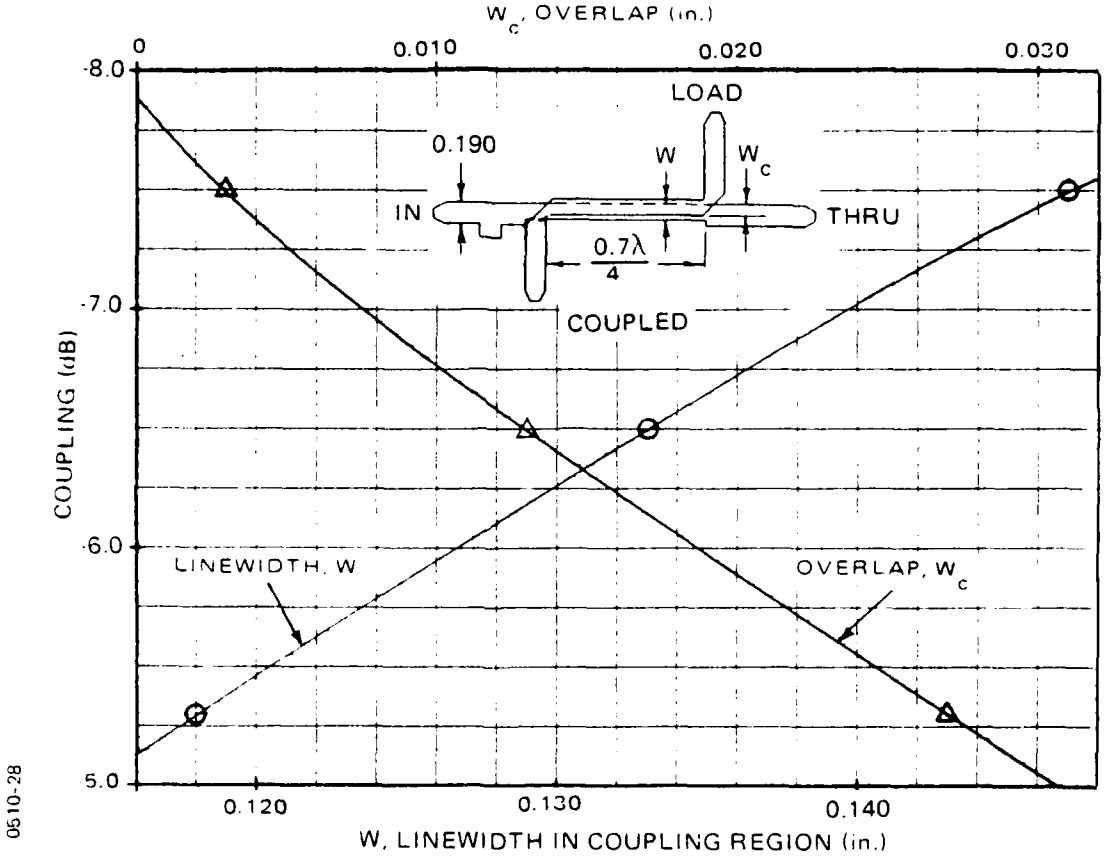

Figure 5-7. Design curve for modified λ/4 overlap directional coupler

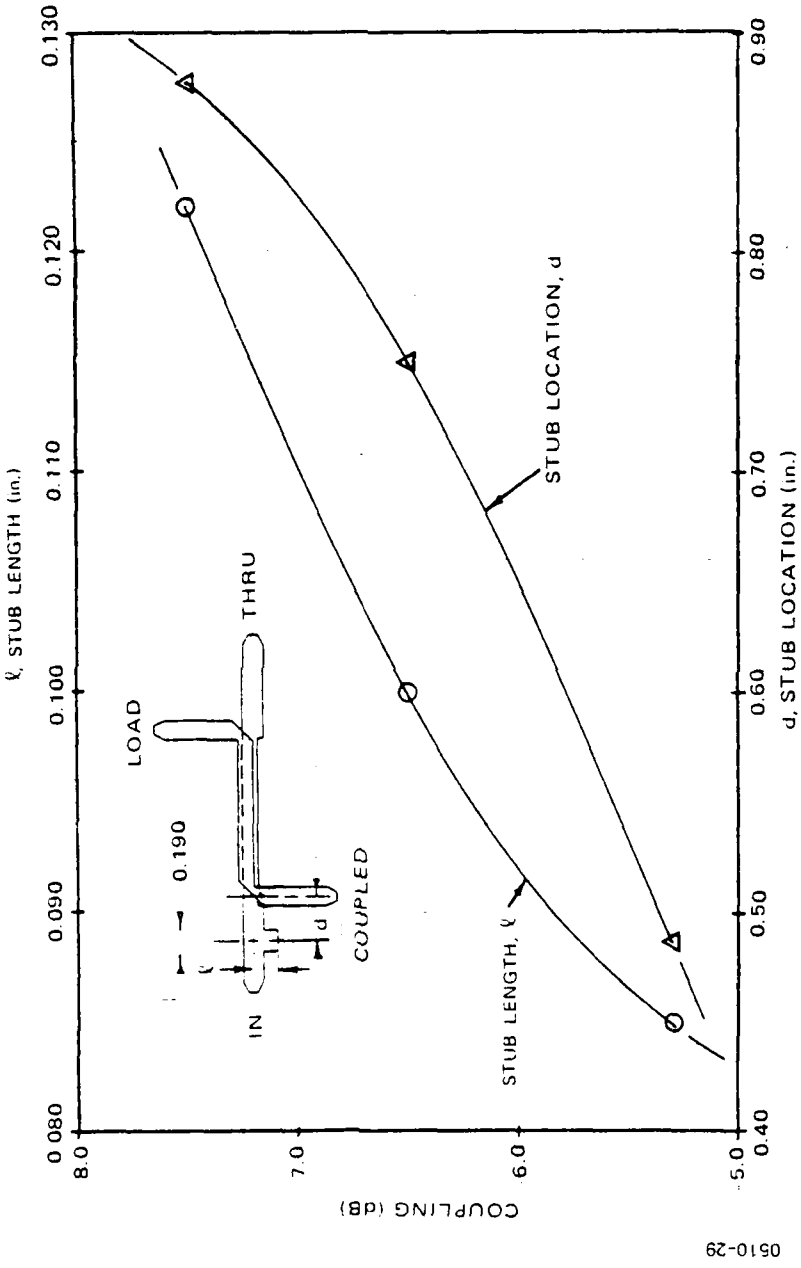

Figure 5-8. Matching stub length and location

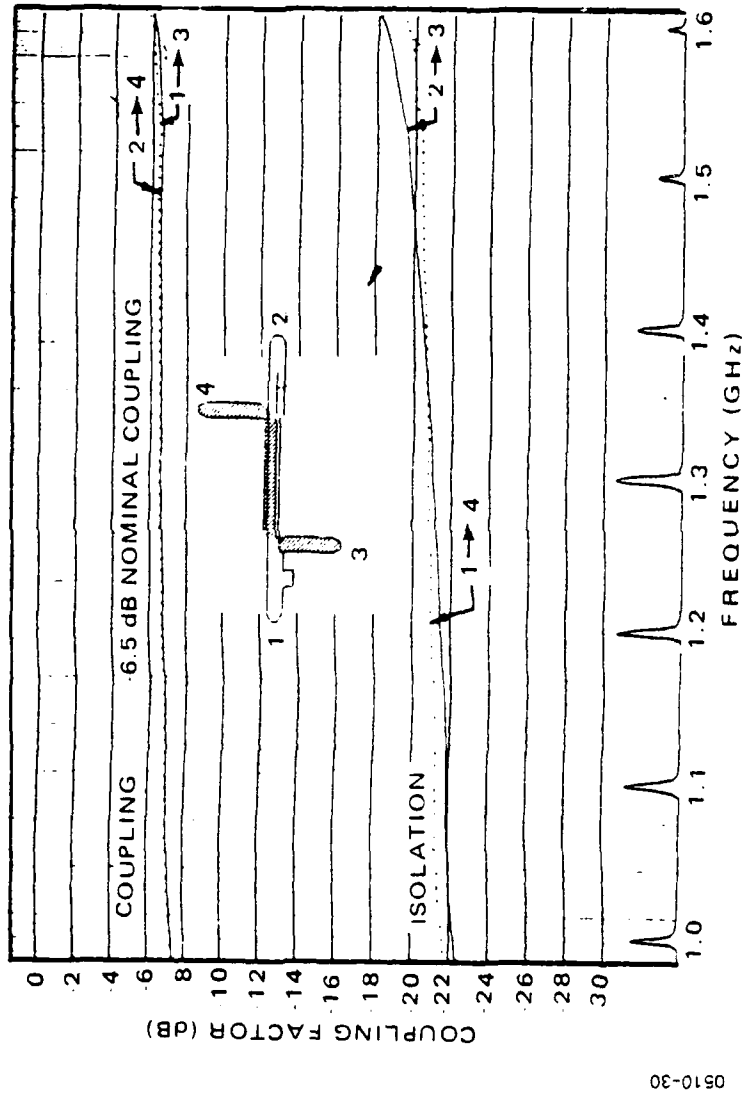

Figure 5-9. Measured coupling and isolation vs frequency of modified coupler

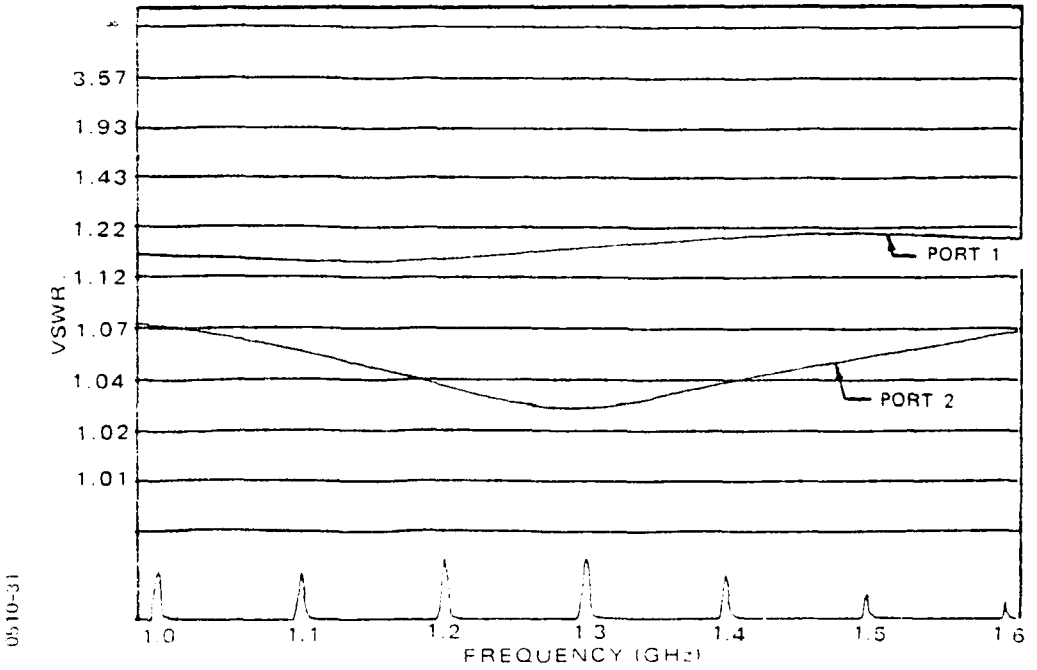

Figure 5-10. Measured VSWR vs frequency of modified N/4 overlap directional coupler

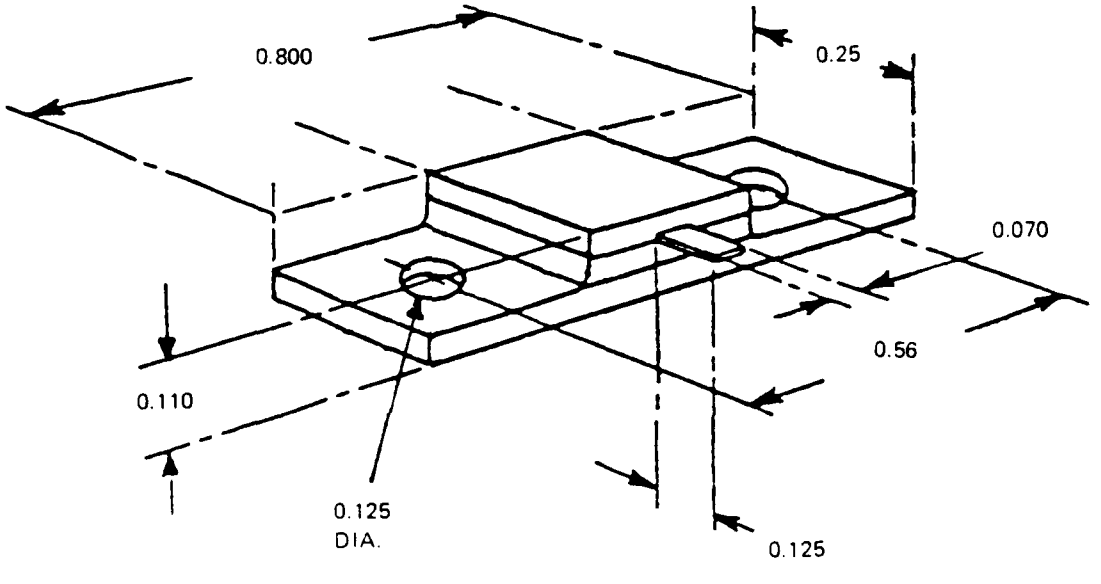

Figure 5-11. Flanged 50-ohm load

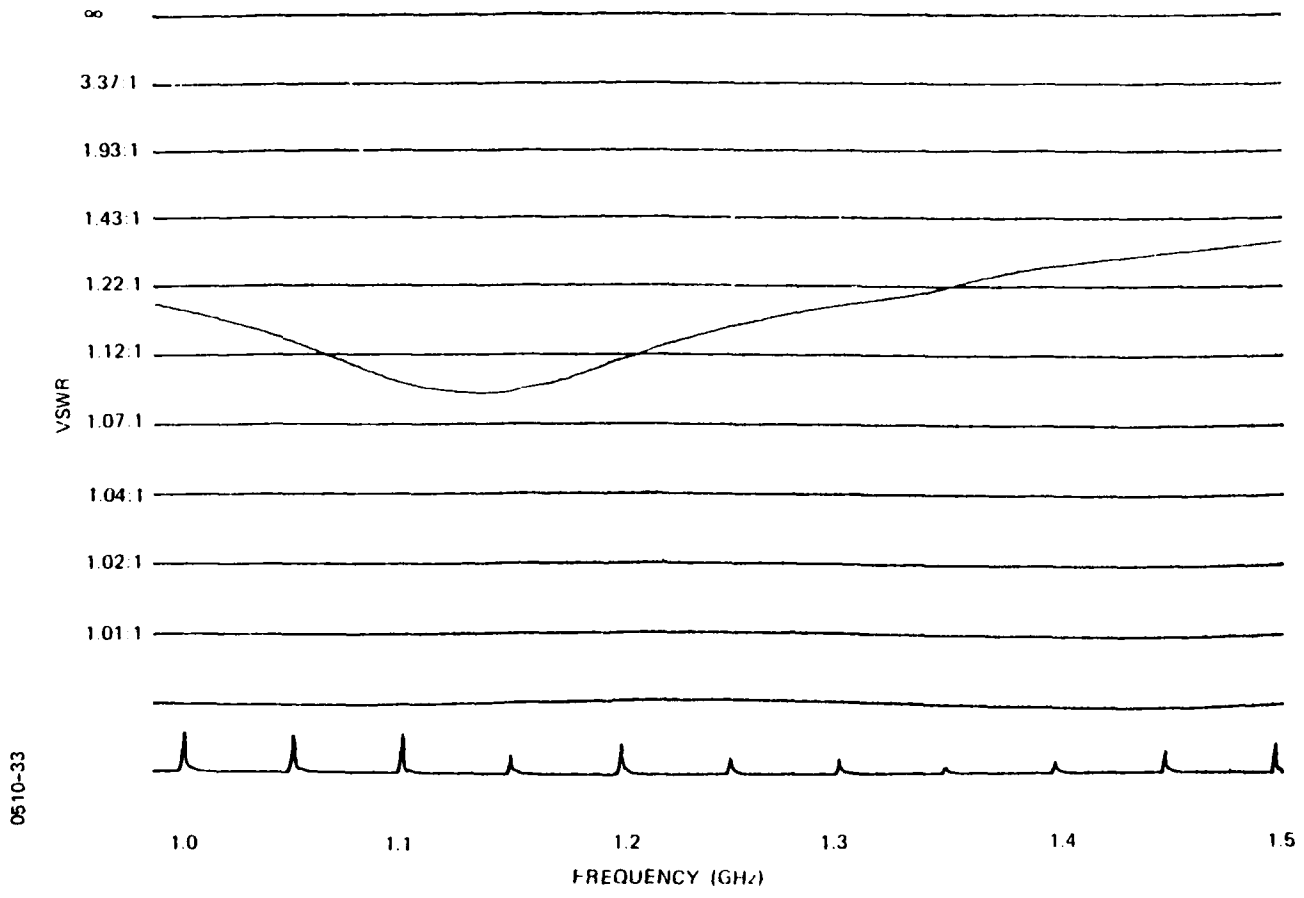

Figure 5-12. Swept-frequency VSWR of typical flanged 50-ohm load measured in stripline test circuit

Table 5-2 summarizes the characteristics of the load.

Table 5-2. SUMMARY OF FLANGED 50-OHM LOAD CHARACTERISTICS	
Frequency of Operation	DC to 4.0 GHz
Resistor Value	50 ± 2.5
VSWR	1.3:1 Maximum
Power Dissipation	25 watts *

95MD27

* De-rate to zero watts at 150°C case temperature.

5.3.3 Delay Lines and Phase Trimmer

A small stripline test fixture, containing eight 90-degree miter bends, was constructed and tested in order to obtain a precise value of insertion phase due to the miters. It was found that the electrical path length is six degrees per bend shorter than the geometrical path length. This correction factor is used for the delay lines in the stripline test fixtures described in Sections 5.3.5 and 5.3.6, as well as in the stripline assembly of the experimental model.

A stripline test fixture, incorporating the double-stub phase trimmers shown earlier in Figure 3-17, was built and tested. Phase adjustment of greater than 15 degrees was measured over the frequency band of 1.2 to 1.4 GHz without any appreciable increase in VSWR.

5.3.4 Stripline Coupling Loop and Matching Stub

As noted earlier, fabrication and assembly of the rotor loops can be improved significantly by etching them directly on the stripline

circuit board, as shown in Figure 5-13. Five different loop widths ranging from 0.2 to 0.4 inch, were compared, with the 0.25-inch wide loop giving the best performance.

A stripline matching stub is required at the location where each rotor loop extends beyond the edge of the dielectric boards. At this point, the ground-plane spacing abruptly changes from 0.270 inch to about 0.500 inch, and would introduce an appreciable VSWR if not otherwise matched.

5.3.5 Five-Coupler Stripline Test Fixture

A test fixture consisting of the last five couplers of the stripline feed network, for elements 1 through 5, was built and tested. Figure 5-14 is a photograph of this circuit. The measured insertion loss referenced to the input port, as a function of frequency, is shown in Figure 5-15. The numbers in parentheses represent predicted losses which are based on the coupler design values and theoretical line losses of 0.015 dB per inch. These results are summarized in Table 5-3.

Table 5-3. SUMMARY OF FIVE-COUPLER STRIPLINE TEST FIXTURE PERFORMANCE

Element	Measured Ins. Loss(dB)	Theoretical Ins. Loss(dB)	Variance(dB)
5	6.0	6.5	-0.5
4	8.0	8.3	-0.3
3	9.8	9.7	+0.1
2	10.8	10.7	+0.1
1	11.3	11.1	+0.2

Figure 5-13. Printed-circuit rotor loops

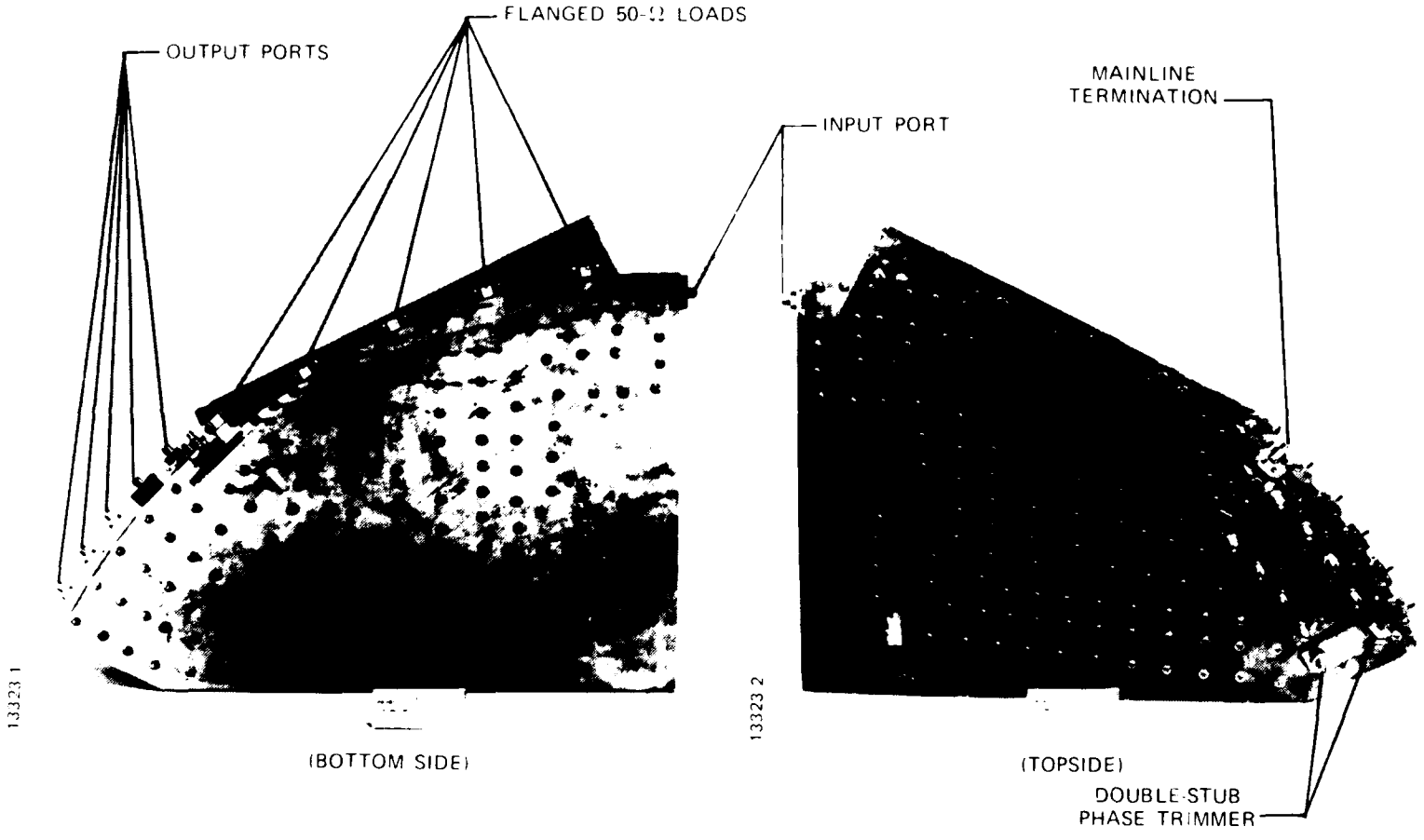

Figure 5-14. Photograph of five-coupler stripline test fixture

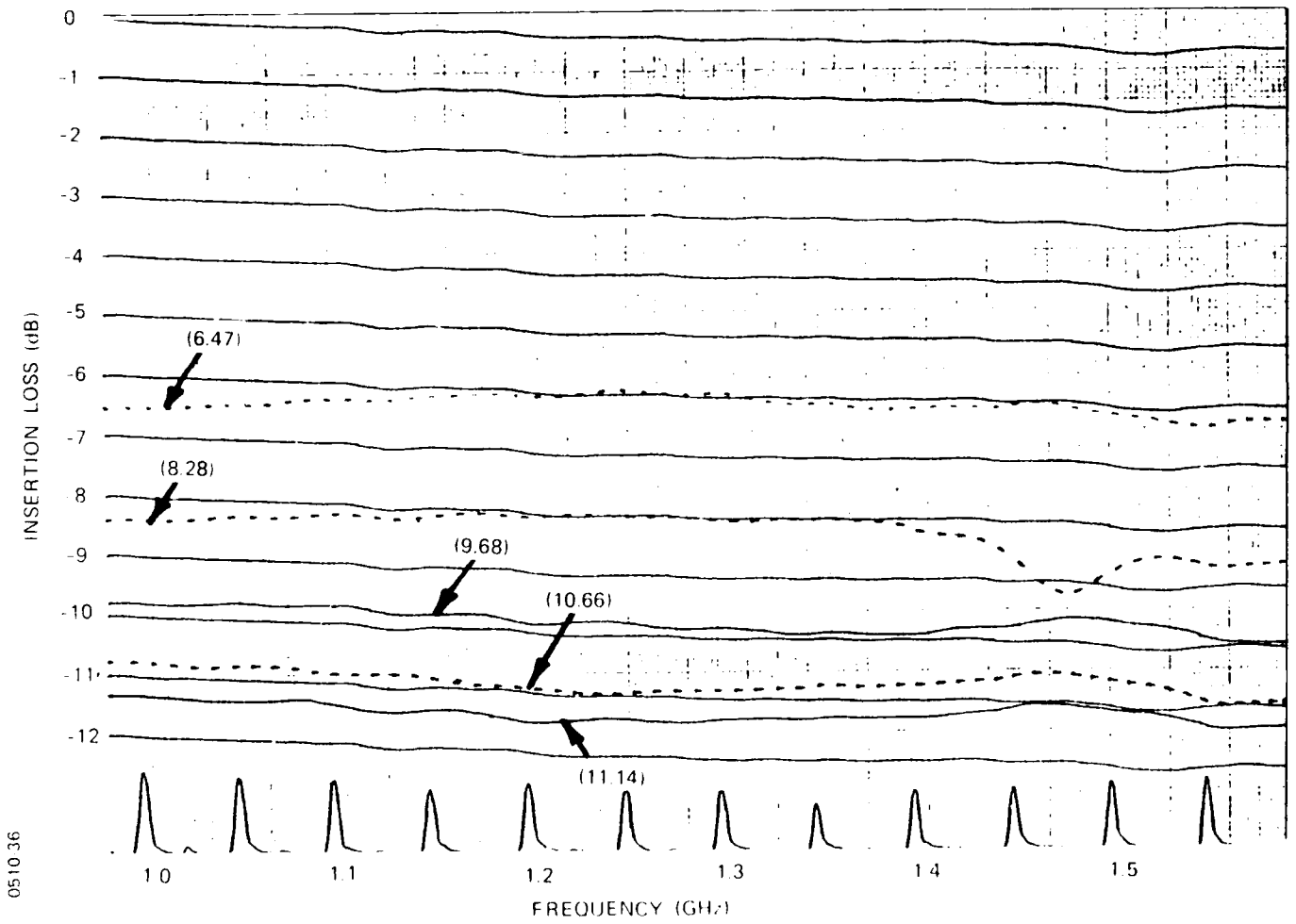

Figure 5-15. Measured insertion loss vs frequency of five-coupler stripline test fixture

On the final stripline circuit layout, a slight correction will be made to the overlap region of each coupler to keep the variance within $\pm$ 0.2 dB. The measured swept-frequency VSWR of this test circuit is shown in Figure 5-16. The input match is less than 1.12:1 over the 1.2 to 1.4 GHz band.

5.3.6 13-Coupler Stripline Test Fixture

One-half of the complete stripline feed network, shown in Figure 5-17, was built and tested. Coaxial connectors replace the 13 printed-circuit rotor loops and matching stubs which are to be incorporated in the final stripline assembly. This allows direct measurement of the amplitude and phase distribution of the network, without introducing potential errors by the loop couplers.

The measured insertion loss referenced to the input port, as a function of frequency, is shown in Figure 5-18. The numbers in parentheses represent predicted losses which are based on the coupler design values and theoretical line losses of 0.015 dB per inch. These results are summarized in Table 5-4.

Table 5-4. Summary of 13-Coupler Stripline Test Fixture Performance

Element	Measured Ins. Loss (dB)	Theoretical Ins. Loss (dB)	Variance (dB)
13	8.0	8.5	-0.5
12	8.5	8.7	-0.2
11	9.1	9.2	-0.1
10	9.9	9.9	0
9	11.1	10.7	+0.4
8	12.3	11.8	+0.5

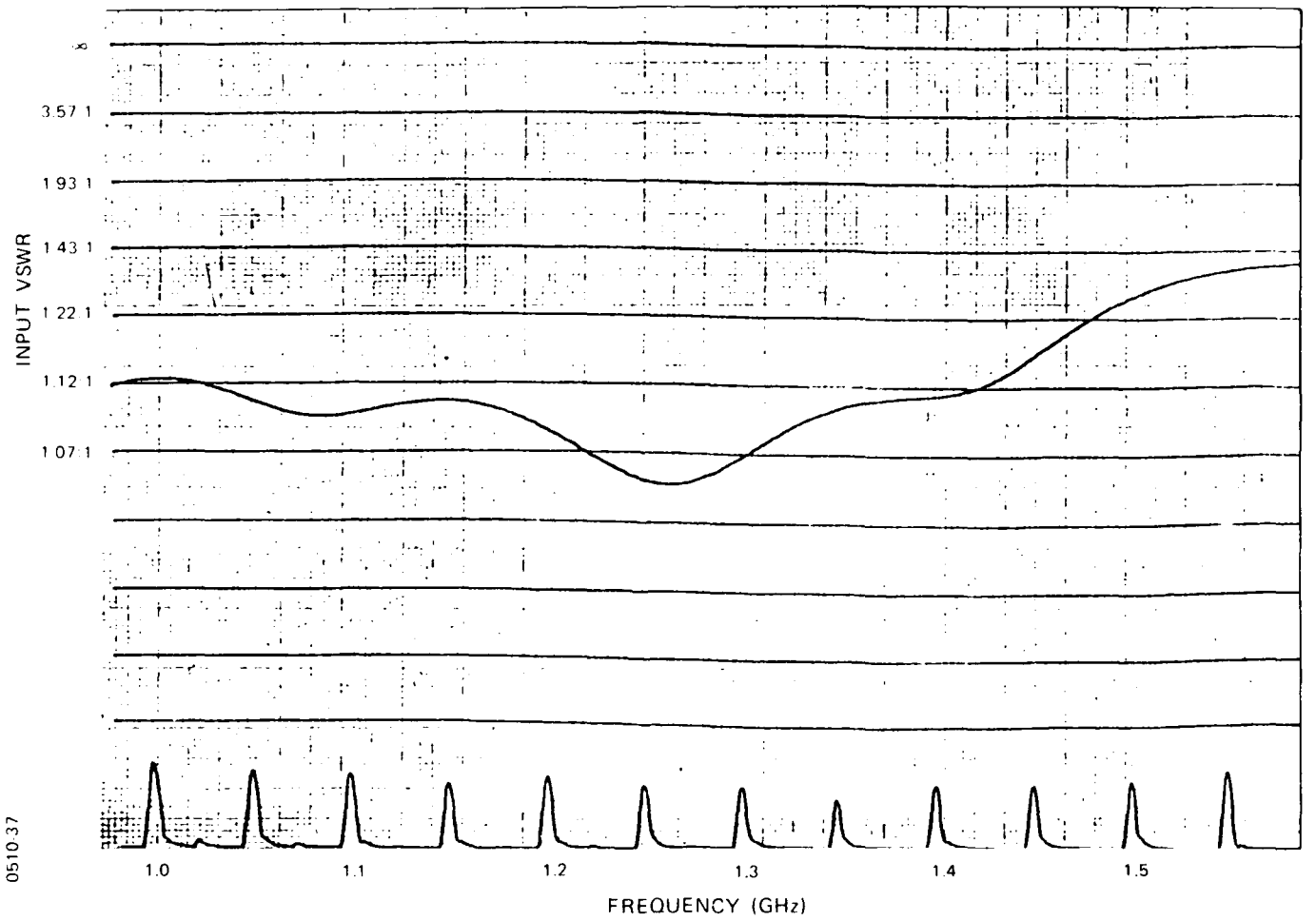

Figure 5-16. Measured swept-frequency VSWR of five-coupler stripline test fixture

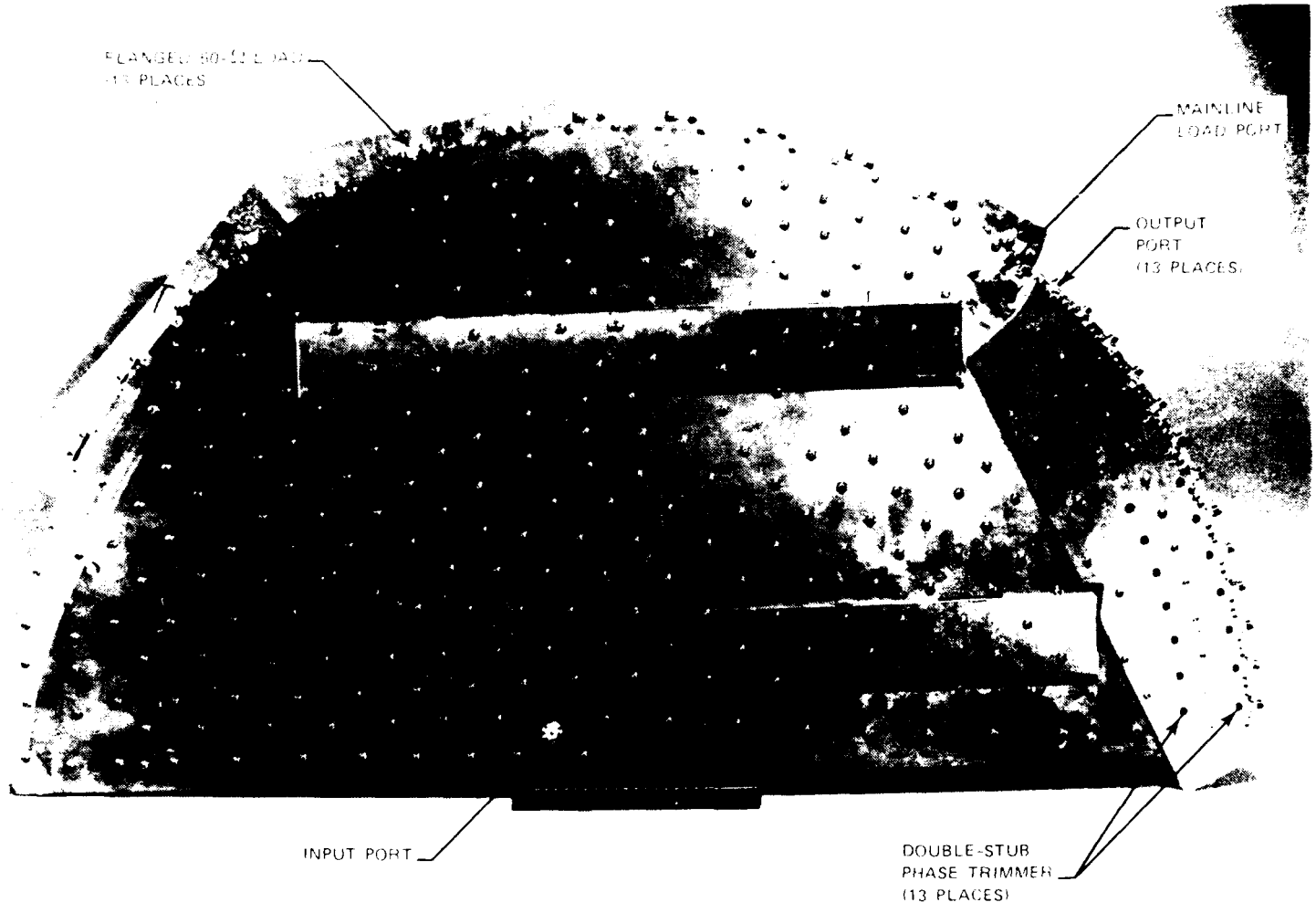

Figure 5-17. Thirteen-coupler stripline test fixture

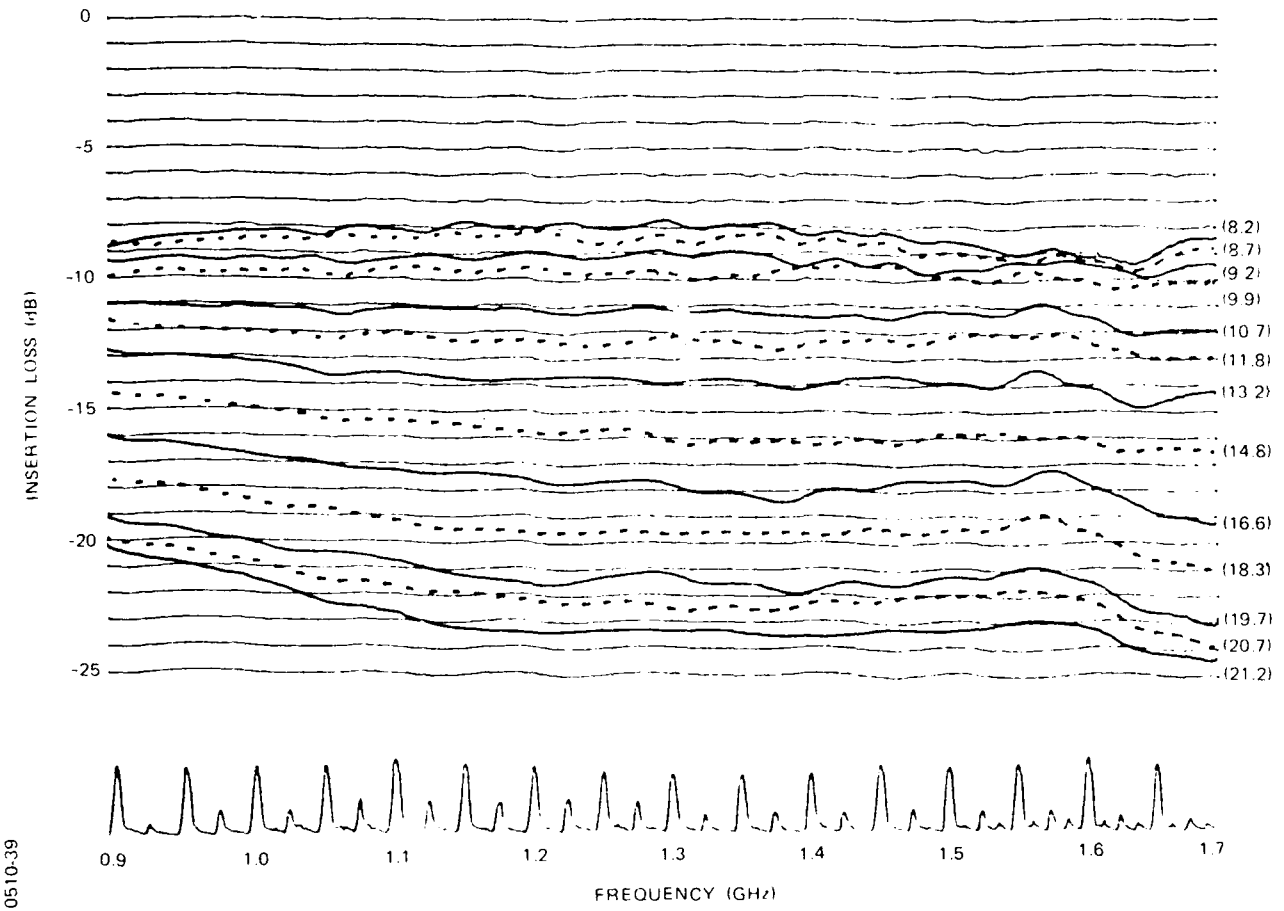

Figure 5-18. Measured insertion loss vs frequency of 13-coupler test fixture

(Table 5-4 Continued)

Element	Measured Ins. Loss (dB)	Theoretical Ins. Loss (dB)	Variance (dB)
7	13.8	13.2	+0.6
6	16.1	14.8	+1.3
5	18.0	16.6	+1.4
4	19.7	18.3	+1.4
3	21.4	19.7	+1.7
2	22.5	20.7	+1.8
1	23.3	21.2	+2.1

It might appear at first glance that the measured amplitude distribution deviates extensively enough from the desired values so as to produce unacceptable azimuth patterns. The actual effects however, are those of a more highly tapered aperture illumination: a decrease in aperture efficiency of about 0.1 dB, and a reduction in sidelobe levels of about 1.0 dB. The explanation is that the variances are not due to random amplitude errors, but rather represent a uniform coupling error of about 0.5 dB in each of the 13 couplers. This is illustrated in the graphs of Figure 5-19. The central curve marked "design" gives the coupled level, relative to the input, for each element of the -29 dB, $\bar{N} = 4$ Taylor distribution. Similarly, the outer curves give the amplitude distributions that occur when every coupler is either 0.5 dB too tight or 0.5 dB too weak. The effect in a series feed is cumulative, so that the variance at the end element can be much greater than the error of the individual couplers. The measured points in Figure 5-19 are seen to fit very nearly the curve marked "design +½ dB".

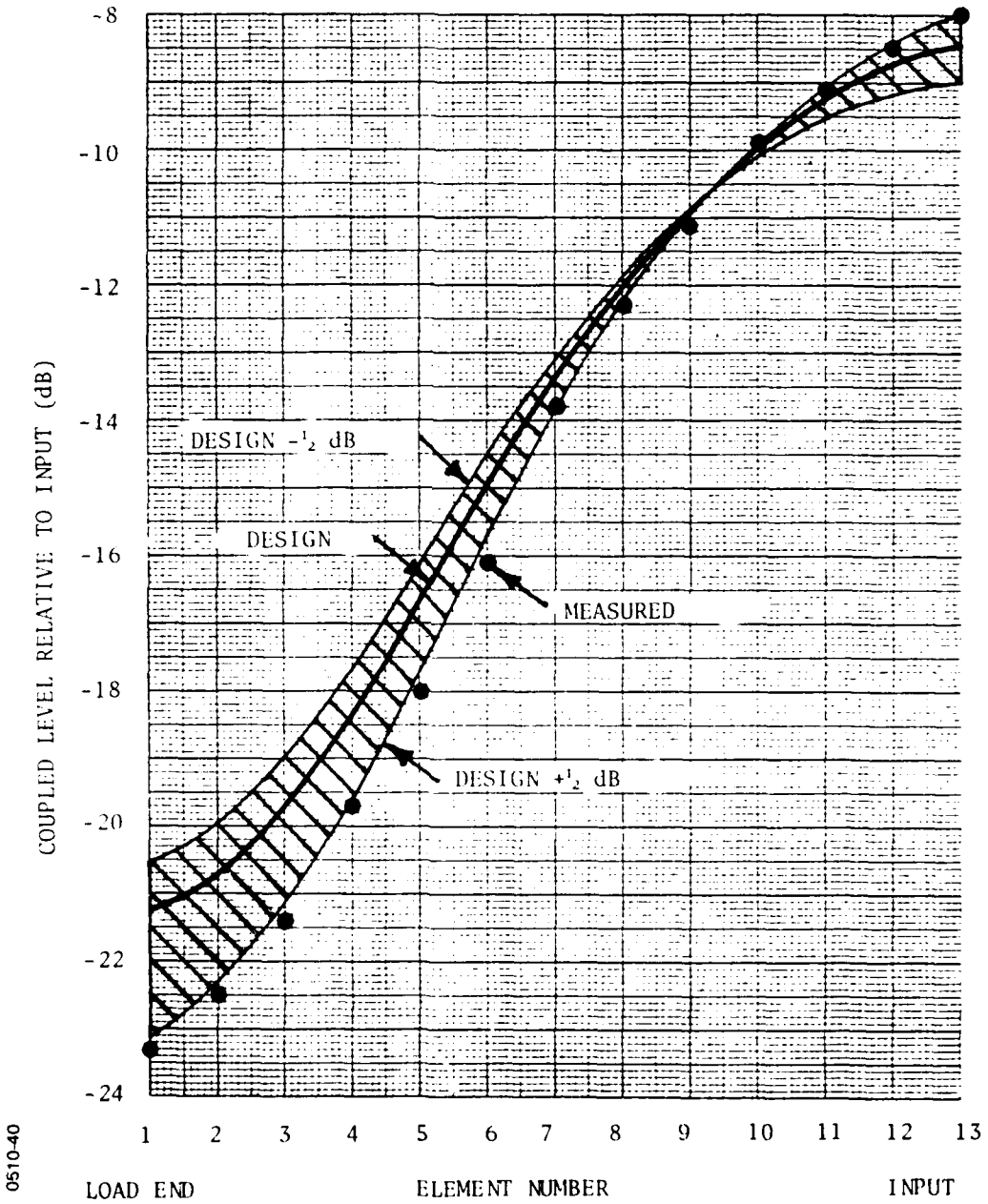

Figure 5-19. Effect of uniform coupling on 13-element series feed

A uniform coupling error of 0.5 dB could be produced by a multitude of factors, some of which are listed in Table 5-5.

Table 5-5. Causes of Overlap Coupler Errors

Cause of Error	Nominal Value	Tolerance	Coupling Error (dB)
ε_r	2.50	$\pm$0.05	$\mp$0.03
Overlap	Varies	$\pm$0.001"	$\pm$0.20
Z_o (Linewidth)	0.190"	$\pm$0.001"	$\mp$0.05
Centerboard Thickness	0.020"	$\pm$0.001"	$\mp$0.17

After carefully measuring ε_r, Z_o and centerboard thickness, these parameters were eliminated as probable causes of the 0.5 dB coupling error. The effect, however, can be explained by a 0.002 or 0.003 inch shift in alignment of the top and bottom photomasks, producing excessive overlap of the quarter-wave coupling sections. Although the two photomasks are pinned to be accurately aligned while lying flat, the upper negative gets displaced slightly when the centerboard is inserted for the exposure. By the time this problem had been identified, the centerboards for the experimental model had already been etched. As the effect of the 0.5 dB over-coupling is not detrimental, it was decided to use these boards without further correction.

The input VSWR of the 13-coupler stripline test fixture is shown in Figure 5-20.

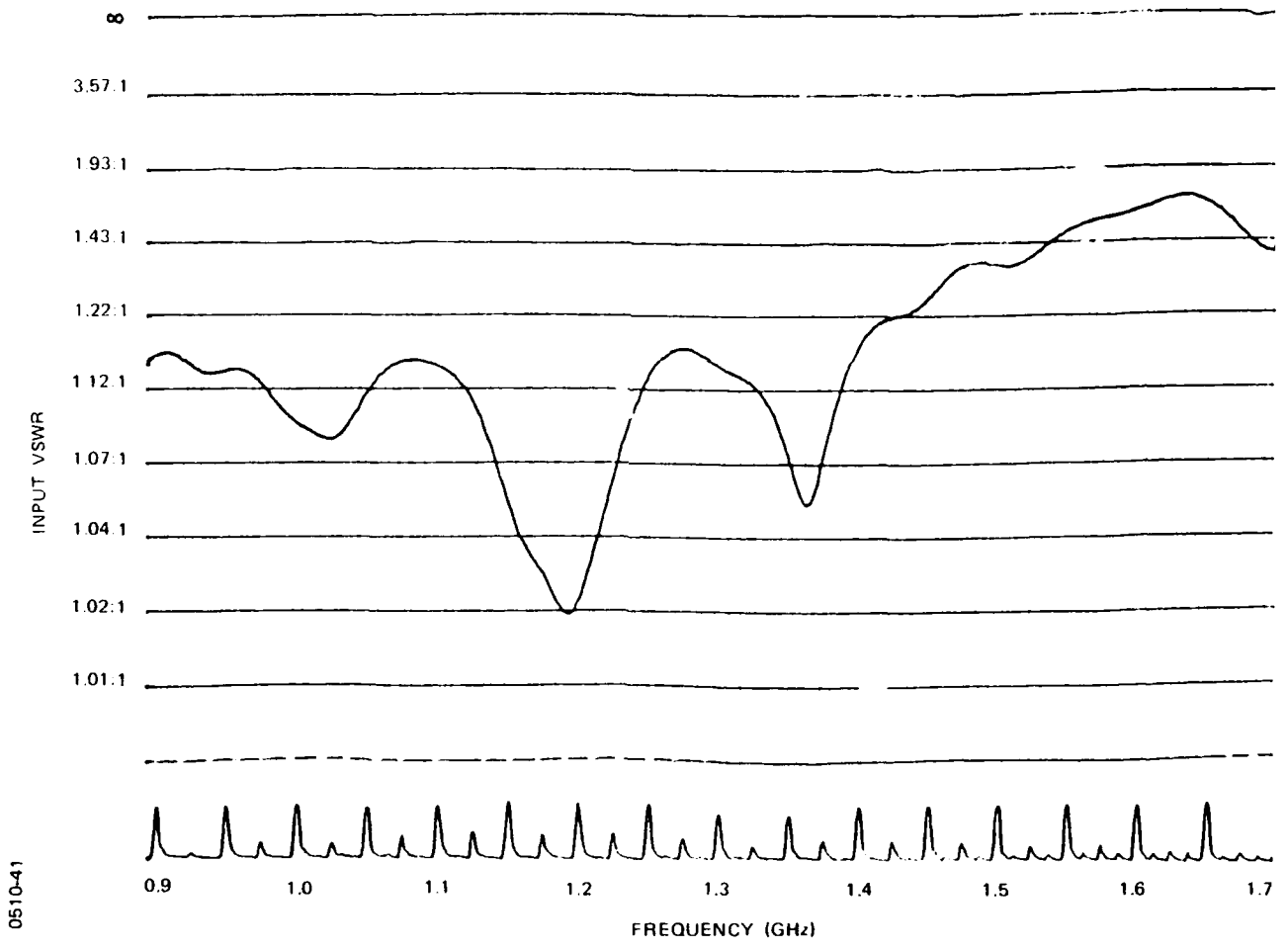

Figure 5-20. Measured swept-frequency VSWR of 13-coupler stripline test fixture

5.4 Loop Couplers

5.4.1 Loop-Coupler Test Fixture

The design of the rotor and stator loops was optimized with the use of several test fixtures, the first of which is shown in Figure 5-21. Five rotor loops of different widths from 0.2 to 0.4 inch can be seen. This test fixture is constructed such that the ground-plane spacing of the rotor loops, as well as the separation between rotor and stator loops, can be varied. For simplicity, the RF shorts between the rotating and fixed sections were made using adjustable spring contacts rather than non-contacting RF chokes. The measured swept-frequency insertion loss for the 0.25-inch wide rotor loop, positioned directly over a stator loop, is shown in Figure 5-22. The two deep resonances at 1.05 and 1.60 GHz are due to the RF shorting arrangement used in this test fixture. Note that insertion loss of less than 0.2 dB can be achieved over a 200 MHz band.

5.4.2 RF Chokes

A second loop-coupler test fixture that includes upper and lower RF chokes was built. A cross section of this test fixture, seen in Figure 5-23, shows how the folded choke sections are implemented. Figure 5-24 shows a close-up view of the baseplate with stator loops and lower RF choke.

The measured swept-frequency insertion loss of the second loop-coupler test fixture is shown in Figure 5-25. Note that the deep resonances that existed with the first test fixture are gone, and the insertion loss is only 0.3 dB from about 1.15 to 1.45 GHz.

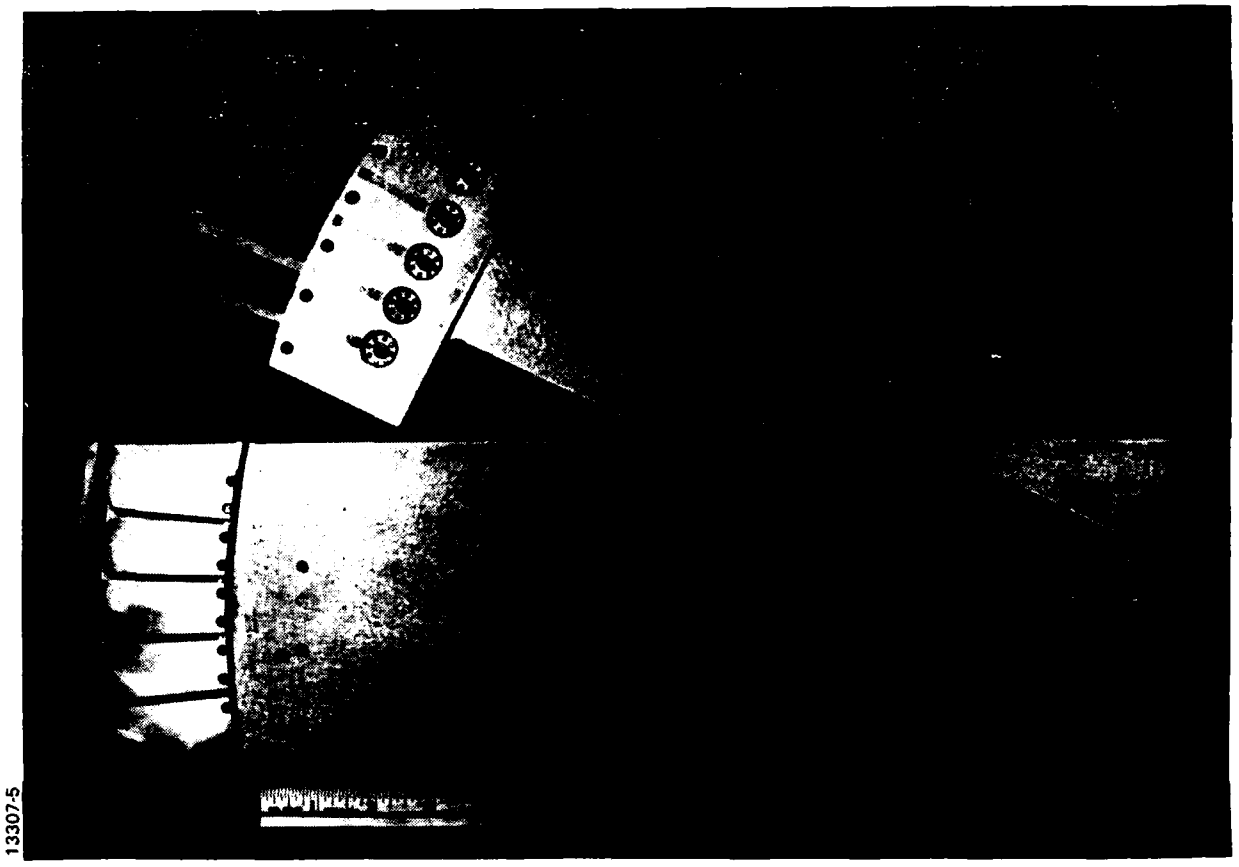

Figure 5-21. First loop-coupler test fixture

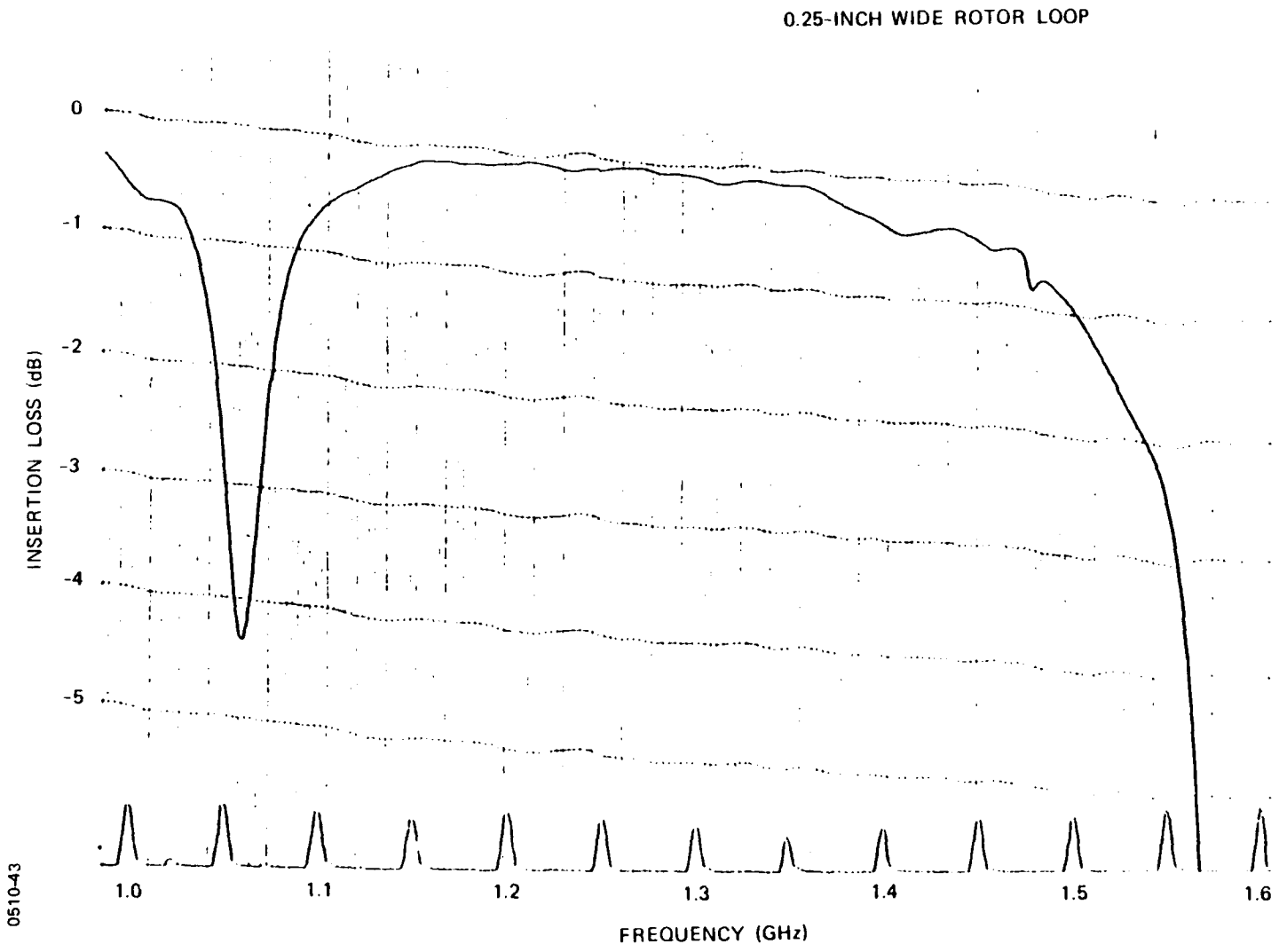

Figure 5-22. Swept-frequency insertion loss of first loop-coupler test fixture

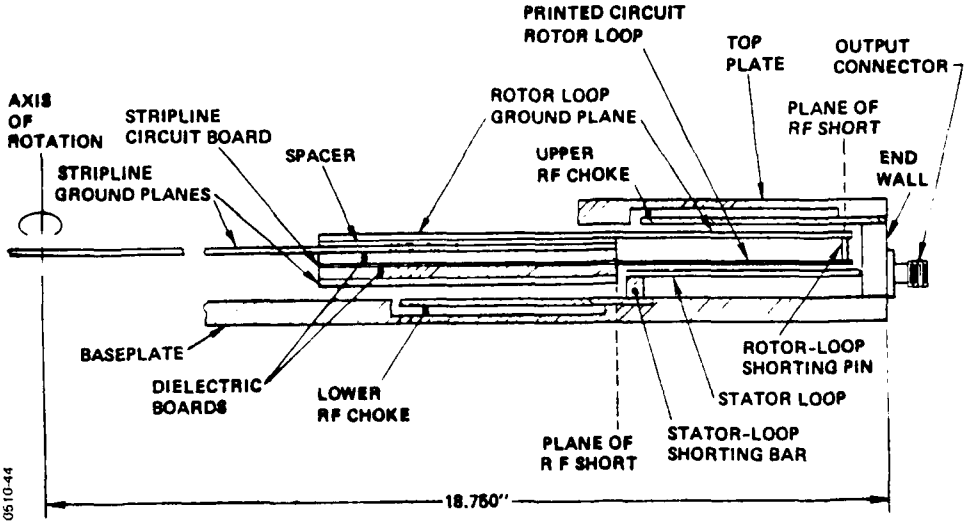

Figure 5-23. Cross section of loop-coupler test section

Figure 5-24. Baseplate with stator loops and lower RF choke

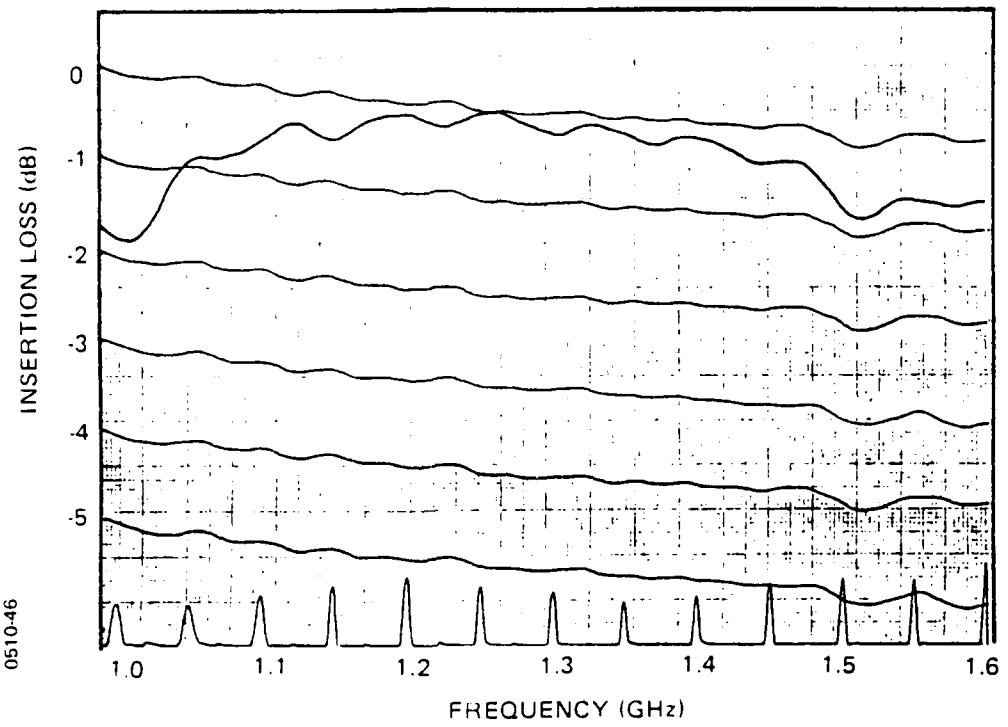

Figure 5-25. Measured insertion loss vs frequency of second loop-coupler test fixture

Coupling performance varies somewhat as the rotor loops transverse the stator loops. The magnitude and interval of these variations can be minimized by using narrow rotor loops and much wider stator loops. The result is relatively flat coupling over most of the cycle, with a gradual decrease as the rotor loop approaches the stator-loop edge. When centered directly over the gap, equal coupling to the two adjacent stator loops occurs; this effect is seen in Figure 5-26, which was measured at 1.3 GHz for a 0.25-inch wide rotor loop.

The coupling situation in the commutating feed assembly is different from the simplified picture described above. Instead of a single rotor loop coupling to only one or two stator loops, there are 26 rotor loops that couple to 26 or 27 stator loops at any given time. Furthermore, the amplitude and phase excitation of the 26 rotor loops is symmetrically tapered. Thus, the voltage that appears at a particular stator loop is the vector sum of all significant contributions from nearby rotor loops. Measured results of this effect are given in Section 6.4.5.

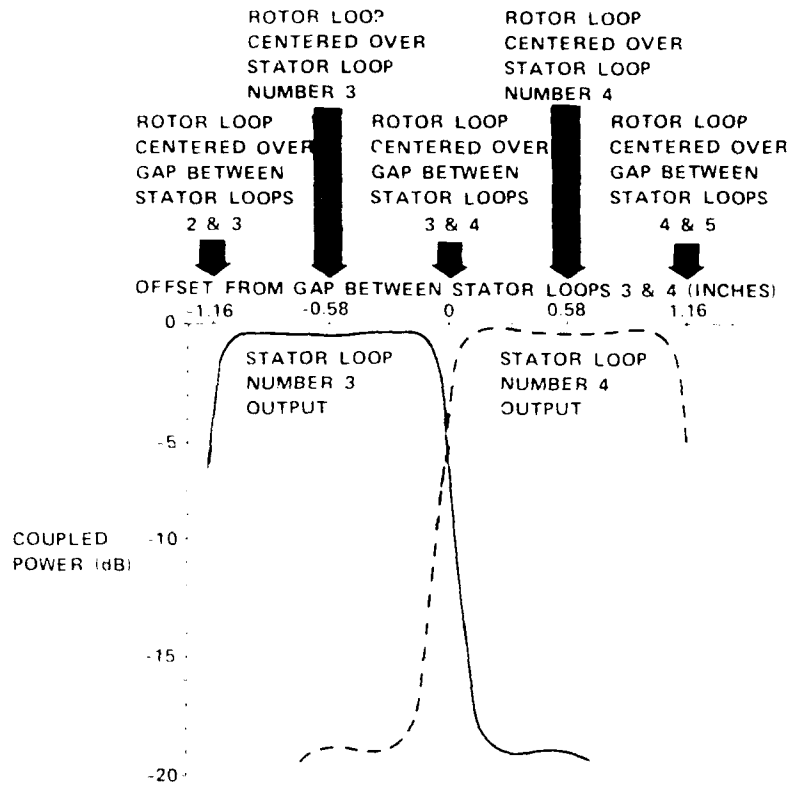

Figure 5-26. Measured loop-coupler power vs offset

AD-A094 470 ITT GILFILLAN VAN NUYS CA F/G 17/9
COMMUTATING FEED ASSEMBLY.(U)
JUN 80 R I WOLFSON F19628-79-C-0034
UNCLASSIFIED RADC-TR-80-180 NL

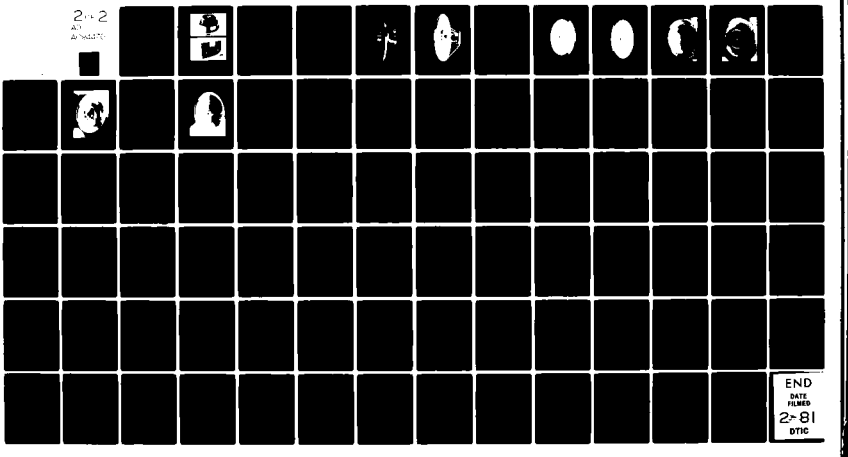

SECTION 6

EXPERIMENTAL MODEL

6.1 Description of Operation

The rotator pedestal assembly and control unit, shown in Figure 6-1, are interconnected through a 10-foot shielded cable. These units are designed to operate in a laboratory environment from a 115 VAC, 60 Hz power source. A regulated power supply which is contained within the control unit provides +24 volts at five amperes required by the servo power amplifier and dc torque motor.

Line power to the control unit is provided through the ON/OFF switch on the front panel. The slotted-shaft potentiometer, labeled AZ RATE, changes the rotational speed of the pedestal from zero to about 40 rpm when turned clockwise. This control has been adjusted and locked at 15 rpm.

The zero index pulse, which appears at connector J3, indicates that instant of each cycle when a particular angular relationship exists between the rotating and stationary parts of the commutator. This angle can be fixed by loosening the set screws in the flexible shaft coupler just above the pedestal, manually rotating the pedestal platform to the desired position, and retightening the set screws. See Figure 6-2.

CAUTION: do not attempt to rotate the stripline assembly unless the set screws that lock the cylindrical bracket to the drive shaft are

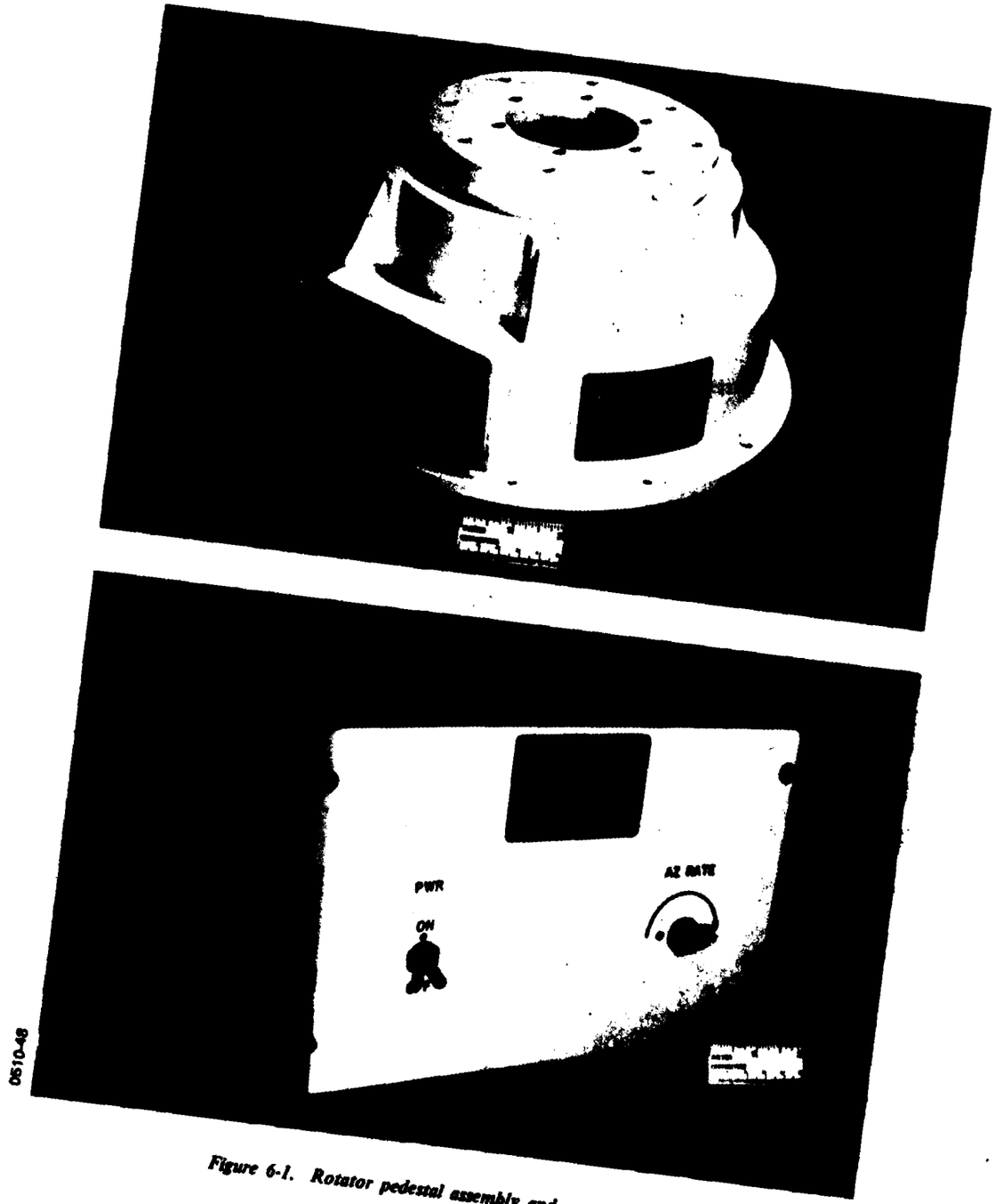

Figure 6-1. Rotator pedestal assembly and control unit

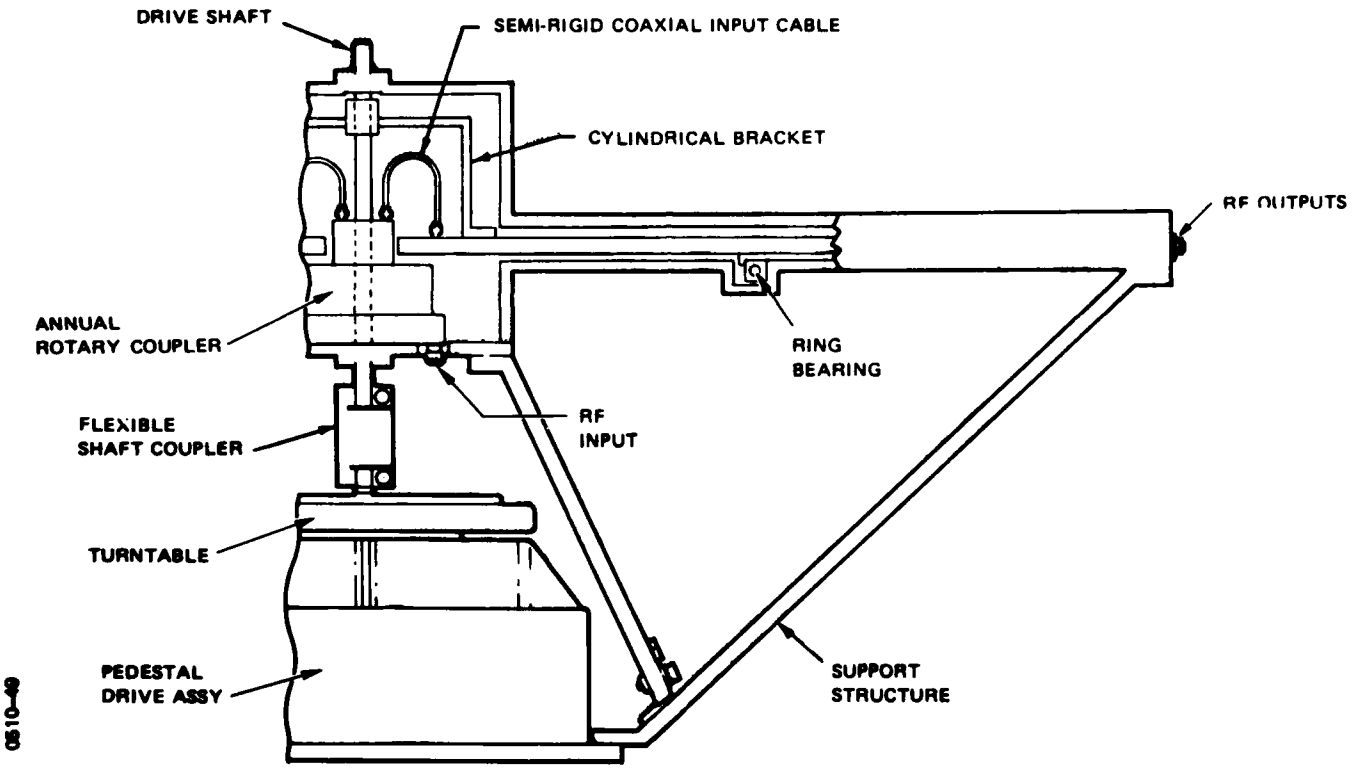

Figure 6-2. Cross section of commutating feed assembly

securely fastened. Otherwise, torque will be transmitted to the rotating stripline assembly wholly through the pair of semi-rigid coaxial input cables, which can easily be damaged by twisting.

6.2 Fabrication and Assembly

The experimental commutator model, shown in Figures 6-3 and 6-4, was fabricated in the ITT-Gilfillan Engineering Model Shop, and assembled and tested in the Antenna and Microwave Department Laboratory. A layout drawing is included at the end of this report.

6.2.1 Stripline Assembly

The circuit layout of the stripline feed network is shown in Figure 6-5. The halves of the circuit are identical mirror images of one another, and are driven by equal-amplitude, in-phase signals derived from the twin outputs of the annular rotary coupler. The small and large diameters of the circuit board are approximately 31.9 and 36.8 inches, whereas the Teflon-fiberglass material used is available in sheets no larger than 17.5 by 37.5 inches. Thus, it was necessary to make the circuit in two pieces, as shown in Figures 6-6 and 6-7. This presents no problems, however, as the circuit halves are electrically independent, with no direct interconnection across the line of separation.

The rotating stripline feed assembly is shown in Figures 6-8 and 6-9. The 90-degree annular sector on the right, which

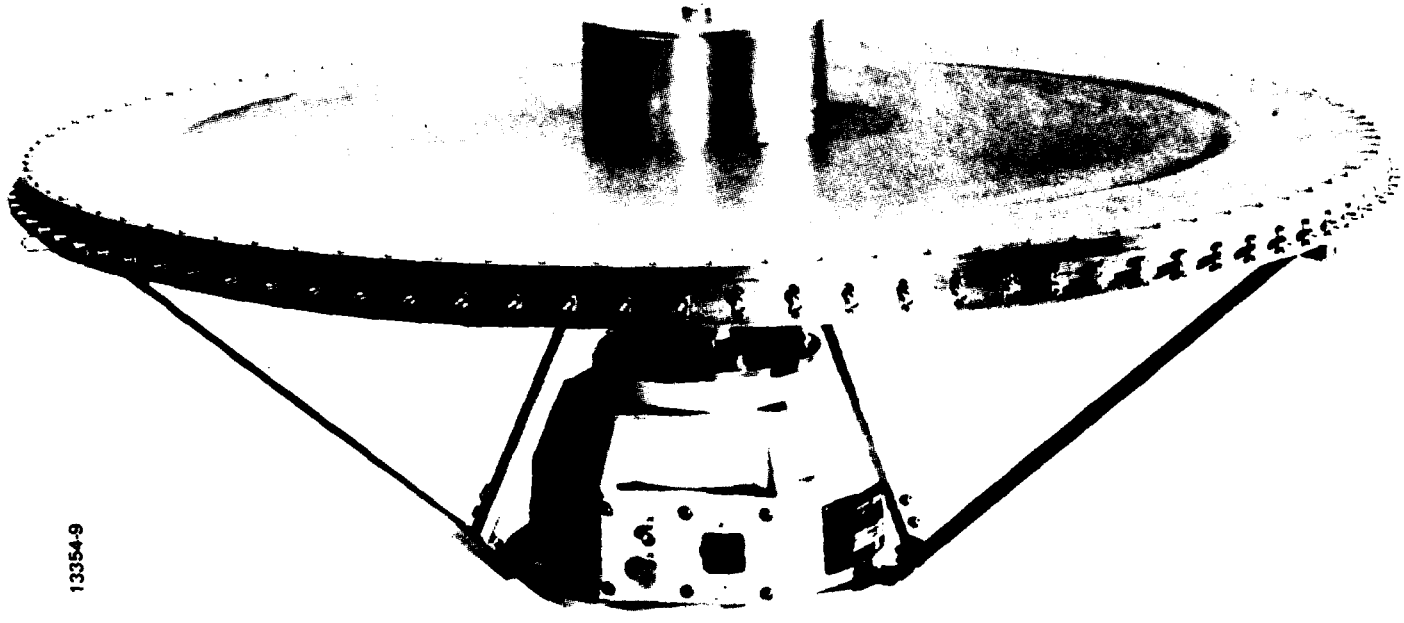

13354-9

Figure 6-3. Experimental commutator model, topside

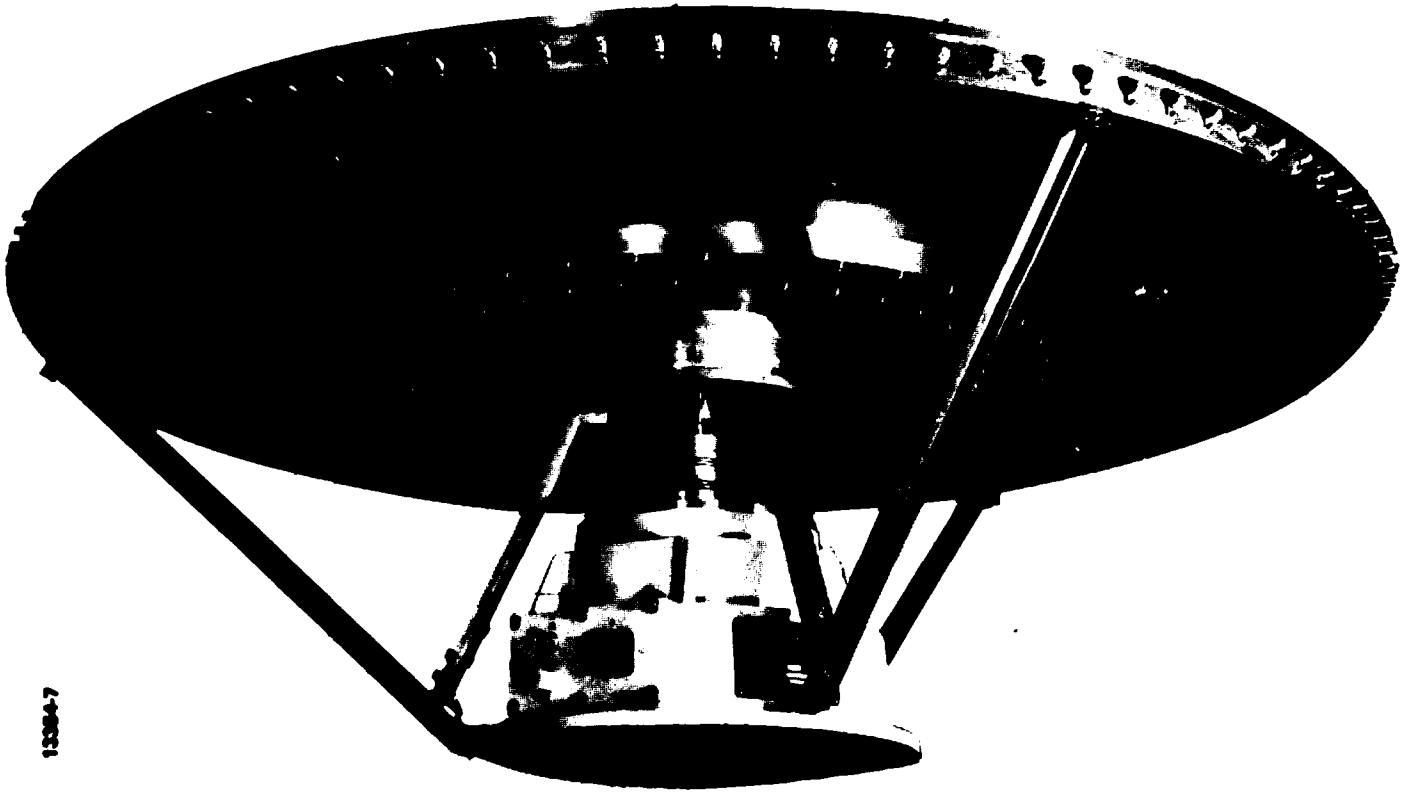

13364-7

Figure 6-4. Experimental commutator model, underside

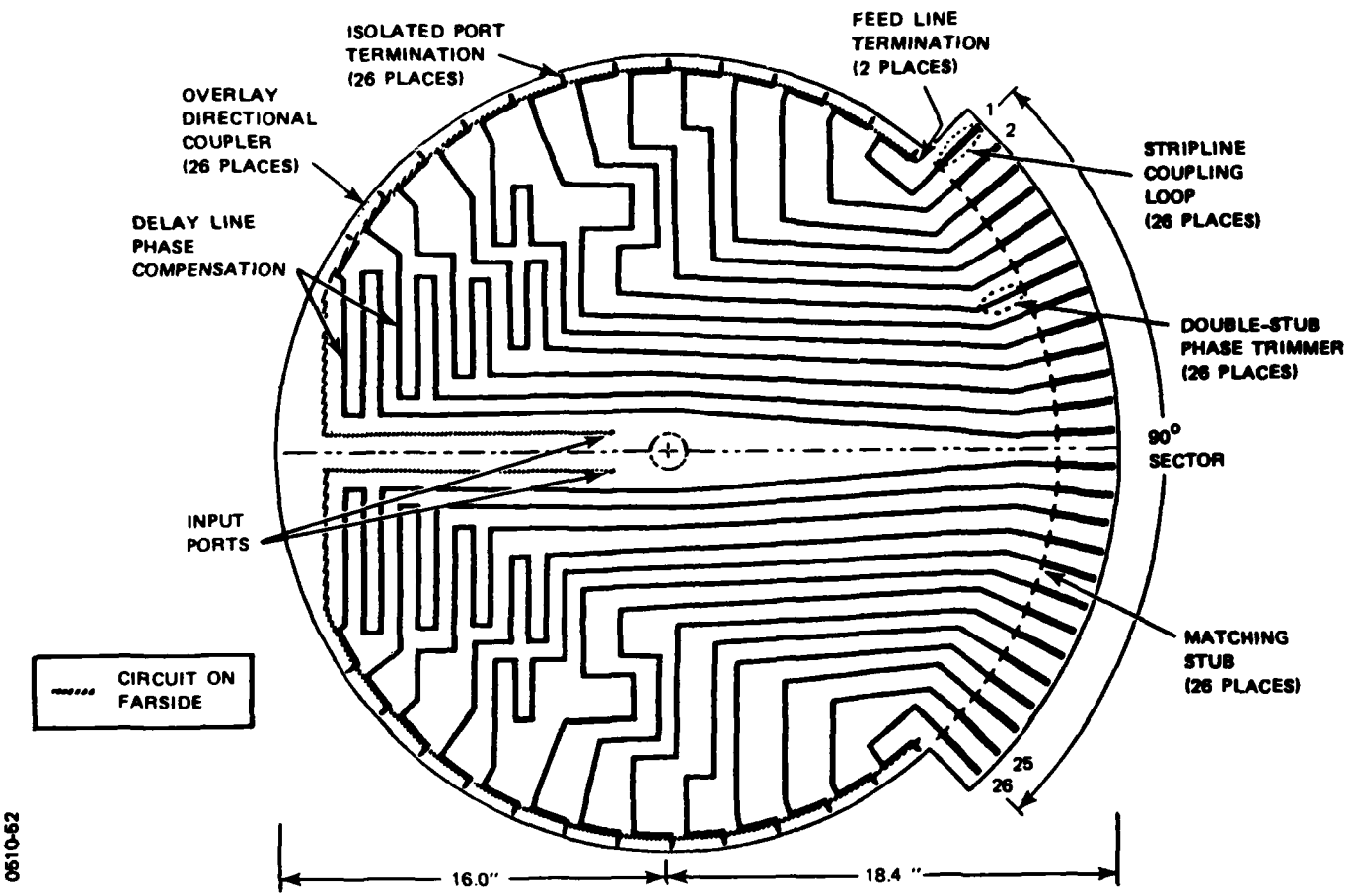

Figure 6-5. Layout of stripline feed network

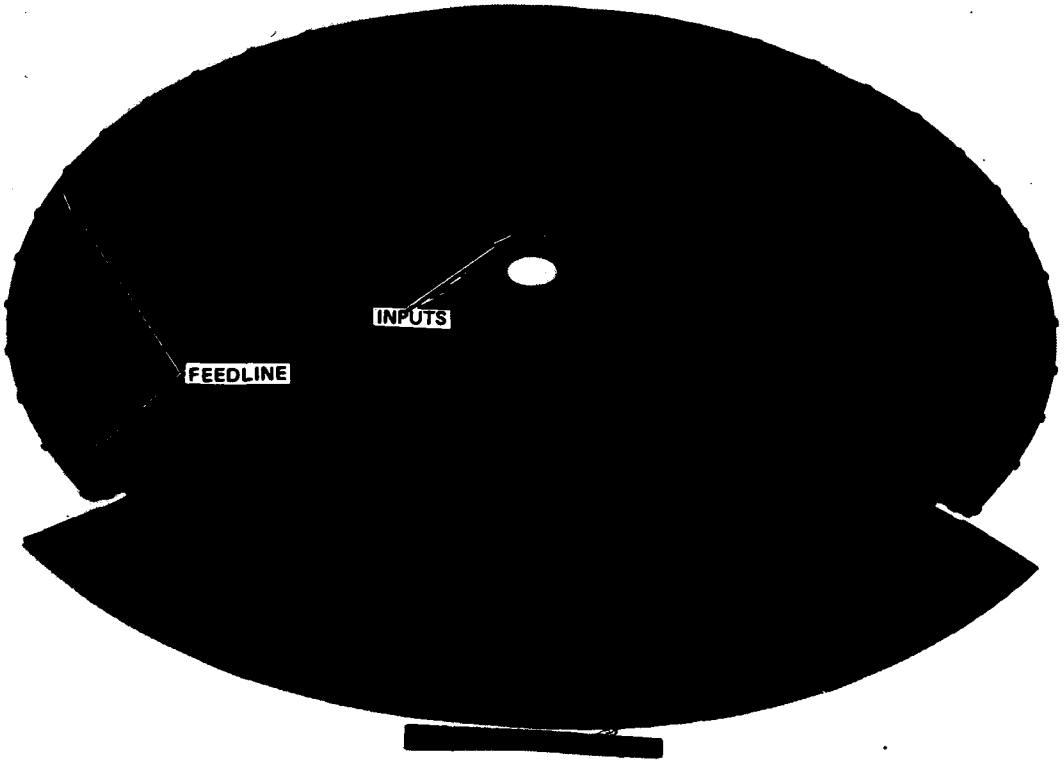

Figure 6-6. Stripline feed network circuit board, input side

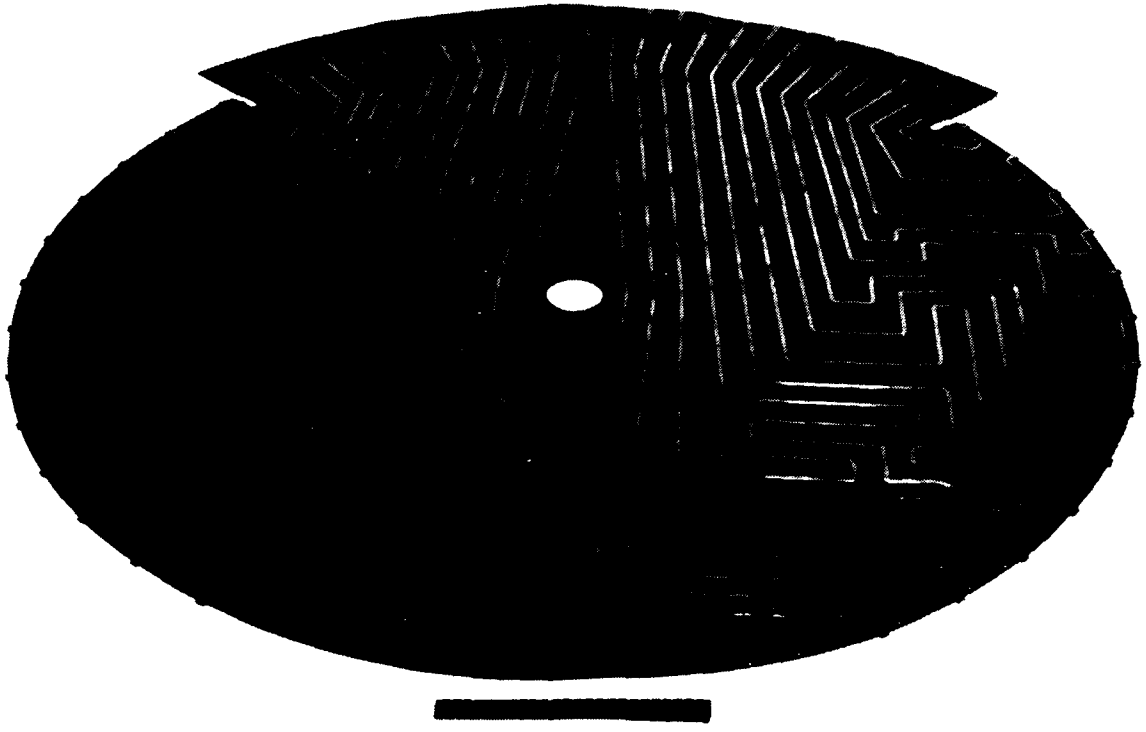

13354-5

Figure 6-7. Stripline feed network circuit board, coupled side

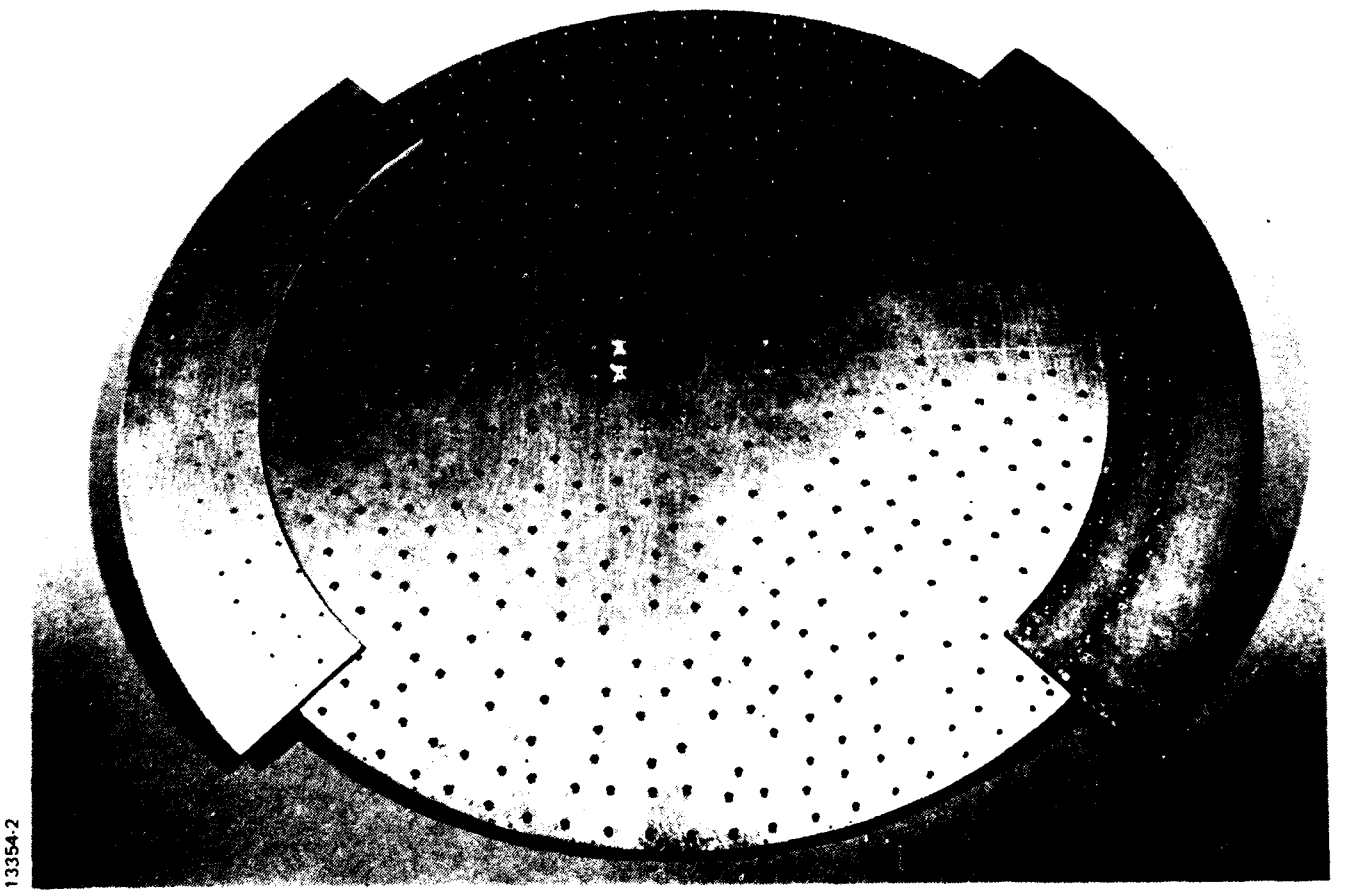

Figure 6-8. Rotating feed assembly, top side

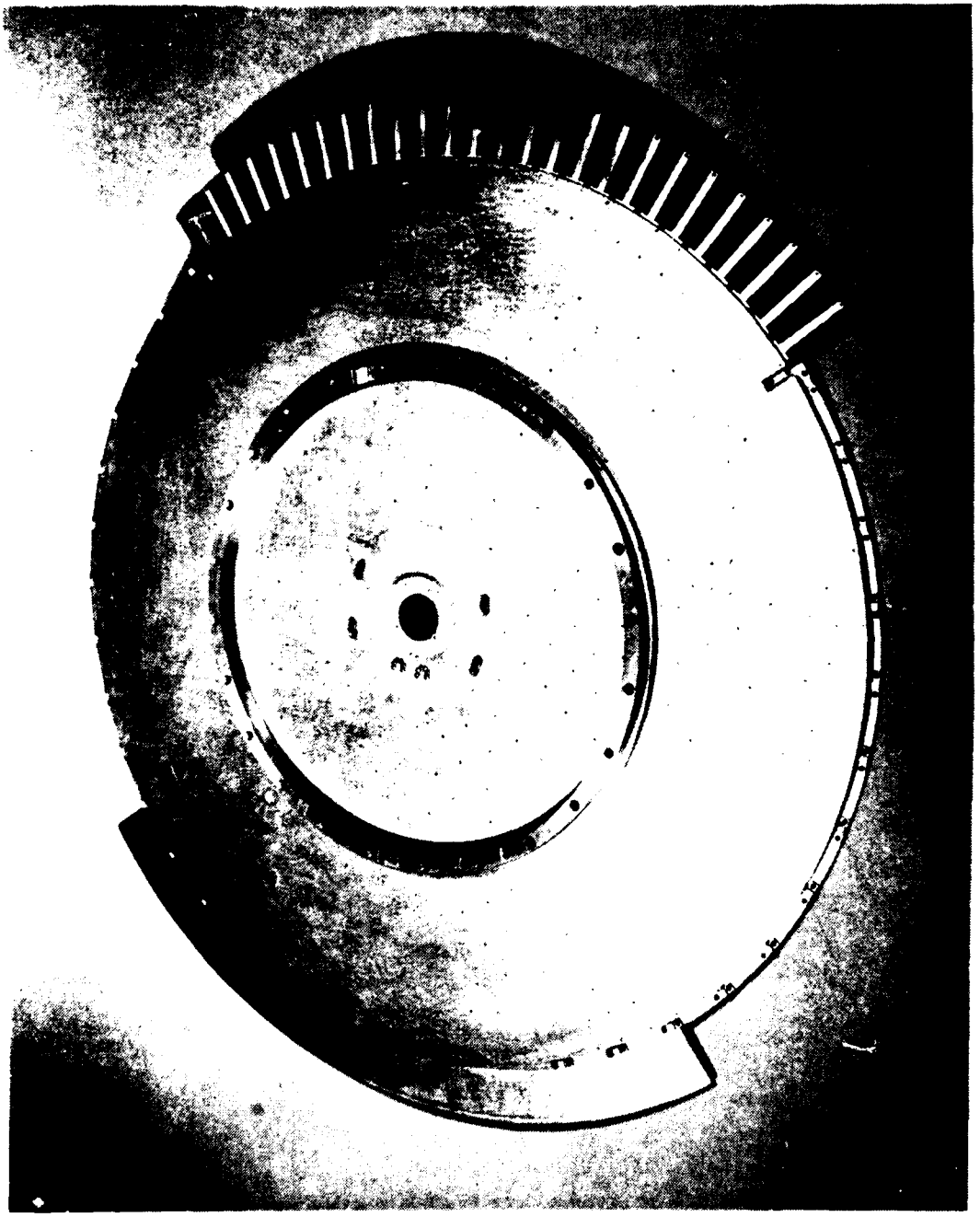

13354-1

Figure 6-9. Rotating feed assembly, under side

is riveted to the upper ground plane, serves as an extended ground plane for the rotor coupling loops, and contains 26 pairs of phase-trimmer screws. The other annular sector provides dynamic balance to avoid excessive vibration as the assembly rotates.

The five-layer stripline assembly, consisting of upper and lower ground planes, two dielectric sheets, and the etched circuit board are fastened together by several hundred #2-56 screws. These screws are threaded flush into tapped holes in the lower ground plane, providing maximum clearance between it and the housing.

Figure 6-9 also shows the rotating assembly support ring that rests on an 18-inch diameter bearing, the 50-ohm stripline load terminations, and the printed-circuit rotor loops. Each rotor loop is short-circuited at the end by means of a #2-56 flathead screw threaded into the extended ground plane through a 0.250-inch spacer. It is essential that all rotor loops lie flat within the plane of rotation, as coupling value and VSWR are extremely sensitive to spacing between rotor and stator loops. To achieve the desired flatness, it was necessary to bond a sheet of low-density foam between the rotor-loop circuit board and extended ground plane.

6.2.2 Stationary Housing

The lower housing, which contains the large bearing, the lower annular RF choke, and 100 stator loop couplers, is shown in

Figure 6-10. During assembly and subsequent preliminary electrical test, excessive variation in the coupling gap dimension was observed as the stripline feed assembly rotated. This produces modulation of the coupled power as large as 6 dB. The mechanical sources of error were found to include the following:

a) warpage of the lower housing due to stress relief during machining;

b) misalignment in seating the main bearing;

c) non-parallel surfaces on stripline feed assembly mounting ring;

d) non-parallel surfaces on the lower RF choke ring, upon which the 100 stator loops are seated;

e) the height at which each stator loop is soldered to the output connector center pins;

f) variations in thickness and flatness of the seven layers that comprise the stripline feed assembly: printed circuit board, two dielectric boards, two ground planes, metal shim, and rotor-loop ground plane;

g) the length of each rotor-loop shorting pin.

A combination of remachining, grinding, shimming, reshaping and reassembly was used to reduce the coupling-gap variations from nearly $\pm$0.050 inch to only $\pm$0.003 inch. The variations in coupled power were thus reduced to the tolerable limits of 0.28 dB rms.

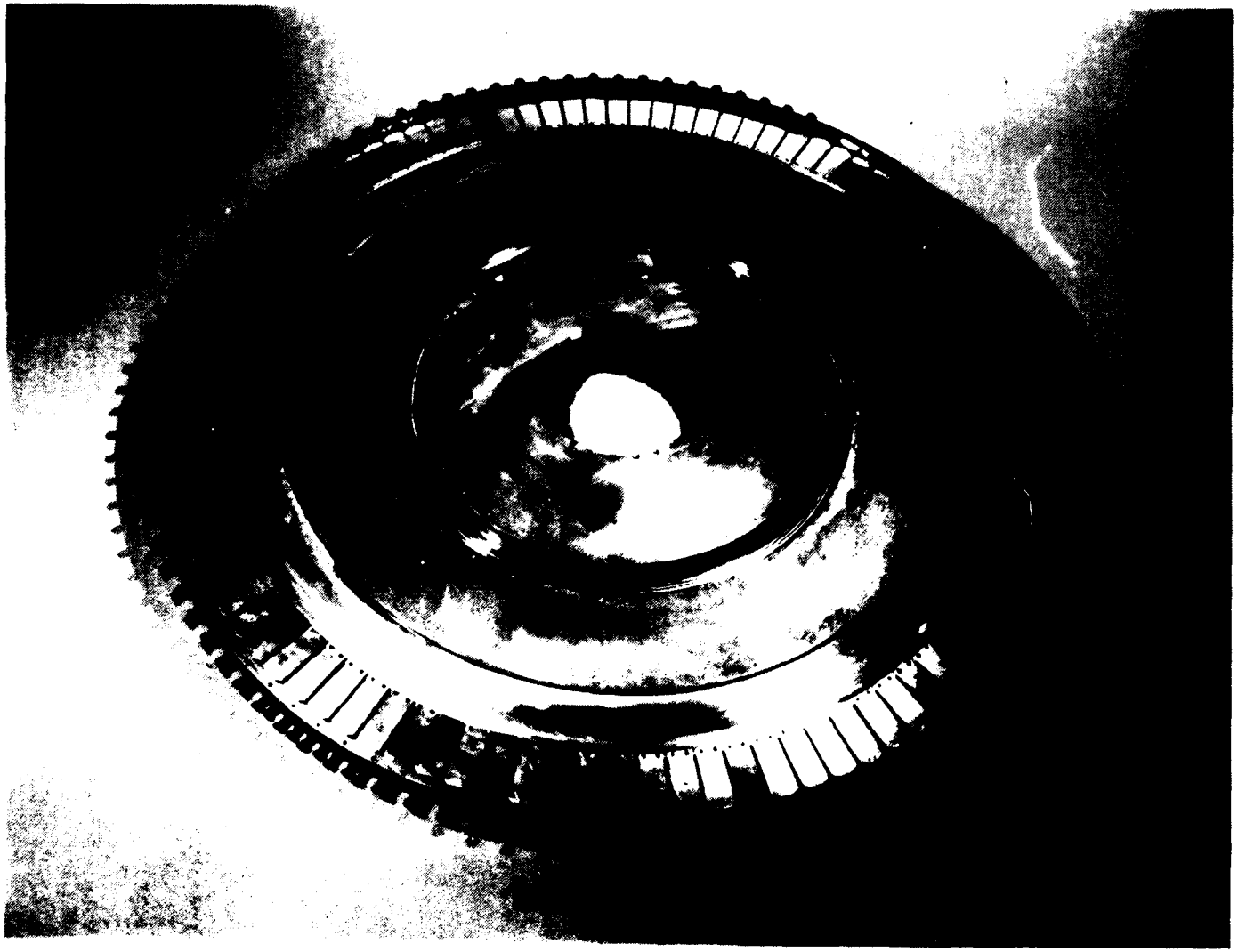

Figure 6-10. Lower housing assembly

The lower housing, with rotating stripline assembly in place, is seen in Figure 6-11.

6.2.3 Support Structure

The support structure, shown in Figure 6-2 and consisting of three short and three long braces, was adjusted and tightened so that the commutator housing is held securely to and level with the pedestal. Any slight misalignment in the turntable and drive shaft is taken up in the flexible shaft coupler.

6.3 Mechanical Test Results

Mechanical test results of the completed experimental commutator model are given in this section.

6.3.1 Dimensions and Weight

Overall Diameter:	38.63 inches (0.981m)
Overall Height:	15.63 inches (0.397m)
Weight (Less Control Unit):	146 lbs (66.2 kg)
Weight, Control Unit:	12 lbs (5.4 kg)

6.3.2 Torque Requirements

@ 15 rpm:	15 inch-lbs (0.17 kg-m)

6.3.3 Rotational Speed

Range of Adjustment:	0 to 40 rpm

6.4 Electrical Test Results

During assembly of the experimental commutator model, electrical measurements were taken at various stages to insure that the unit was

Figure 6-11. Lower housing with rotating stripline assembly in place

functioning properly. Particular attention was given to unresolved moding problems that had been observed earlier in the breadboard test fixtures. The annular RF choke design, which produces an RF short to the desired radial TEM mode, has little effect on the unwanted circumferential mode. Variations in coupled amplitude as great as ±3dB, due to energy coupled to non-adjacent stator loops by means of the circumferential mode, were observed.

As the circumferential mode is orthogonal to the desired radial TEM mode, it should be relatively simple to suppress without drastically affecting the latter. However, as time was running out on the project, it was decided to determine the essential performance potential of the commutator. RF shorts between the rotating and fixed sections were made using adjustable spring contacts, rather than relying on the non-contacting RF chokes.

6.4.1 Drive Power

Drive power requirements for the dc torque motor and power servo amplifier were measured at a constant rotational rate of 15 rpm.

Voltage	+24.2V
Current	2.5 A
Power	60.5W

As noted in Section 5-1, much of this drive power is dissipated in the power servo amplifier, and could be reduced to about 12 watts with optimum selection of the motor winding.

6.4.2 Insertion Loss

Insertion loss of the commutator is determined by measuring amplitude and phase at 26 output ports within a 90^{o} excited sector, and computing the far-field vector sum. The results are given in Table 6-1.

TABLE 6-1 INSERTION LOSS OF EXPERIMENTAL COMMUTATOR MODEL

Frequency (GHz)	Insertion Loss (dB)
1.2	1.58
1.3	1.41
1.4	1.84

In Section 5.2 it was noted that the annular rotary coupler had not been optimized over the band for minimum insertion loss. It can be seen in Figure 5-3 that at the upper band edge, insertion loss increases about 0.2 dB. This higher loss is observed in the data above.

6.4.3 Input and Output VSWR

The input VSWR of the experimental commutator model, measured at the input to the annular rotary coupler, is shown in Figure 6-12. Typically, the input VSWR is less than 1.15:1 over 25 percent of the band, less than 1.5:1 over 65 percent of the band, and less than 1.8:1 overall. Although the annular rotary coupler, the stripline feed network, the loop-coupling region, and the stator loops had been carefully matched in the various breadboard test fixtures, no

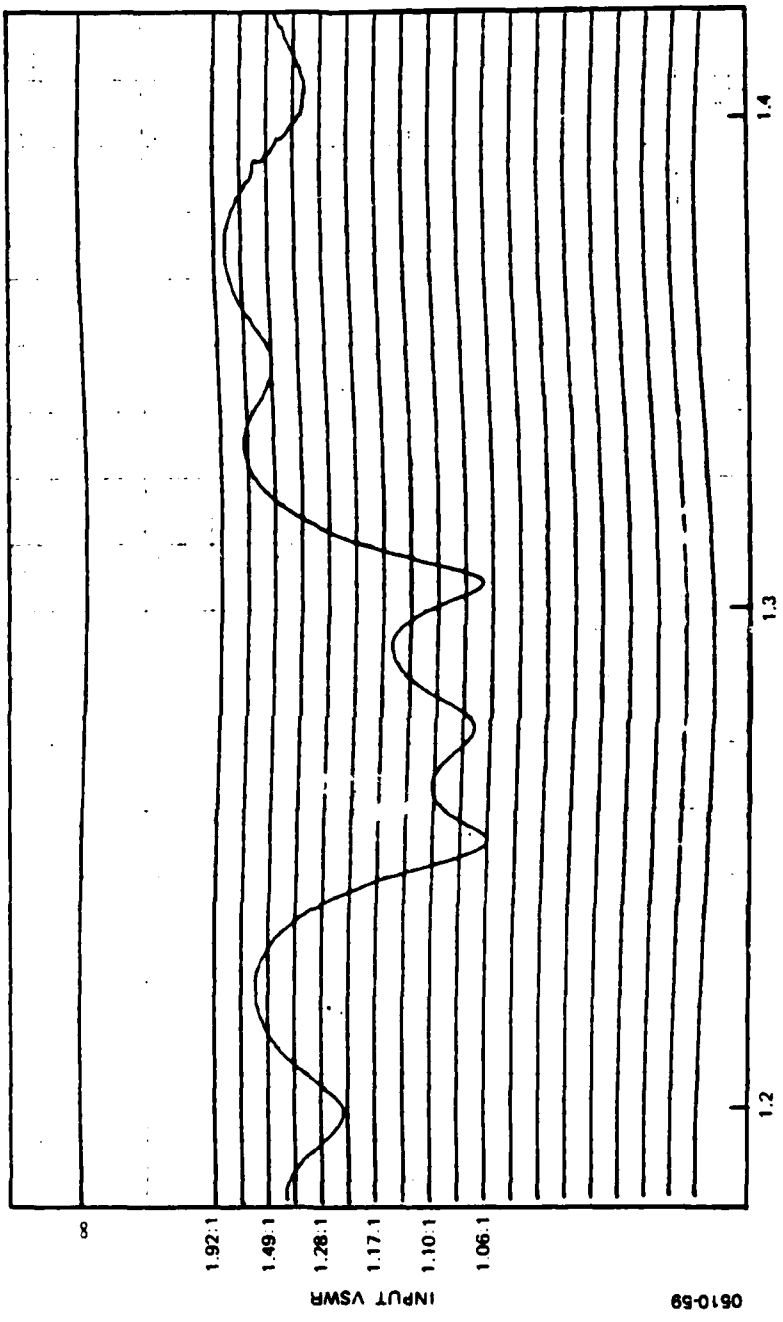

Figure 6-12. Input VSWR of experimental commutator model

attempts were made to improve the overall input VSWR of the completed model.

The VSWR's of 26 output ports, excited by the stripline feed network, are shown in Figures 6-13 through 6-18 for the case where the rotor loops are located directly over the stator loops. Note that on elements number 24 through 26, the match is poor. The assembly was rotated to several other angular positions to eliminate the possibility that the mismatch might be associated with a particular set of stator loops or output connectors. The load termination and rotor-loop ground were examined for elements 24 through 26, but no defect was found. The stripline package was not taken apart, as it is difficult to visualize anything within that could cause the observed problem, and the degradation to performance is not serious enough to justify that effort.

6.4.4 Amplitude and Phase Distribution

The coupled amplitude and phase excitation of the 26-element feed was measured with the rotor loops located directly over the stator loops. The swept-frequency amplitude is shown in Figures 6-19 and 6-20. Note once again that elements 24 through 26 do not appear to be functioning properly.

Coupled amplitude, measured at 1.2, 1.3 and 1.4 GHz, is shown in Figure 6-21 along with the ideal design illumination for a lossless network. The data in each case have been normalized to the peak value, which occurs at one of the center elements, number 13 or 14.

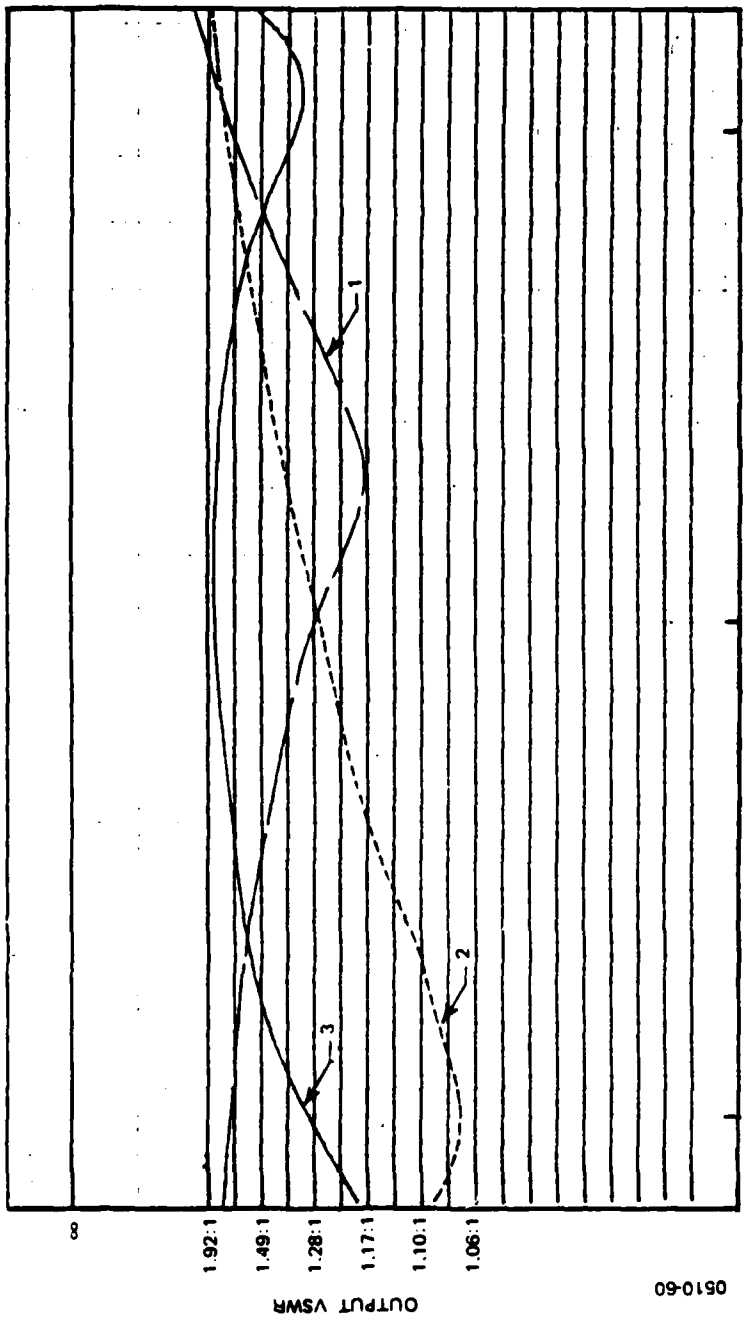

Figure 6-13. Output VSWR, elements 1 through 3

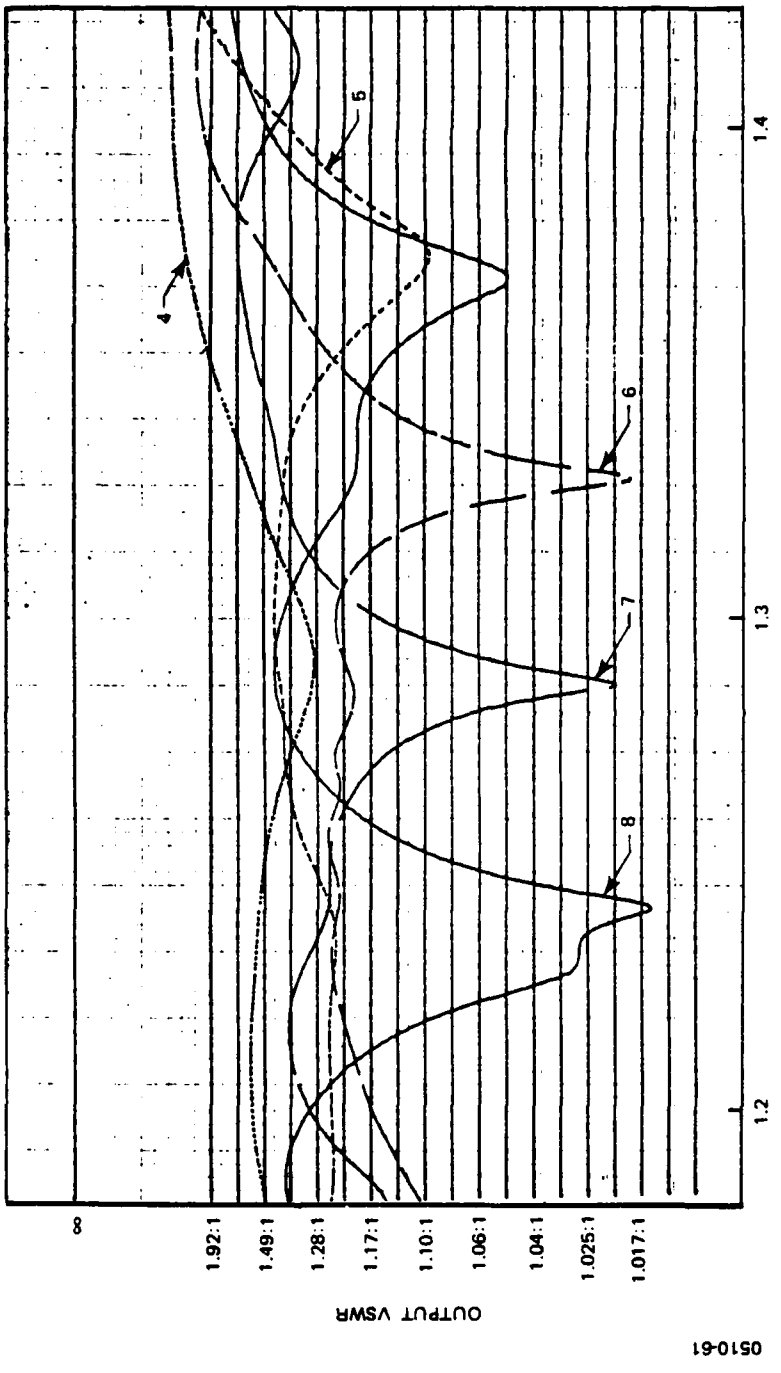

Figure 6-14. Output VSWR, elements 4 through 8

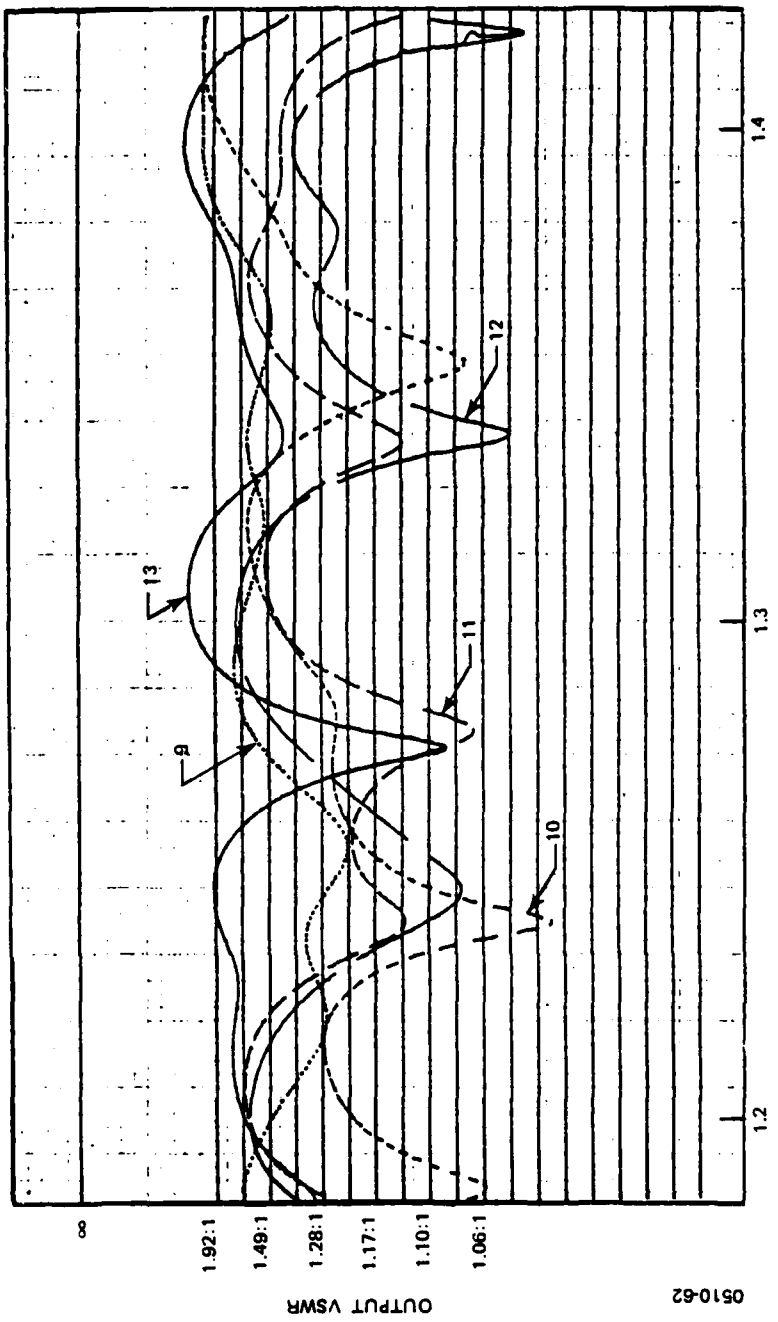

Figure 6-15. Output VSWR, elements 9 through 13

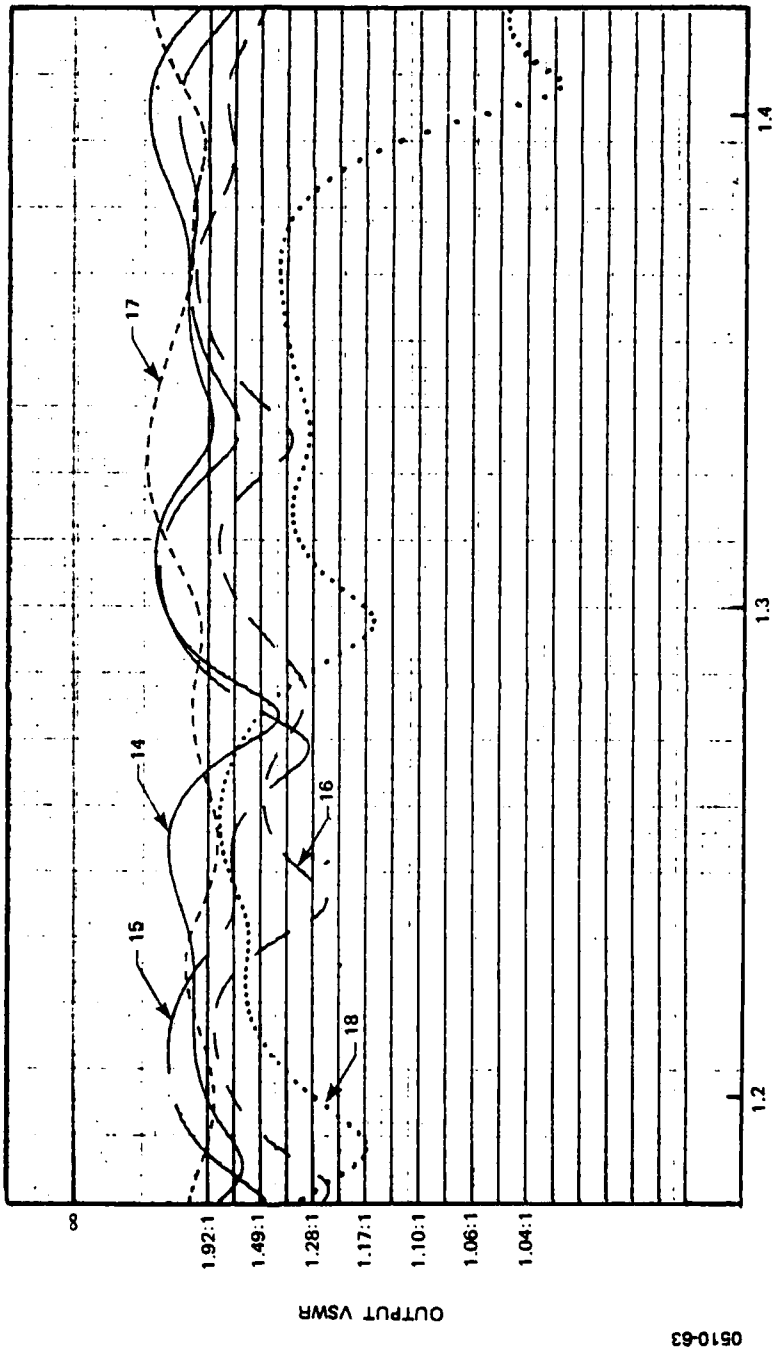

Figure 6-16. Output VSWR, elements 14 through 18

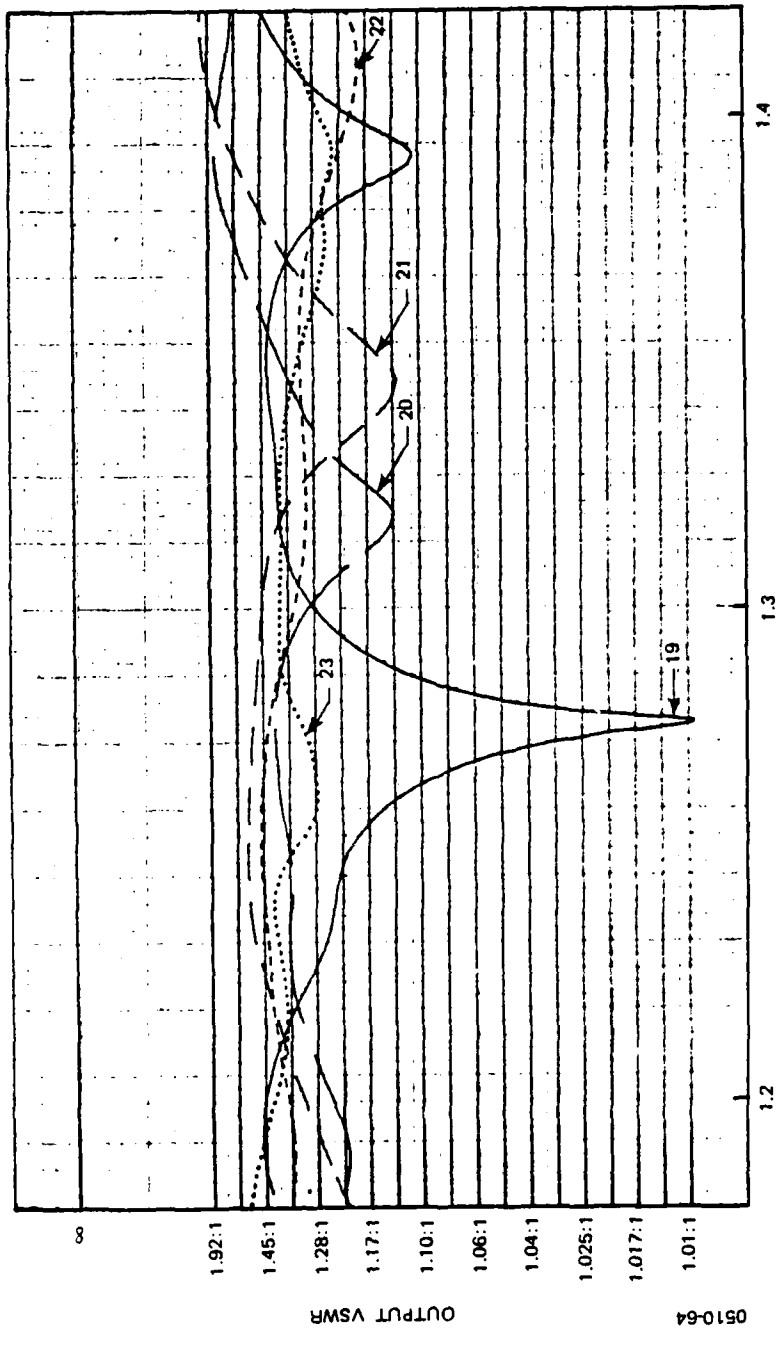

Figure 6-17. Output VSWR, elements 19 through 23

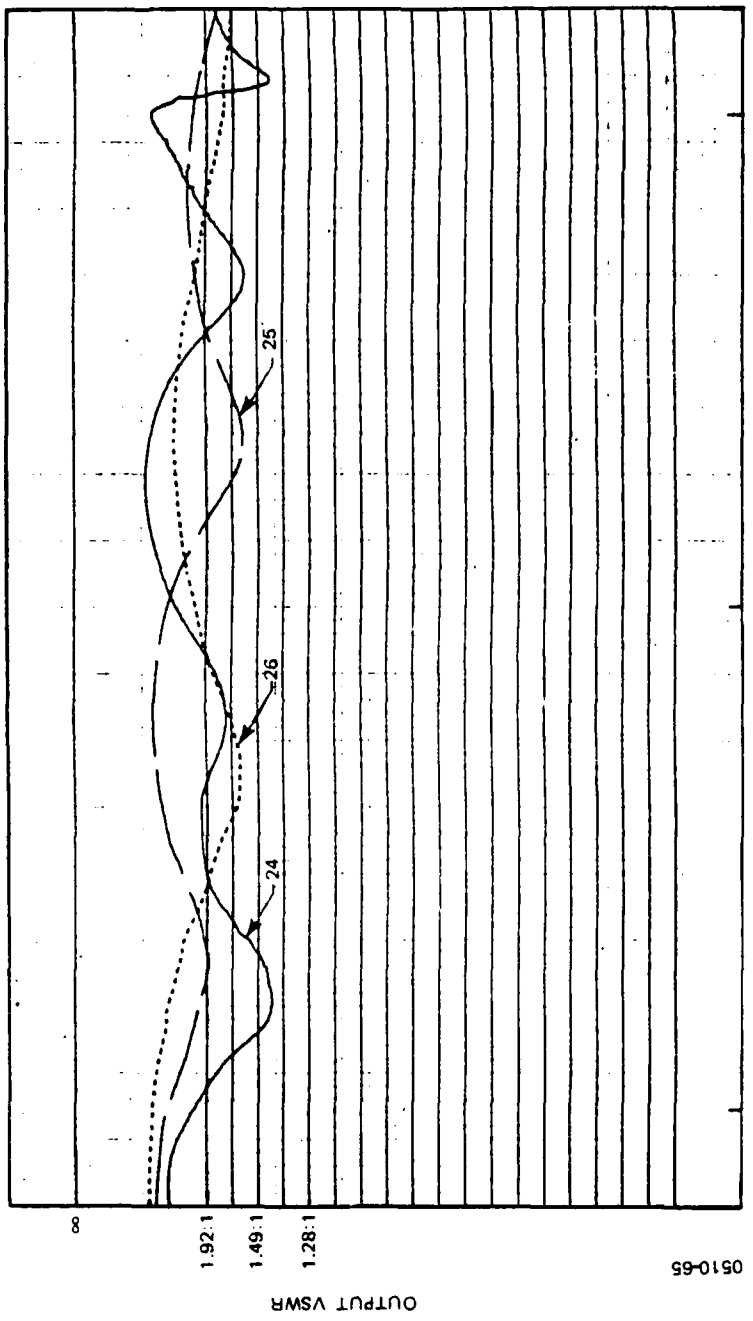

Figure 6-18. Output VSWR, elements 24 through 26

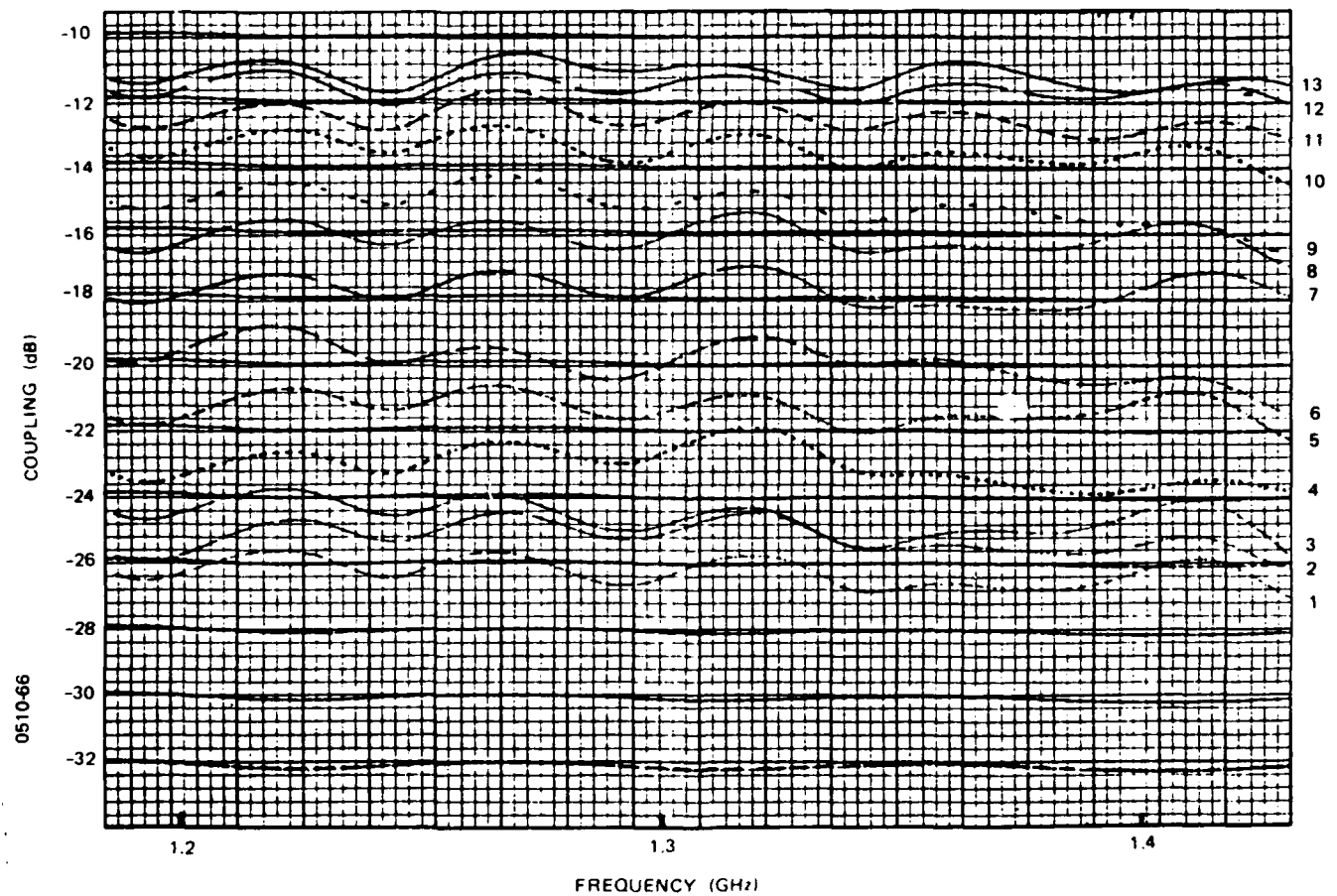

Figure 6-19. Coupling to output ports 1 through 13 versus frequency

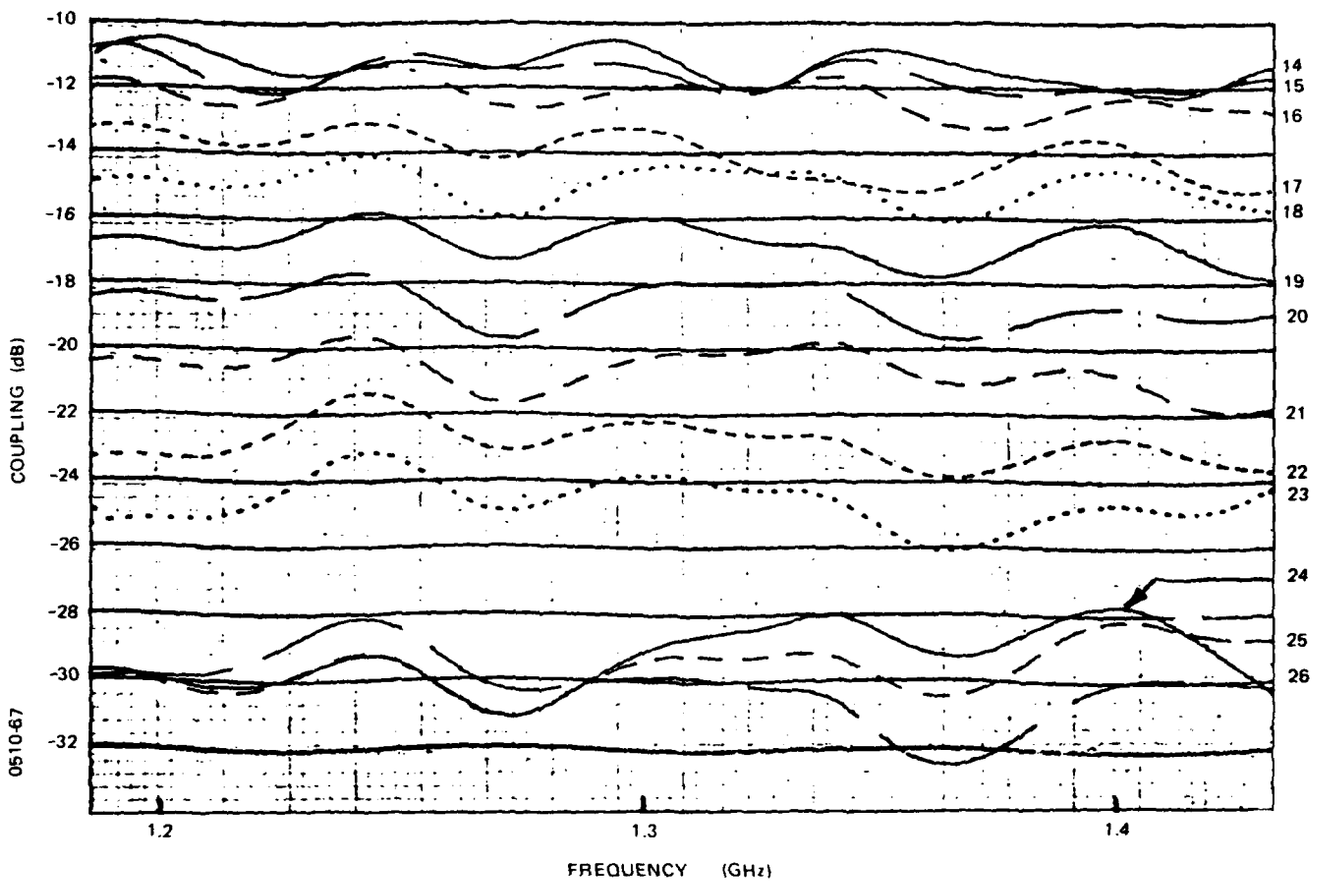

Figure 6-20. Coupling to output ports 14 through 26 versus frequency

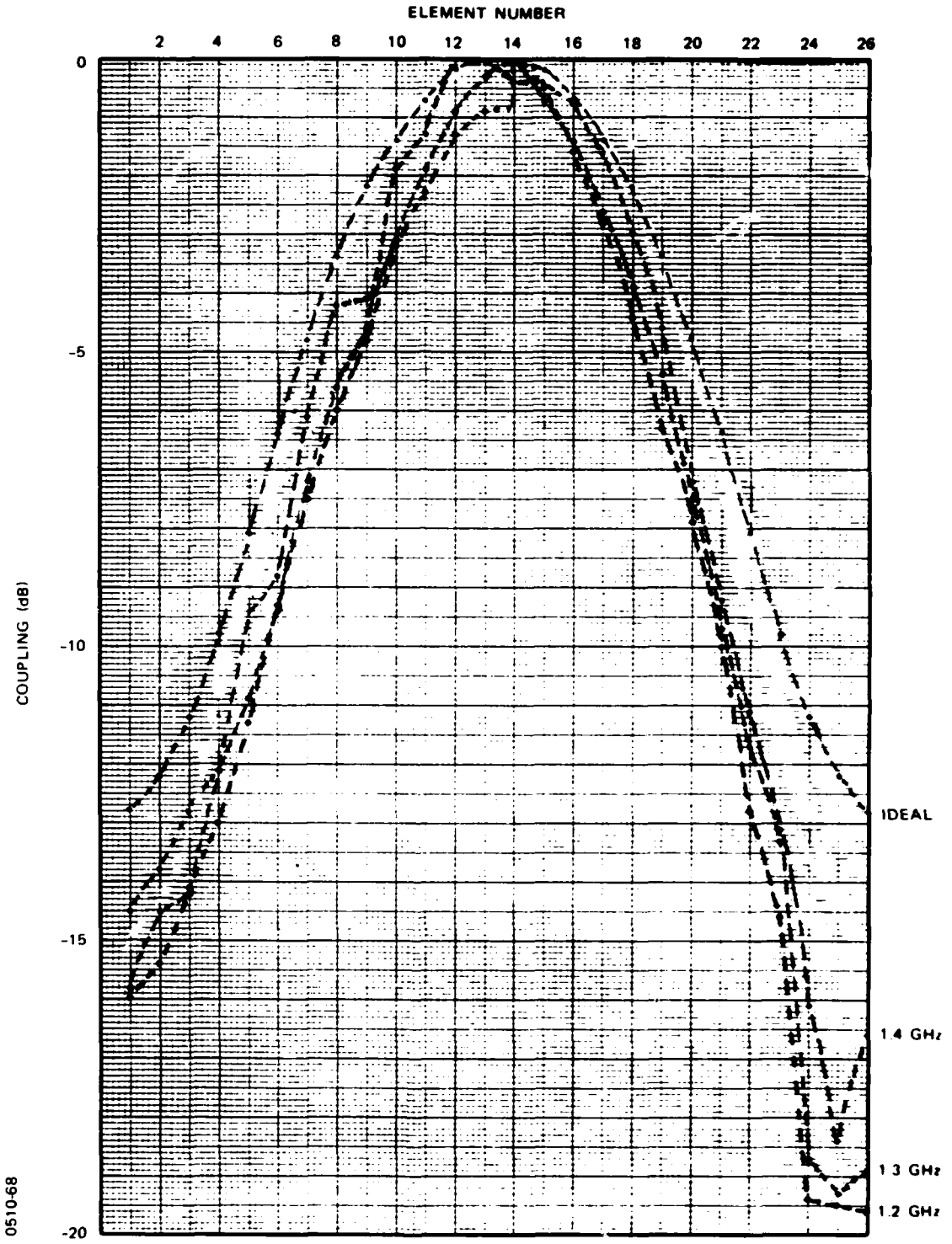

Figure 6-21. Coupling versus element number at 1.2, 1.3 and 1.4 GHz

Phase error, defined as the difference between the measured value and the ideal design value, is shown in Figures 6-22 through 6-24 for 1.2, 1.3 and 1.4 GHz.

6.4.5 Variation of Parameters with Rotation

The measured values of insertion loss, VSWR, and amplitude and phase distribution which are given in Sections 6.4.2 through 6.4.4 were taken with rotor loops centered directly above stator loops. The data presented in this section show the effects of rotation on these parameters.

Two distinct sources of variation can be identified. The first is associated with mechanical differences amongst the 100 stator loops, which were noted in Section 6.2.2.. As rotation occurs, any given rotor loop couples in sequence to each of the stator loops, and irregularities appear as amplitude and phase variations. Thus, these excitation errors are essentially a measure of the precision with which the experimental commutator model has been constructed. Figures 6-25 and 6-26 show the relative amplitude and phase fluctuations as a single rotor loop sequentially couples to the 100 rotor loops. The rms variations of these parameters are 0.28dB and 2.18 degrees, respectively. During actual operation of the commutating feed, smaller errors would be expected because of the averaging effect of multiple coupling from all 26 rotor loops.

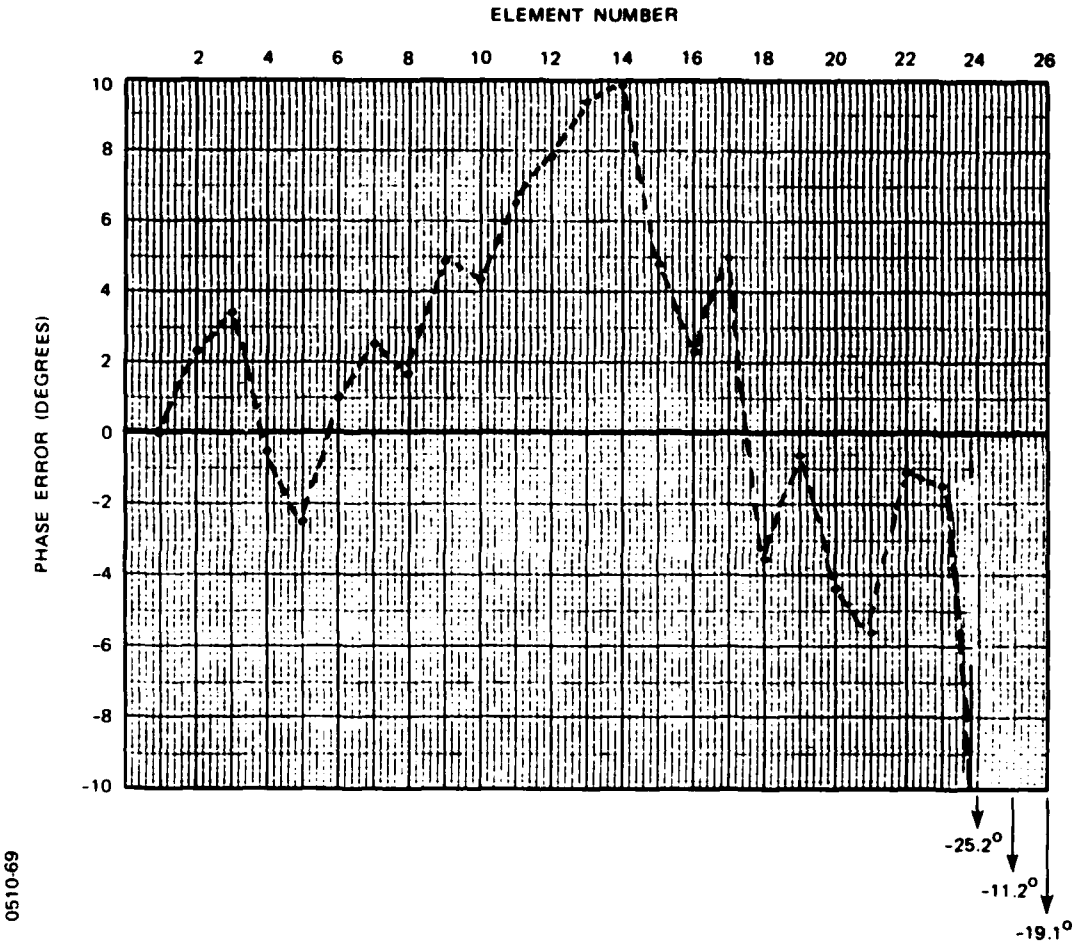

Figure 6-22. Phase error versus element number at 1.2 GHz

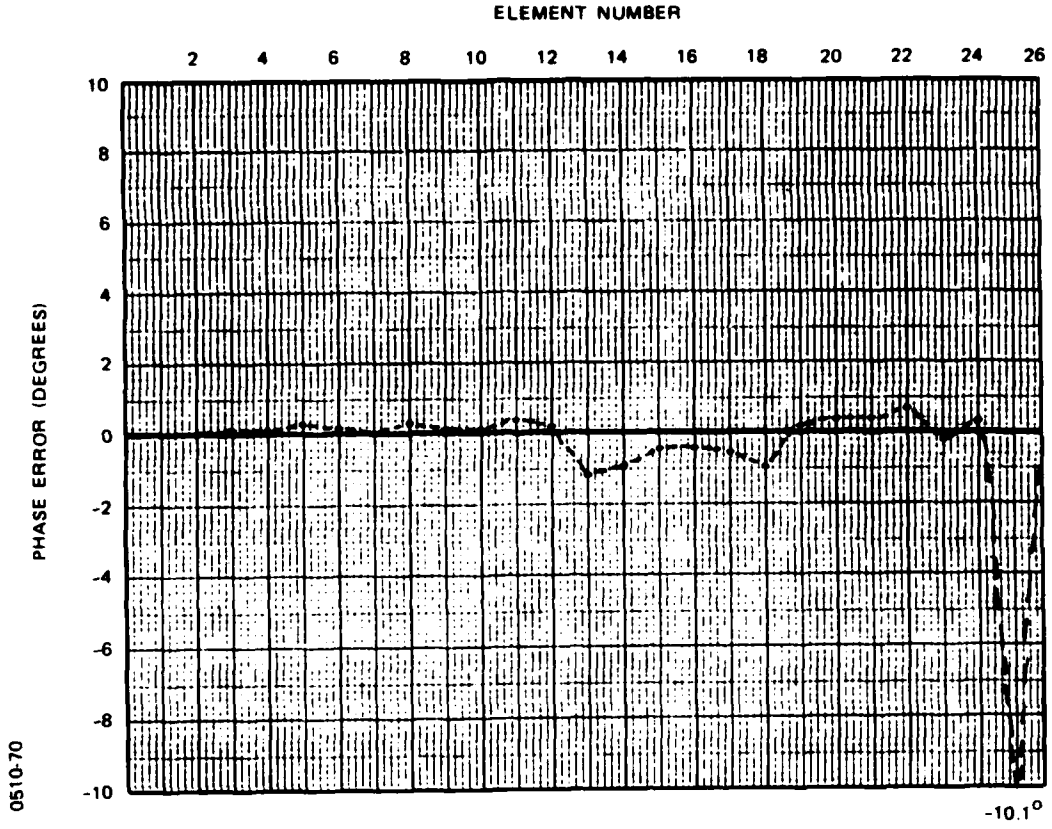

Figure 6-23. Phase error versus element number at 1.3 GHz

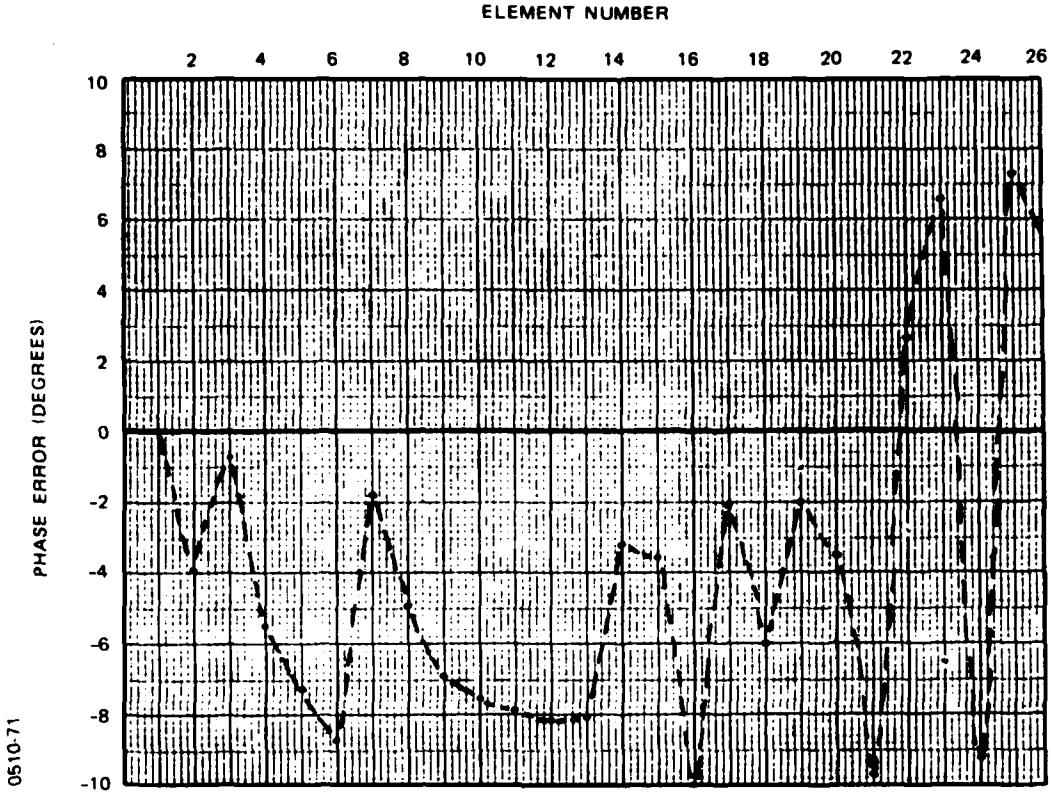

Figure 6-24. Phase error versus element number at 1.4 GHz

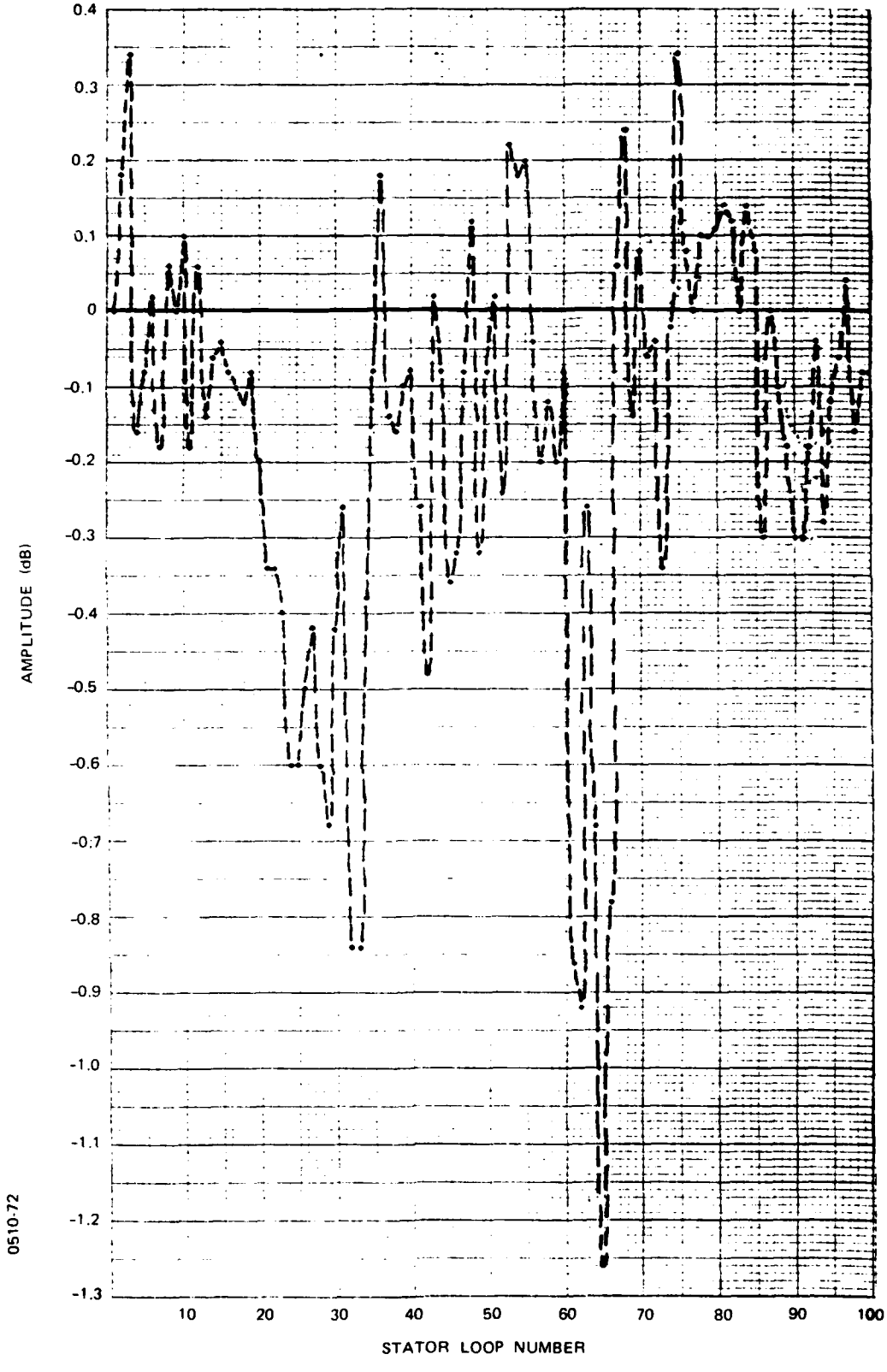

Figure 6-25. Amplitude variations of stator loops

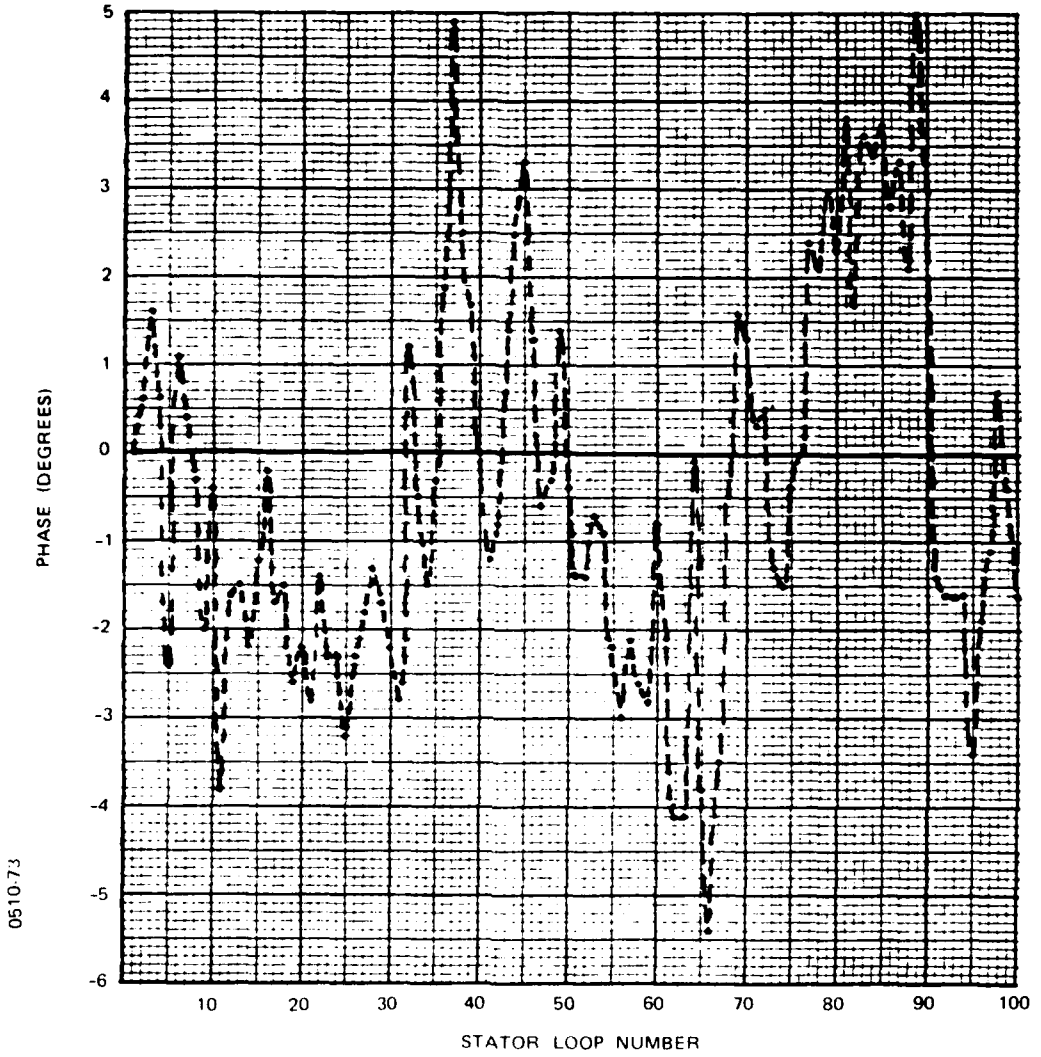

Figure 6-26. Phase variations of stator loops

The second source of variation arises because adjacent rotor loops, which have dissimilar amplitude and phase excitations, couple in changing proportion as they move in the vicinity of the stator loops. The effect is most noticeable when the rotor loops are aligned with the gaps between stator loops. The magnitude and slope of the variations can be minimized over an appreciable percentage of rotational angle by using narrow rotor loops and much wider stator loops. In the experimental commutator model, the rotor loops are 0.25 inch wide, and the stator loops are approximately 1.00 inch wide separated by 0.10-inch gaps.

Figure 6-27 shows amplitude measured at 13 consecutive output ports as the rotating stripline feed network is stopped at ten incremental positions between adjacent stator loops. At fractional offset "0", rotor loops 1 through 13 are centered directly over corresponding stator loops. At "0.1", the rotor loops have been rotated one-tenth the distance toward stator loops 2 through 14. At "0.5", rotor loop 1 is over the gap between stator loops 1 and 2, and so forth. At "1.0", the rotor loops have moved over one complete stator-loop spacing. Thus, the amplitude distribution that was originally at output ports 1 through 13 has now been commuted to output ports 2 through 14. This effect can be seen in the data. The coupled levels at the left-hand edge of the graph correspond to the coupled levels for the next-higher numbered output ports at the right-hand edge. Most of the change in coupled levels take place in the vicinity of the gaps. The transition is very moderate at the six highest-level ports, 8 through 13; however,

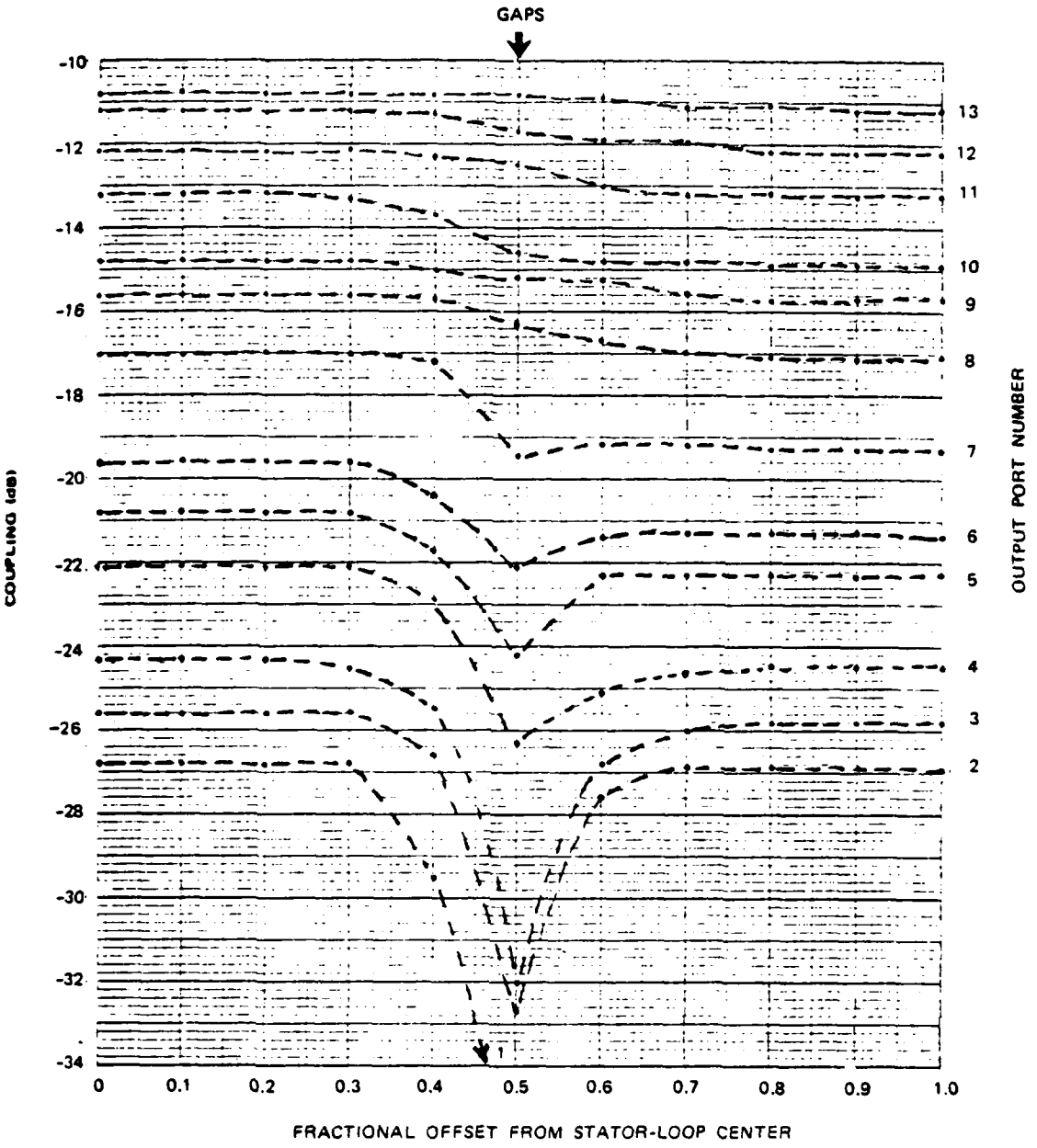

Figure 6-27. Measured loop-coupled amplitude versus offset

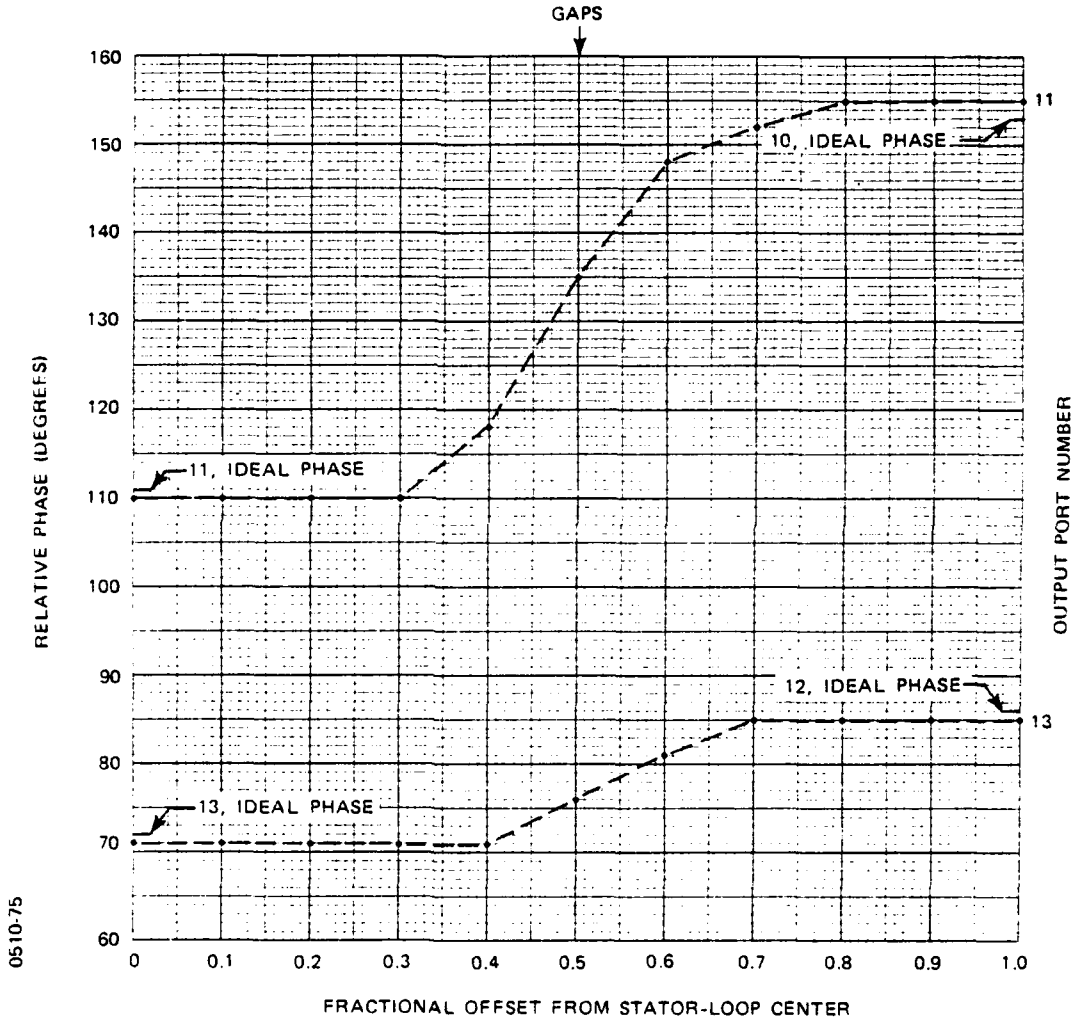

Figure 6-28. Measured loop-coupled phase versus offset

at the weaker-coupled ports, progressively larger excursions occur. No signal appears at port 1 for a fractional offset greater than 0.5, as the last rotor loop has passed beyond the range of stator loop 1.

Figure 6-28 shows the phase characteristics measured at output ports 11 and 13 as the stripline feed network assumes various offsets. The transition region for phase appears to be larger than for amplitude.

With a fractional offset of 0.5, input VSWR remains less than 1.5:1 over 65 percent of the band, and less than 1.8:1 overall. Output VSWR, however, varies from about 2.5:1 to 3.5:1.

Patterns computed from amplitude and phase data taken at various fractional offsets are given in Section 6.4.7. It will be seen that even with an offset of 0.5, excellent patterns are obtained, although insertion loss increases to 1.91dB due to the higher mismatches.

6.4.6 Operation at IFF

Although the experimental commutator model is not required to operate over the IFF frequency band, 1.03 to 1.09 GHz, measurements were made at 1.03 GHz in order to demonstrate the extremely wide-band performance of the device.

The insertion loss, computed from measurements of amplitude coupling factors, is 1.53dB.

Input VSWR, measured at the input to the annular rotary coupler, is 1.44:1. The VSWR sampled at several output ports is typically less than 1.60:1.

The coupled amplitude and phase excitation for one-half of the commutating feed assembly was measured at 1.03 GHz with the rotor loops located directly over the stator loops. Figure 6-29 shows the coupled amplitude for the 13 elements, along with the ideal design illumination for a lossless network. Phase error is shown in Figure 6-30. The azimuth pattern was computed from these data at 1.03 GHz, and is given in the next section.

6.4.7 Computed Patterns

In this section, computed azimuth patterns are given for an 180-inch diameter circular array of 100 uniformly-spaced elements. Although the feed network was designed to be phase compensated at an elevation scan angle of 15 degrees, these patterns are computed at zero elevation scan, which represents a slightly worse situation in terms of sidelobe levels.

Figures 6-31 through 6-33 show patterns computed at 1.2, 1.3 and 1.4 GHz, using the amplitude data of Figure 6-21 along with associated phase data. The reference lines represent the sidelobe specification limit, -20dB, and the sidelobe design limit that would be realized with ideal excitation, -30dB. Table 6-2 summarizes the results of these pattern computations.

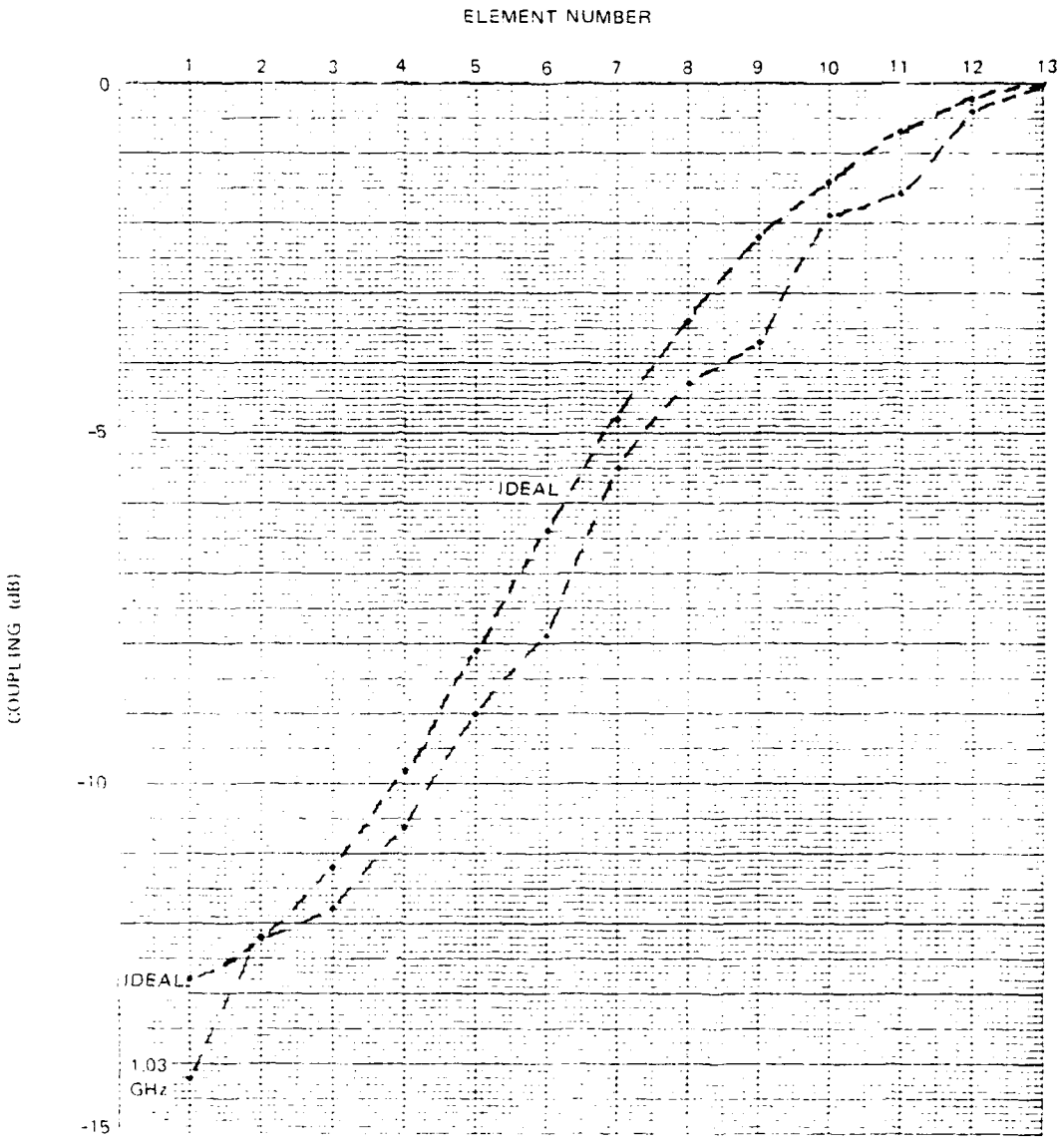

Figure 6-29. Coupling versus element number at 1.03 GHz

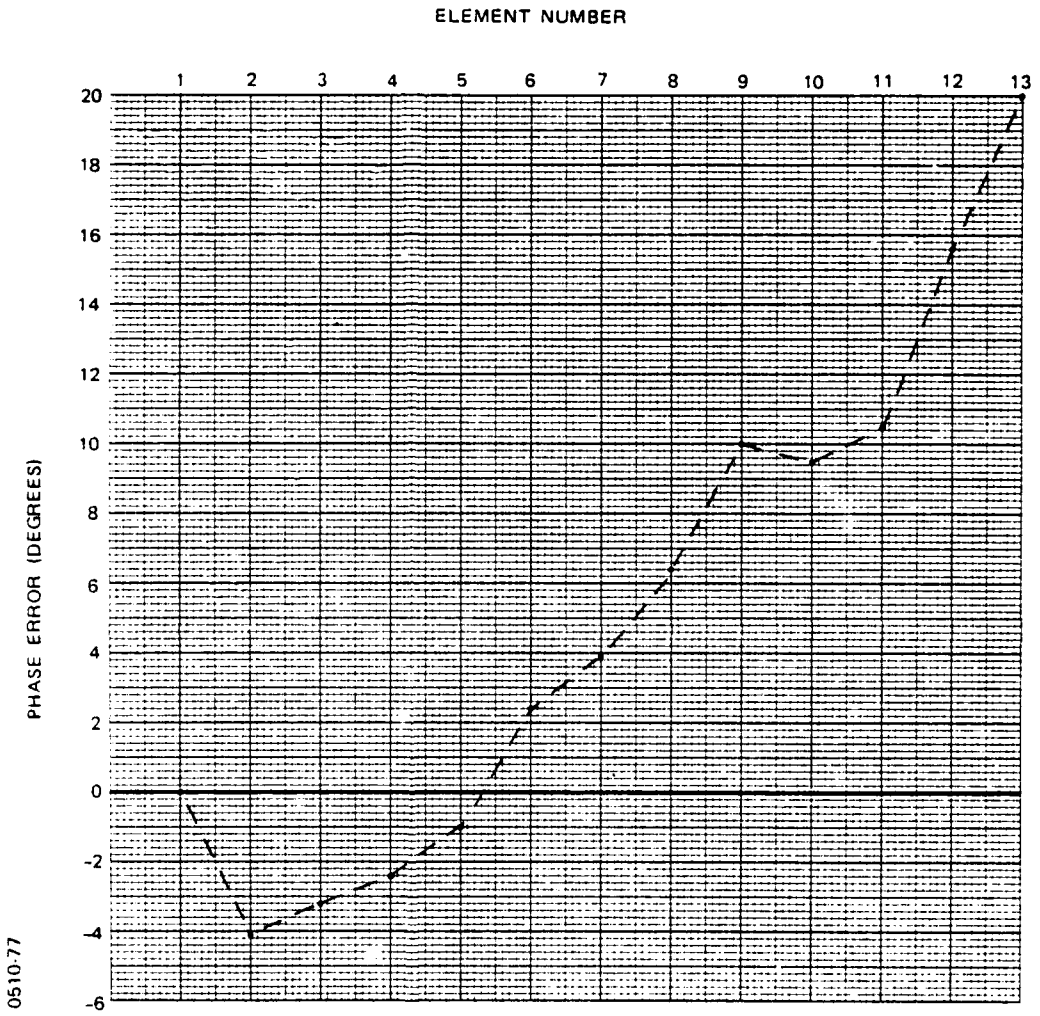

Figure 6-30. Phase error versus element number at 1.03 GHz

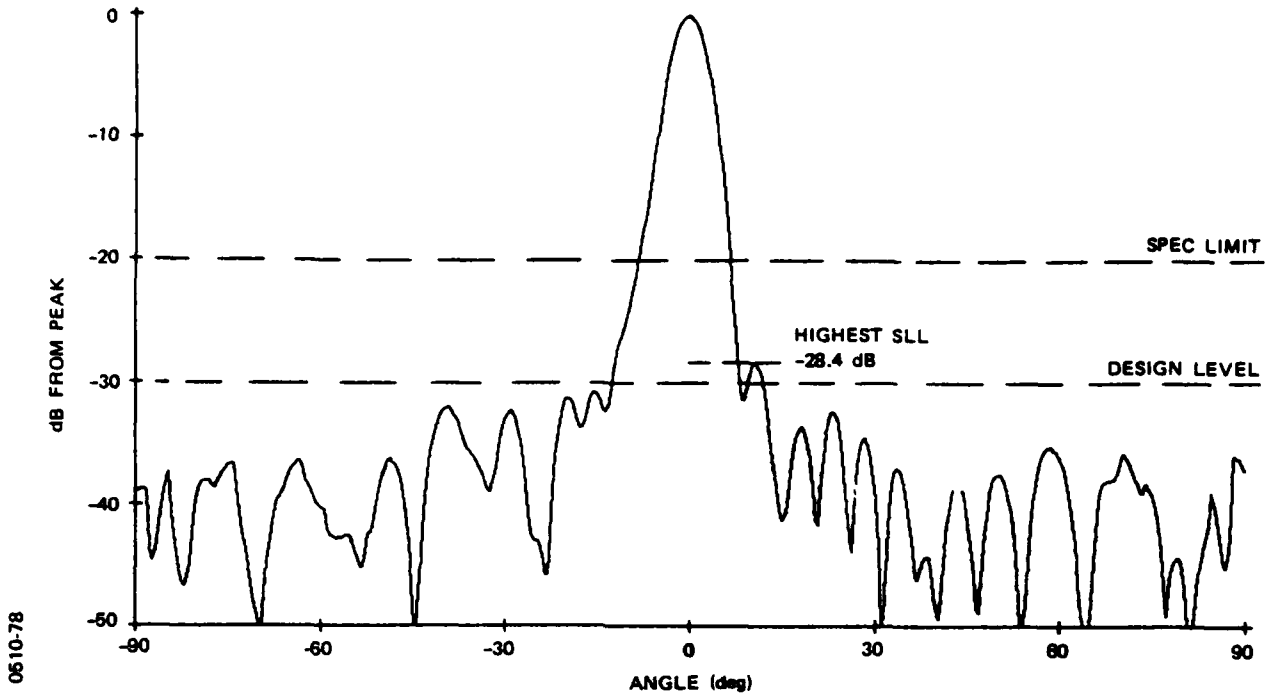

Figure 6-31. Computed azimuth pattern of experimental commutator model at 1.2 GHz

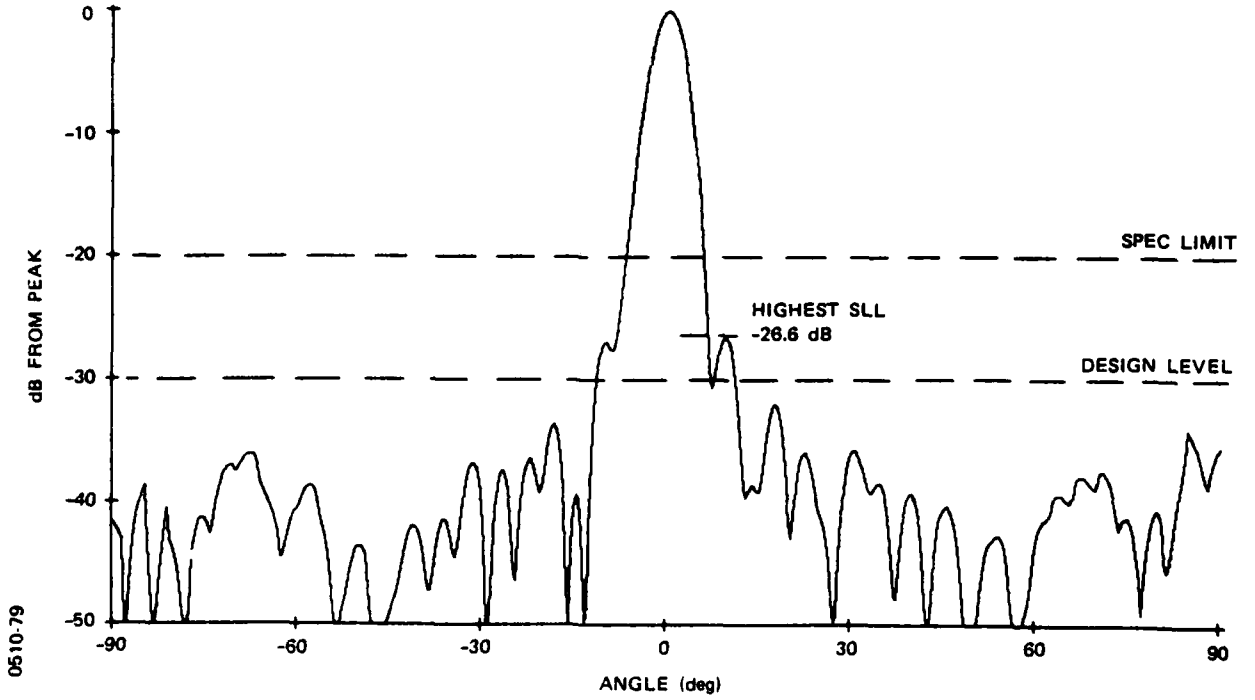

Figure 6-32. Computed azimuth pattern of experimental commutator model at 1.3 GHz

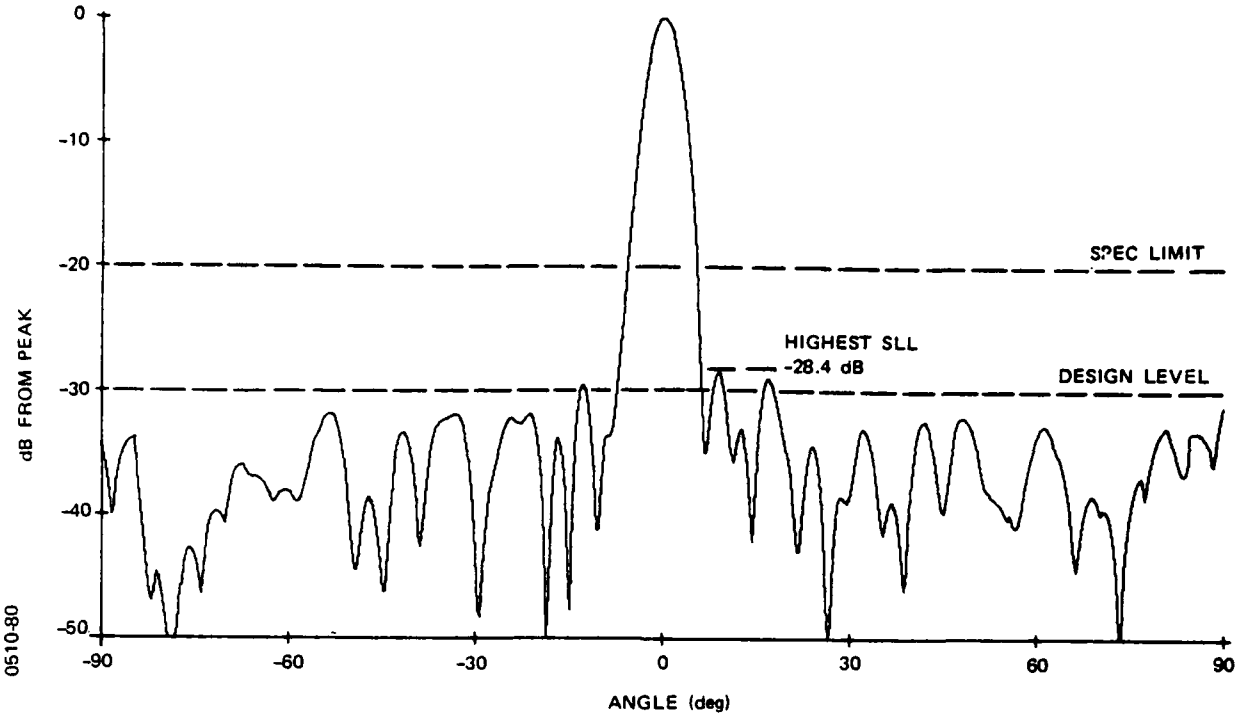

Figure 6-33. Computed azimuth pattern of experimental commutator model at 1.4 GHz

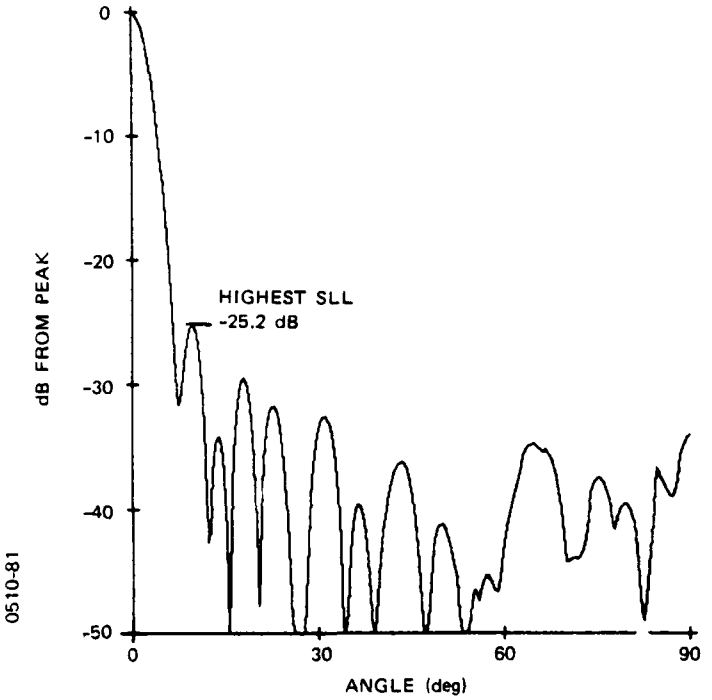

Figure 6-34. Computed azimuth pattern at zero fractional offset

TABLE 6-2. RESULTS OF PATTERN COMPUTATIONS			
Frequency (GHz)	1.2	1.3	1.4
Highest Sidelobe (dB)	-28.4	-26.6	-28.4
Aperture Efficiency (dB)			
Theoretical	-1.25	-1.27	-1.28
Measured	-1.84	-1.69	-1.59
Dissipation Loss (dB)	-1.58	-1.41	-1.84

The remaining patterns in this section were computed using amplitude and phase data measured for one-half of the feed network, and assuming symmetrical excitation. Therefore, only one-half of each pattern is shown.

Figures 6-34 through 6-39 were computed from measured data taken at 1.3 GHz. The rotor loops were centered directly above the stator loops in Figure 6-34, which serves as a reference pattern.

The pattern of Figure 6-35 is identical to the reference pattern, except that excitation was measured at 17 output ports rather than at just 13. The additional four ports, which are adjacent to the edge port, are in theory not excited; however, because isolation is limited by rf leakage in the coupling region, excitation is not abruptly truncated at the edge elements. The measured amplitudes for one-half of the commutating feed assembly, plus four adjacent elements, are given in Table 6-3.

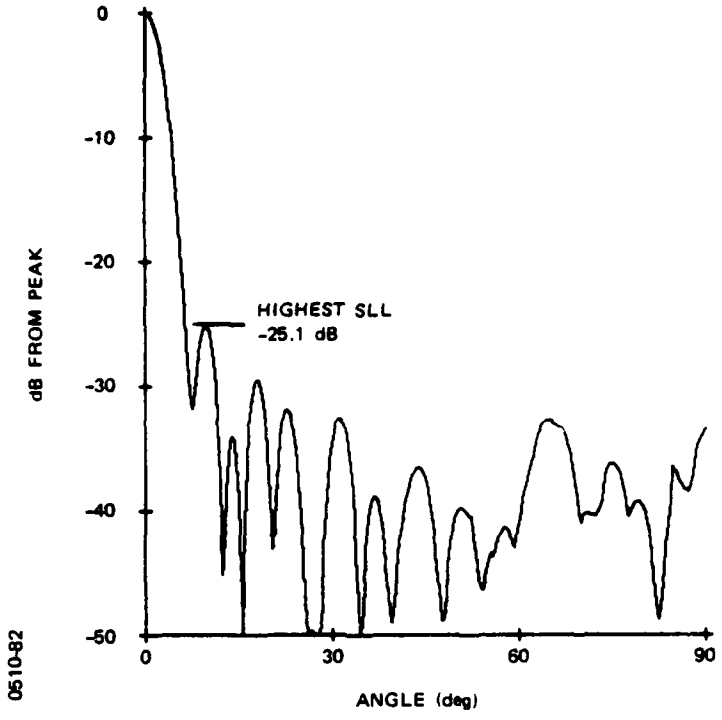

Figure 6-35. Computed azimuth pattern at zero fractional offset (34 elements)

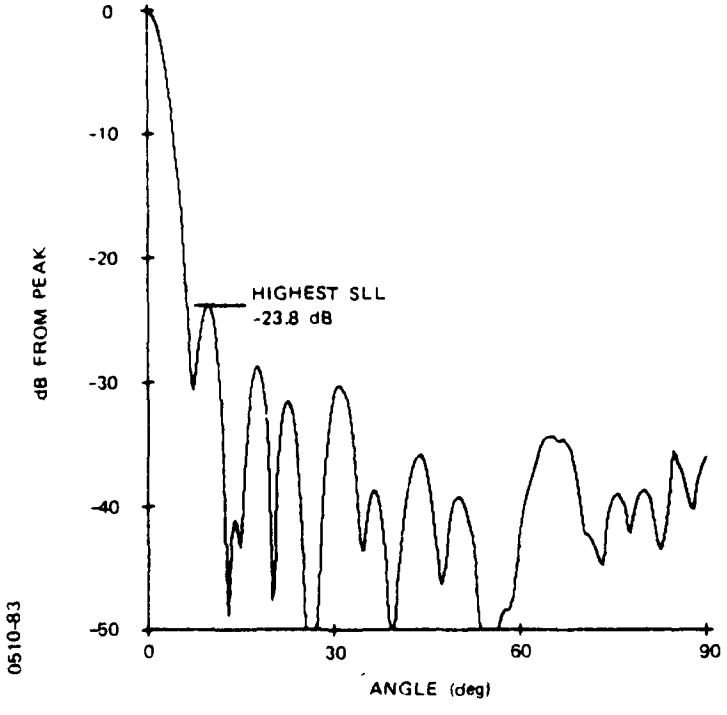

Figure 6-36. Computed azimuth pattern at 0.375 fractional offset

TABLE 6-3. MEASURED AMPLITUDE WITH EDGE EFFECTS	
Element Number	Amplitude (dB)
-4	-39.1
-3	-38.1
-2	-34.9
-1	-30.7
1 (Edge Element)	-15.2
2	-14.3
3	-13.5
4	-11.6
5	-10.4
6	-8.8
7	-6.6
8	-4.9
9	-3.9
10	-2.4
11	-1.7
12	-0.5
13 (Central Element)	0 (Reference)

The leakage illumination is about 15dB to 25dB below the signal level at element number 1; hence, it should have no perceptible effect on the patterns for the case of zero coupling-loop offset. Although no measurements were made of edge effects that occur as fractional offset increases, some skewing of the excitation would be expected, along with an increase in the sidelobe level.

The patterns in Figure 6-34 and Figures 6-36 through 6-39 show the performance of the experimental commutator model as fractional offset is increased from zero to 0.5. Table 6-4 summarizes these results.

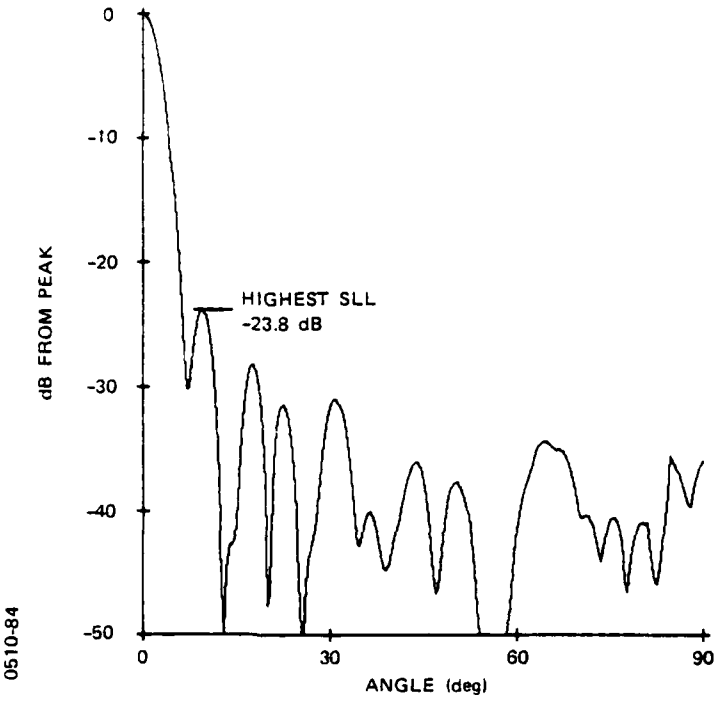

Figure 6-37. Computed azimuth pattern at 0.400 fractional offset

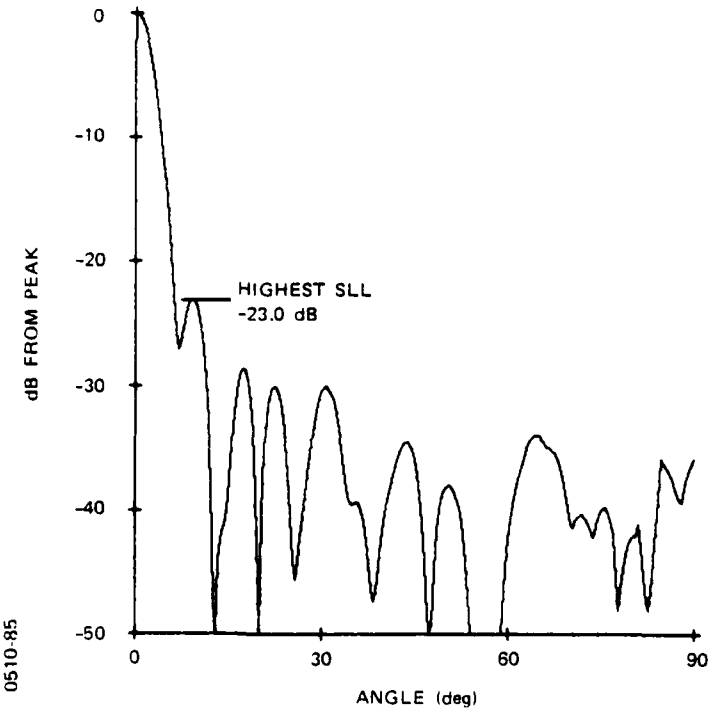

Figure 6-38. Computed azimuth pattern at 0.425 fraction offset

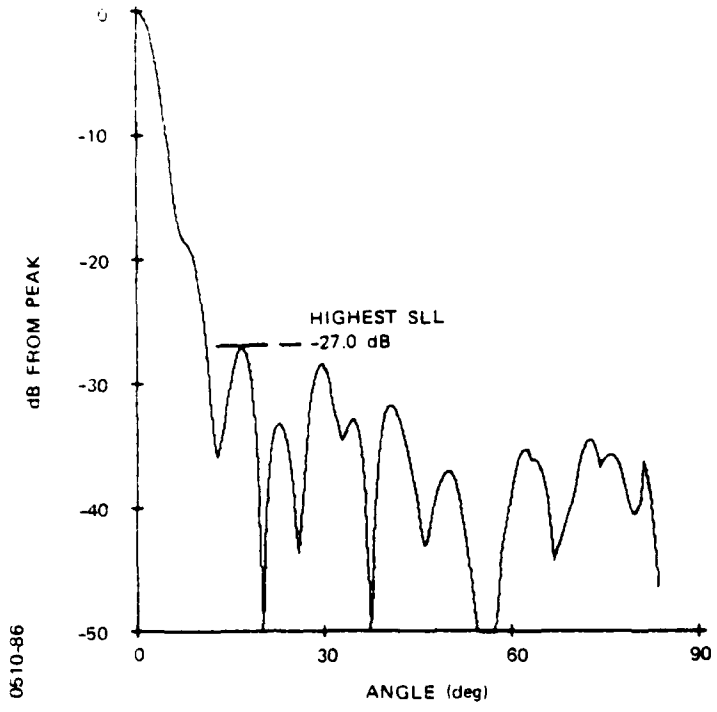

Figure 6-39. Computed azimuth pattern at gap (0.500 fractional offset)

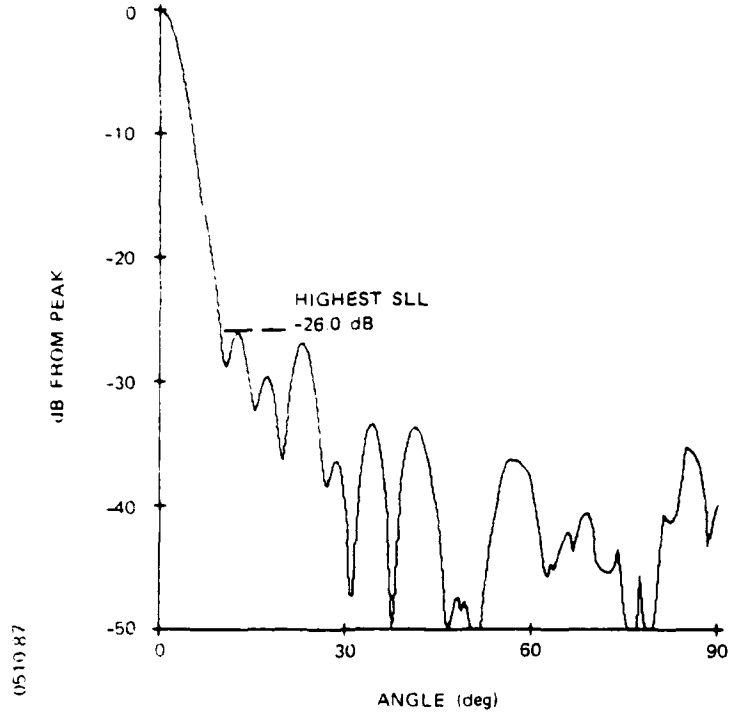

Figure 6-40. Computed azimuth pattern at 1.03 GHz

TABLE 6-4. RESULTS OF PATTERN COMPUTATIONS WITH FRACTIONAL OFFSETS

Fractional Offset	0	0.375	0.400	0.425	0.500
Highest Sidelobe (dB)	-25.2	-23.8	-23.8	-23.0	-27.0*
Aperture Efficiency (dB)	-1.51	-1.54	-1.55	-1.60	-1.99
Dissipation Loss (dB)	-1.30	-1.42	-1.29	-1.33	-1.91

* Shoulder at -18dB

Figure 6-40 is the computed azimuth pattern at 1.03 GHz, more than 20 percent below the design center frequency. Note that an excellent pattern is still obtained, with the highest sidelobe at -26.0 dB.

6.4.3 Power-Handling Capability

The power-handling capability of the commutating feed assembly is essentially determined by the power ratings of the annular rotary coupler and of the main feed line in each half of the stripline assembly. The power levels in the delay lines and loop couplers are not a serious problem, as these circuits are decoupled from the power incident at the commutator input by at least 10dB. The annular rotary coupler is rated at 15kW peak and 500 watts average, and meets commutator requirements.

Incident power to each half of the stripline assembly is reduced to 5kW peak and 250 watts average because of the 3-dB

power split in the output of the annular rotary coupler. These levels are well within the capability of the three-layer stripline, shown in Figure 3-15, which is used in the experimental commutator model.

High-power tests were not performed on the completed experimental commutator model, as considerable expense would be incurred to buy the 100 medium-power coaxial loads required. A high degree of confidence, however, was obtained by successfully testing a 4x12 inch breadboard stripline circuit, containing two overlap directional couplers, at 16 kilowatts peak and 400 watts average power. Test conditions are given in Table 6-5.

TABLE 6-5. STRIPLINE CIRCUIT HIGH-POWER TEST CONDITIONS

Frequency	1.3 GHz
Power	
Peak	16.0kW
Average	400W
Pulse Width	125 μsec
Duty Cycle	2.5%
Duration of Test	30 minutes
Environment	Room

The test circuit used had been bonded with an adhesive film into a unitized assembly under temperature and pressure. This effectively prevents voids between layers, and seals the assembly against humidity and contaminants. Although the stripline assemblies of the experimental commutator model are not bonded, this process would be incorporated into the production version.

SECTION 7

STUDY OF A PRODUCTION-VERSION COMMUTATOR

In order to reduce development cost while retaining the essential features of the system, the experimental commutator model was configured to have 100 output ports with a 90° illuminated sector. The number of array elements chosen is roughly one-half that required for a full-size antenna, and the 90° sector may likewise be less than dictated by mission requirements.

This section of the report discusses a study of the fabrication techniques, costs and reliability for a production version of this commutator which can drive 200 elements with the same inter-element spacing of 0.62λ, and for the two cases of 90° and 120° illumination sectors.

7.1 Alternative Approaches for Full-Size Commutator

The salient differences in requirements between the experimental commutator and a full-size production model are given in Table 7-1.

TABLE 7-1. DIFFERENCES IN COMMUTATOR MODEL REQUIREMENTS

Parameter	Experimental Model	Full-Size Production Model
Number of Output Ports	100	200
Number of Excited Ports	26	50 or 68
Excited Sector	90°	90° or 120°

The full-size commutator has 200 ports, compared to 100 ports for the experimental model. This can be accomplished by any of the following approaches, or combinations thereof:

(a) increase diameter of commutator;

(b) increase stripline dielectric constant;

(c) modify design configuration.

7.1.1 Increased Diameter

If the present loop-coupler size and circumferential spacing are maintained, the diameter of the full-size commutator will double. The stripline series feed network and phase compensating delay lines would need to be redesigned as a result of changing the number of excited ports and the array diameter. The loop-coupling region and RF chokes, however, would essentially retain their original cross sections at larger radial locations, as shown in Figure 7-1. The disadvantages of doubling the diameter of the commutator are that stripline area, hence material cost, is increased by a factor of four, and the overall commutator weight would be approximately three times greater. Although the moment of inertia of the rotating assembly increases 16-fold, the dc torque motor requires only double the drive power for start up, and essentially the same drive power for continuous rotation at 15 rpm. RF losses will increase regardless of the approach chosen, as the lengths of delay lines required for phase compensation are directly proportional to the radius of the circular array.

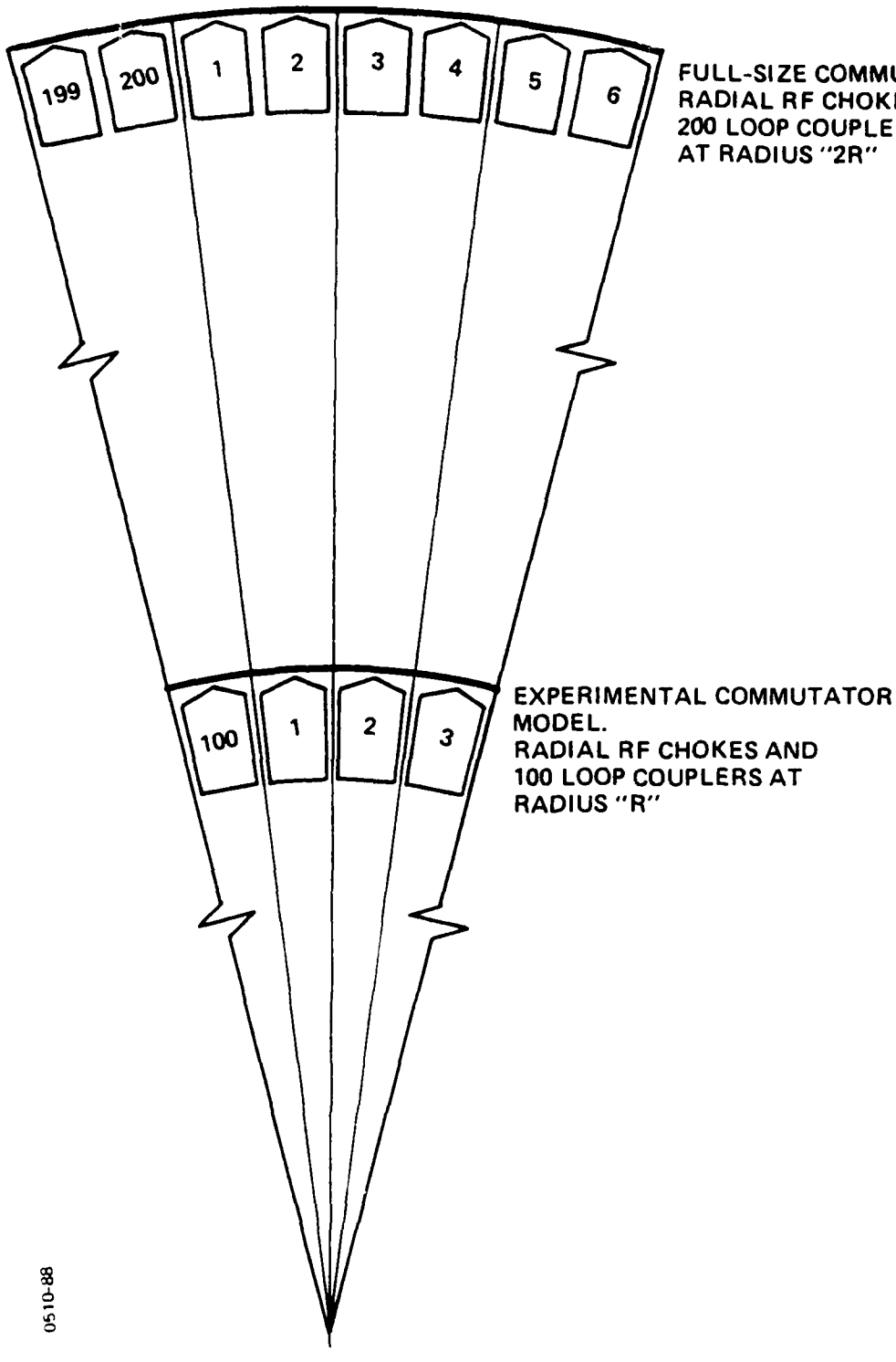

Figure 7-1. Two-fold radius increase for 200 loop couplers

7.1.2 Increased Stripline Dielectric Constant

The second approach, using high-dielectric-constant material in the stripline assembly, allows the feed-line couplers and delay lines to be reduced in size. A dielectric constant of about 10 is required for a two-fold reduction in the size of the present stripline package. Epsilam-10, manufactured by 3M Company, is a potential candidate; however, this material costs about $300 per square foot, and is currently available in sheets no larger than 9 x 9 inches. Another consideration is that making the rotating stripline assembly smaller does not solve the problem of how to fit 200 stator loops within the present outline. One solution is to trade off the size of the stripline assembly against the width of the loop couplers, as illustrated in Figure 7-2. This requires a stripline material of intermediate dielectric constant, and a reduction in ground-plane spacing, which results in an increase in insertion loss. Table 7-2 lists these parameters for three dielectric materials. Pathlength within the stripline assembly is assumed to be reduced to a practical minimum.

TABLE 7-2. COMMUTATOR PARAMETERS FOR THREE DIELECTRIC MATERIALS

Material	Teflon-Glass	Epsilam-6	Epsilam-10
Dielectric Constant	2.5	6.0	10.3
Loss Tangent (@10GHz)	0.0018	0.0018	0.0010
Diameter (Inches)			
Stripline Assembly	64.00	41.31	31.53
Commutator	70.63	47.94	38.16
Ground-Plane Spacing (Inches)	0.270	0.170	0.110
Stripline Insertion Loss (dB)	1.68	2.92	3.26

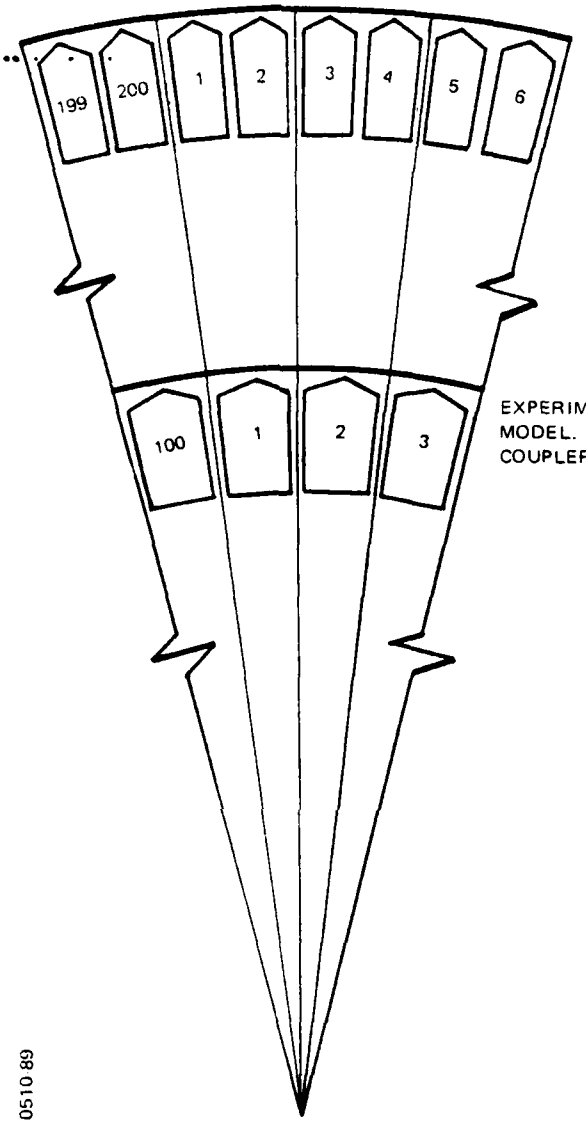

Figure 7-2. Reduced-width loop couplers to minimize radius of commutator

7.1.3 Modified Design Configuration

The third approach to a 200-port commutator is to modify the design configuration such that diameter is minimized without resorting to high-ε_r materials, or without reducing the width of the stator coupling loops. Two concepts are suggested here, although the practicality of the ideas has not been examined in detail.

In one configuration, the complete feed network is distributed between two back-to-back stripline assemblies, which feed alternate rotor loop couplers, and are mounted to a common rotating ground plane. Figure 7-3 shows the odd-numbered and even-numbered feed lines separated, and contained in the upper and lower stripline assemblies respectively. The rotor loops, which are turned perpendicular to the ground plane, couple to two rings of 100 stator loop couplers. Another way in which the feed lines can be apportioned between the two assemblies, rather than odd/even, is by mirror-image halves as in the experimental commutator model.

A second concept for minimizing diameter is to use cylindrical geometry, as illustrated in Figure 7-4, rather than planar geometry. This requires curved stripline assemblies, which are somewhat more difficult to fabricate than flat assemblies. Furthermore, the reduction in diameter is only twice the length of the stator loop couplers: about five inches at L-band.

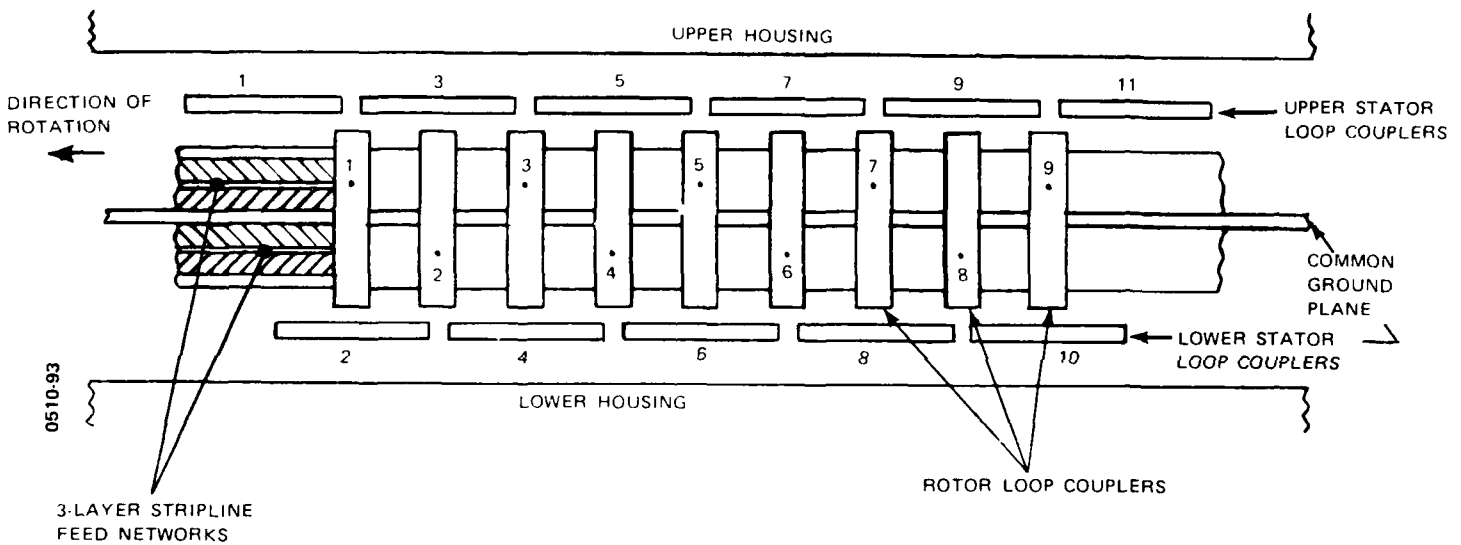

Figure 7-3. Edge view of back-to-back stripline feed networks

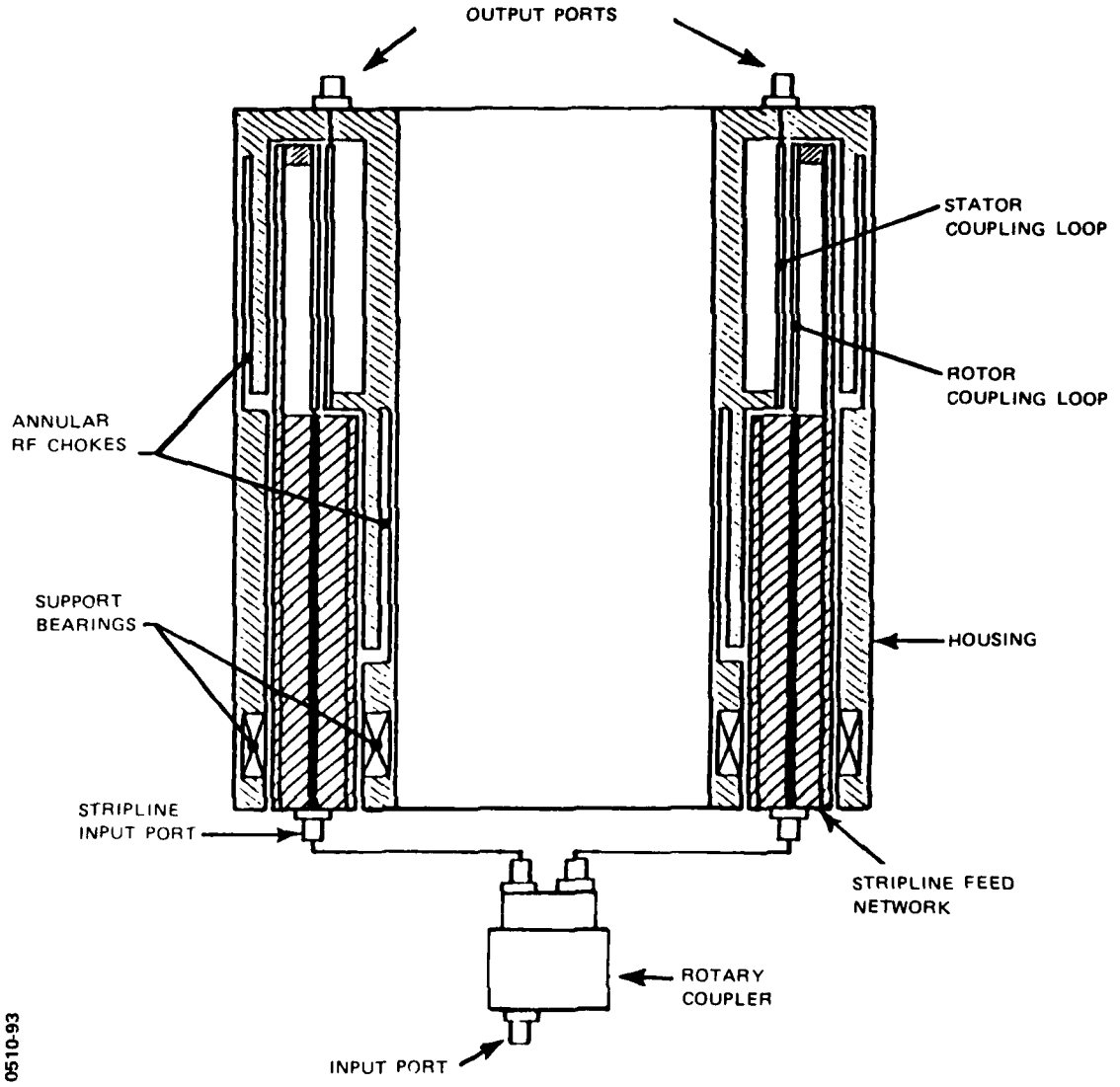

Figure 7-4. Commutating feed assembly using cylindrical geometry

7.1.4 Recommended Approach

After examining the alternative approaches described above, the use of Epsilam-6 in a configuration similar to that of the experimental commutator model is selected as the recommended approach for a full-size production unit. This represents a realistic trade-off amongst insertion loss, size, complexity and cost. Estimated features of a production version of this design are given in Table 7-3.

TABLE 7-3. ESTIMATED FEATURES OF PRODUCTION-VERSION COMMUTATOR

Frequency Band	1.0 to 1.4 GHz
Number of Output Ports	200
Number of Excited Ports	50 or 68
Excited Sector	90^{o} or 120^{o}
Azimuth Sidelobe Level	<-25dB
VSWR	
Input Port	1.5:1 maximum
Output Ports	1.5:1 maximum
Insertion Loss	3.5 dB maximum
Power Capacity	
Peak	10.0 kW
Average	500 W
Rotation Rate	15 rpm
Drive Power (2 Stacked Units)	25 Watts maximum
Environment	-35^{o}F to $+100^{o}$F (as encountered in Arctic)
Reliability	100,000 hrs MTBF
Size	48 inches diameter
Weight	210 lbs
Cost per Unit (Qty 100)	$23,547

7.2 Environmental Conditions

The commutating feed assembly is a rugged mechanical structure that is not unduly susceptible to normal shock and vibration. The major environmental conditions of concern, temperature and humidity, are discussed below.

7.2.1 Temperature

All active electronic circuits, which are located in the pedestal, are selected for the specified ambient temperature of $-35^{\circ}F$ to $+100^{\circ}F$. The materials and components used in the stripline feed network and housing present no problems over the temperature range.

The 18-inch diameter ring bearing is made from vacuum processed high carbon chromium steel identified as SAE 52100 or AISI E-52100. With standard heat treatment, this bearing steel can be operated satisfactorily at temperatures as high as $+250^{\circ}F$. Prelubricated bearings, packed with high quality grease, provide years of maintenance free operation at low speeds over a temperature range of $-70^{\circ}F$ to $+225^{\circ}F$.

7.2.2 Humidity

For the production-version commutator, a bonded stripline assembly will be used. Thin adhesive films are placed between dielectric layers, and with the application of heat and pressure, the entire assembly is formed into a single, trouble-free unit.

Voids between layers are eliminated, and the assembly is effectively sealed against humidity and contaminants. This not only enhances power-handling capability, but assures repeatability of attenuation and insertion phase characteristics.

The incursion of moisture into the housing will have negligible effect on performance, unless condensation and collection of water takes place. This is easily avoided by allowing the structure to breathe, and providing drainage holes in the bottom.

7.3 Fabrication Techniques

The key fabrication techniques for a production-version commutator focus on producing a lightweight, precision, low-cost housing and on bonding the stripline laminations to form a trouble-free, unitized assembly.

7.3.1 Housing

The 48-inch diameter of the production-version housing makes investment casting impractical. The top and bottom sections, however, can be made as sand or plaster-mold castings from A35o aluminum alloy, which is then solution heat treated and artificially age hardened to a T6 condition. The castings would be ribbed for strength, and machined to final dimensions.

7.3.2 Stripline Assembly

Each half of the stripline assembly requires a board size approximately 20x40 inches; however, Epsilam-6 is a relatively new material presently available in sheets only 12x12 inches maximum.

The outer dielectric sheets of the three-layer stripline construction contain no etched circuitry, and can therefore be easily fashioned from the smaller sheets. One attractive approach is to laminate the 12x12 inch squares to an aluminum alloy back-up plate large enough to form one entire ground plane of the rotating stripline assembly. After this is machined to final dimensions, cracks between squares of Epsilam-6 can be filled and sealed with a suitable high-dielectric cement.

It would be difficult to fabricate the thin dielectric circuit board from smaller pieces, as the etched network circuitry would be required to bridge seams in many places. Unless large sheets of Epsilam-6 become available, another material will have to be used. The dielectric constant can differ appreciably from that of the outer dielectric sheets, where most of the electric field is concentrated, without greatly affecting the composite dielectric constant. The primary effect of center-board dielectric constant is on the coupling value of the overlap directional couplers.

The center board containing the etched feed network is bonded to the previously laminated outer sections. This process similarly uses heat and pressure, but at a lower temperature so as not to destroy the existing bond.

One method of accomplishing the bonding process is to put a thin adhesive film between each layer, pin or clamp the pieces in position, and place the assembly within an autoclave. A vacuum

bag is used around the stripline assembly to assure that all air bubbles between layers are evacuated during the curing cycle.

The bonded stripline assembly is a trouble-free unit that is sealed against humidity and contaminants. All components, such as connectors, load terminations, phase trimmers, and rotor-loop ground connections are externally located and readily accessible for adjustment or maintenance actions.

7.4 Reliability

The predicted failure rate and mean-time-between-failure (MTBF) of a single-layer, production-version commutator are 17.728 $f/10^6$ hours and 56,407 hours respectively. This predicted reliability is in accordance with MIL-STD-756 and MIL-HDBK-217 procedures. Tables 7-4 and 7-5 contain detail parts and failure rates for the commutating feed assembly and rotary pedestal subassembly. Parts failure rates, excepting bearings, are taken from MIL-HDBK-217C, Section 2, and are based upon assumed typical worst case application stresses achieved on similar equipments and through reliability management controls. The parts failure rates are based upon a fixed ground environment, an equipment ambient temperature of 38 degrees centigrade ($100^{o}F$), and an equipment internal parts temperature of 50 degrees centigrade. Parts to be used in the production configuration are expected to be good military quality, and this prediction reflects those type parts. Semiconductors are assumed to be JANTX, microcircuits are assumed to be M38510 Level B, and discrete resistors are assumed to be established reliability (ER) level P. The quality of non-standard items should be controlled through detailed parts/components specifications.

Table 7-4. EBC for Commutating Feed Assembly

EBC

UNIT NO.	UNIT TITLE: COMMUTATING FEED ASSY.	JOB CONTRACT: 3911000	REV DATE / REV
SCHEMATIC NO.	DESIGN GROUP: ANT	ENGINEER / DATE	SHEET 1 OF 1

REV	QTY PER	CIRCUIT SYMBOL NO.	DESCRIPTION	TYPE OR PART NUMBER	STRESS RATED	STRESS ACTUAL	STRESS RATIO	TEMP	FAILURE RATE (F/10^6 HRS)	SOURCE
	2		CONNECTOR, RF	OSM, No. 2066-1403-00				38°C	0.006 X 2	217C
	200		" "	OSM, No. 2052-1352-00				38°C	0.006 X 200	"
	4		" "	OSM, No. 2001-7761-02				38°C	0.006 X 4	"
	1		CONNECTOR, CIRCULA	MS 3122E 12-10P		10 PINS		50°C	0.003	"
	70		RESISTOR, FILM	CTC, No. TT 40-5K			0.3	50°C	0.022 X 70	217C PIG 2.5.2-9
	1		BEARING	KAYDON, KD180X P0				"	0.001	ITTG
	1		ANNULAR ROTARY COUPLER	KELVIN, No. 21003				38°C	NEGL.	217C
	1		ROTARY PEDESTAL ASSY	RPM, No. 100064					14.948	

		SUBTOTAL	
RELIABILITY ENGR: ORC	DATE: 12-21-79	MTBF (IN HRS): 56,407	TOTAL (IN F/10^6 HRS): 17.728
ITT Gilfillan	CODE IDENT NO. 24930	ENGINEERING BILL OF MATERIAL (CIRCUIT COMPONENT LIST)	

0510-94

Form No. 69572

Table 7-5. EBC for Rotary Pedestal Assembly

EBC

UNIT NO. | SCHEMATIC NO. | UNIT TITLE: ROTARY PEDESTAL ASSY. | DESIGN GROUP: RPM, INC. | JOB CONTRACT: 39/11000 | ENGINEER | DATE | REV DATE | REV | SHEET 1 OF 1

REV	QTY ASSY	CIRCUIT SYMBOL NO.	DESCRIPTION	TYPE OR PART NUMBER	STRESS RATED	STRESS ACTUAL	STRESS RATIO	TEMP	FAILURE RATE (F/10^6 HRS)	SOURCE
	1		MOTOR	DC				50°C	7.164	217C
	1		TACHOMETER					50°C	7.164	"
	1		ENCODER	OPTICAL SHAFT				"	0.276	"
	1		CONNECTOR	CIRCULAR RACK & PANEL		10 PINS		"	0.003	"
	2		MICROCIRCUITS	OPERATIONAL AMPL				T_J=60°C	0.105	"
	4		POWER TRANSISTORS	NPN, SILICON			0.3	50°C	0.049X4	"
	2		TRANSISTORS <1W	" "			0.3	"	0.005X2	"
	2		TRANSISTORS <1W	PNP, "			0.3	"	0.007X2	"
	25		RESISTORS	RCR- - - - P			0.3	"	0.015	"
	1		BEARING					"	0.001	ITTG
								SUBTOTAL		

RELIABILITY ENGR: MRC | DATE: 12-21-7° | MTBF (IN HRS): 66,898 | TOTAL (IN F/10^6 HRS): 14.948

ITT Gilfillan | CODE IDENT NO. 24930 | ENGINEERING BILL OF MATERIAL (CIRCUIT COMPONENT LIST)

Form No. E8672

0510-95

This reliability prediction assumes that the failure distribution is exponential where each part has a constant failure rate throughout the operating time of the equipment. It is further assumed that part failures occur independently, and all equipment failures occur randomly. Failure rates are not duty cycled, and redundancy has not been considered.

During operation of the commutator, a substantial degree of redundancy actually exists in the form of allowable soft degradation. That is, the commutator functions with 68 output ports simultaneously excited, and one or more of these ports can fail without operational performance degradation below the required level. Further analysis and data would verify this redundancy.

The tachometer contained in the rotary pedestal assembly can fail in modes that are not critical to the mission of the commutator. However, the predicted MTBF of 56,407 hours does not assume these mission noncritical failure modes. If these modes had been considered along with the redundancy inherent in the multiple excited output ports, the predicted MTBF of the commutator would exceed 100,000 hours.

7.5 Costs

Cost predictions for a production-version commutator are given in Table 7-6. The figures assume factory cost in 1980 dollars for a dual-beam system (two stacked commutators) manufactured in a production run of 100 units. Non-recurring development costs have not been included.

TABLE 7-6. COST PREDICTIONS FOR A PRODUCTION-VERSION COMMUTATOR (Two Stacked Units)

Assembly/Component	Qty	Factory Cost	
		Material	Labor
Support Structure	1set	$ 20	$ 96
Rotary Pedestal Assembly	1	3,870	48
Stripline Assembly	2		876
Bonded Striplines	2	5,760	96
Load Terminations	138	1,157	
RF Connectors	4	36	
Misc. Hardware	lot	160	
Housing Assembly	2		1,288
Castings	4	1,186	1,200
Annular Rotary Coupler	2	2,322	48
18-Inch Bearing	2	902	
Shaft Bearings	4	24	
RF Connectors	400	1,950	
Stator Loops	400	180	
RF Chokes	4	160	
Misc. Hardware	lot	264	
Final Assembly			328
RF Cables	4	106	
Shaft	2	26	
Shaft Coupler	2	20	
Test			1,424
Total Factory Cost: $23,547			

SECTION 8

FINDINGS AND CONCLUSIONS

The development of an experimental commutator model to feed a 90^{o} sector of a circular array antenna was completed. Performance tests demonstrate the excellent electrical characteristics that can be achieved with this device: wide operating bandwidth, low azimuth sidelobe levels, low RF losses, and high power-handling capability. In addition to this development, a study was conducted on the costs, reliability and fabrication techniques of a larger production version of this commutator.

Two key technological developments were advanced. The first consists of non-contacting magnetic loop couplers, which allow low-loss transfer of RF energy with the precise control of amplitude and phase needed to realize low sidelobe levels. The second is the implementation of a large-scale, rotating stripline distribution network that is used to feed a 90^{o} sector of a circular array antenna.

During the course of the development, numerous technical problems arose that had to be resolved. In most instances, a satisfactory solution was found and implemented. It was often recognized that a significant improvement in performance could be obtained with another design iteration of a particular component; however, due to budget and schedule limitations, it was felt at that time that further effort in these areas was unwarranted. Examples of parameters not fully optimized in the experimental commutator model are:

a) insertion loss and VSWR of annular rotary coupler;

b) amplitude distribution of the 13 overlap couplers in the series line feed;

c) the stripline assembly uses screw fasteners rather than the bonding process described in Section 7.3.2;

d) lack of flatness and uniformity of the rotor and stator loops;

e) composite input VSWR of the completely assembled commutator.

All of the above can be improved with further design effort, and represent negligible technical risk.

One major problem area was not fully resolved: energy coupled to adjacent and non-adjacent stator loops by means of circumferential-mode coupling. The annular RF choke design, which produces the necessary RF short to the desired radial TEM mode, has little effect on the unwanted circumferential mode. In theory, this mode is orthogonal to radial TEM mode, and should be relatively simple to suppress without disturbing the latter. Devices such as radially oriented slots or circumferentially located resistive vanes should prove effective for this purpose. In order to obtain the electrical measurements given in Section 6.4, RF shorts between the rotating and fixed sections of the commutator were made using adjustable spring contacts, rather than relying on the non-contacting RF chokes. After electrical tests were completed, these spring contacts were replaced with a conductive closure material called CONFUZZ. This is a silver impregnated nylon tape covered with a myriad of finely woven monofilaments. CONFUZZ has good

compressibility and recovery characteristics, and is ideally suited for providing a grounding path between rotating surfaces with only light physical contact required. When a ribbon of the 0.125-inch thick CONFUZZ was placed in the 0.063-inch gaps between the stripline ground planes and housing, the assembly would not rotate due to excessive drag. Circumferential slots 0.188 inch wide by 0.040 deep were machined into the upper and lower stripline assembly ground planes so that the CONFUZZ sticks up above the surface only a nominal 0.085 inch. This maintains the contacting RF short, yet allows the rotating assembly to turn freely. In order not to weaken the 0.063-inch thick ground planes and induce warpage, discontinuous slots are used. Segments of CONFUZZ were bonded in the slots with conductive silver epoxy, and the commutator was retested. It was found that while the overall performance of the commutator had not changed greatly, the coupled amplitudes for individual elements varied from the previous data by as much as +1.6 dB to -3.4 dB. The rotating stripline assembly was removed from the housing and inspected. It was noted that the RF shorts produced at the ends of the rotor loops by means of #2-56 screws threaded into the ground plane were loose. These screws were tightened and cemented in place with conductive silver epoxy. The commutator was then reassembled and retested. While some improvement was observed, it was not possible to duplicate the amplitude data previously obtained using spring contacts. It was concluded that the change in performance was due to one or more of the following:

a) the silver epoxy was either marginally old, improperly cured, or less conductive at L-band than supposed;

b) the CONFUZZ is not an effective RF short;

c) the rotor-loop RF shorts are lossy;

d) the stripline assembly was degraded by stress or contaminants while the slots for the CONFUZZ were being machined.

The use of CONFUZZ is a stop-gap measure that would not be required once the unwanted circumferential mode is suppressed. Furthermore, the use of conductive silver epoxy is not recommended as a production technique, and would not be used in a production-version commutator. An acceptable method of making the rotor-loop RF short is to solder the etched copper circuitry directly to silver-plated terminals securely fastened to the ground plane.

The development of the experimental commutator model and study of a production version have clearly demonstrated the viability of this approach for low-cost azimuth steering the beam of a circular array. Excellent electrical performance is obtained, with improvements in reliability, maintenance and life-cycle cost compared to alternative approaches.

SECTION 9

PROGRAM PERSONNEL AND ORGANIZATION

The commutator development and study team are shown in Figure 9-1.

Mr. Wolfson, as Program Manager, was responsible for budget, schedule and technical performance of this development. In addition, his technical contributions included the specification and vendor liaison of major purchased items, design of the loop-coupler test fixtures, and preparation of quarterly and technical reports.

Mr. Charlton proposed the design concept for the commutating feed assembly developed on this program. He also did the antenna system analysis, the azimuth pattern computations, and the analytical design of the stripline feed network.

Mr. Fletcher provided background information on the UAR Program, plus valuable inputs concerning system performance.

Dr. Ching-Fai Cho was responsible for most of the development and evaluation of the stripline feed network and the loop couplers, as well as overall integration of the commutator.

Mr. Fernandez did the mechanical design, including preliminary drive-train analysis, selection of bearings, housing layout, support structure design, and liaison with drafting and model shop.

Mr. Churchill did the reliability study of the production-version commutator.

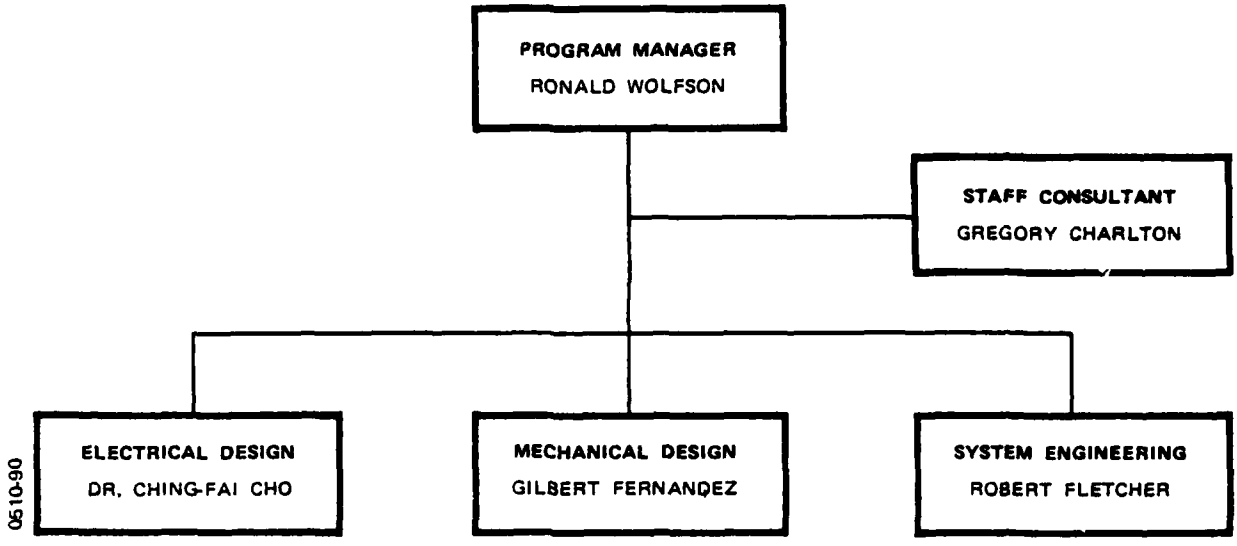

Figure 9-1. Commutator development and study team

APPENDIX A

DERIVATION OF ANALYTICAL EXPRESSIONS FOR LOOP-COUPLER DESIGN

The magnetic loop couplers operate similar to the conventional, -3dB, matched quarter-wave transmission line directional coupler. The coupling coefficient, C_o, for a -3dB coupler is:

$$C_o = \text{ANTILOG}_{10}\left(-\frac{3}{20}\right) = 0.7079 \tag{1}$$

The ratio of even- and odd-mode impedances is given by:

$$\frac{Z_{oe}}{Z_{oo}} = \frac{1 + C_o}{1 - C_o} = 5.8480 \tag{2}$$

Further, to obtain a matched condition, it is required that:

$$Z_o^{\,2} = Z_{oe}\, Z_{oo} \tag{3}$$

where Z_o is the characteristic impedance of the input line. From equations (2) and (3):

$$Z_{oe} = \sqrt{5.8480}\, Z_o \tag{4}$$

and

$$Z_{oo} = Z_o / \sqrt{5.8480} \tag{5}$$

For Z_o equal to 50 ohms:

$$Z_{oe} = 120.91\ \Omega \tag{6}$$

and

$$Z_{oo} = 20.68\ \Omega \tag{7}$$

The geometry and symbols for broadside coupled lines are shown in Figure A-1. For the case where the lines have equal widths ($w_1 = w_2 = w$):

$$\bar{z}_{oe} = \frac{188.3/\sqrt{\epsilon_r}}{\frac{w/b}{1-(s/b)} + \frac{C'_{fe}}{\epsilon_r}} \tag{8}$$

and

$$\bar{z}_{oo} = \frac{188.3/\sqrt{\epsilon_r}}{\frac{w/b}{1-(s/b)} + \frac{w}{s} + \frac{C'_{fo}}{\epsilon_r}} \tag{9}$$

The line widths, w_1 and w_2, of the rotor loops and the stator loops used in the commutating feed assembly are unequal; however, a good approximation is to use the average width:

$$w = \frac{w_1 + w_2}{2} \tag{10}$$

The approximate value of the fringing capacitances is given by:

$$\frac{C'_{fo}}{\epsilon_r} = \frac{C'_{fe}}{\epsilon_r} = \frac{2}{\pi} \text{ LN } 2 = 0.4413 \tag{11}$$

To design loop couplers with these expressions, values of w_1, w_2, s and b are found that, when used in equations (8), (9), (10) and (11), satisfy the required values of even- and odd-mode impedances given by equations (4) and (5).

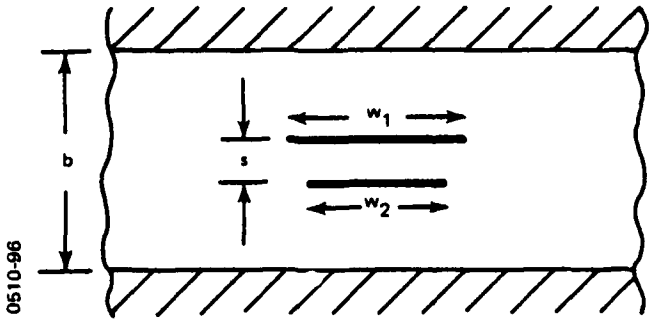

Figure A-1. Geometry and symbols of broadside coupled lines

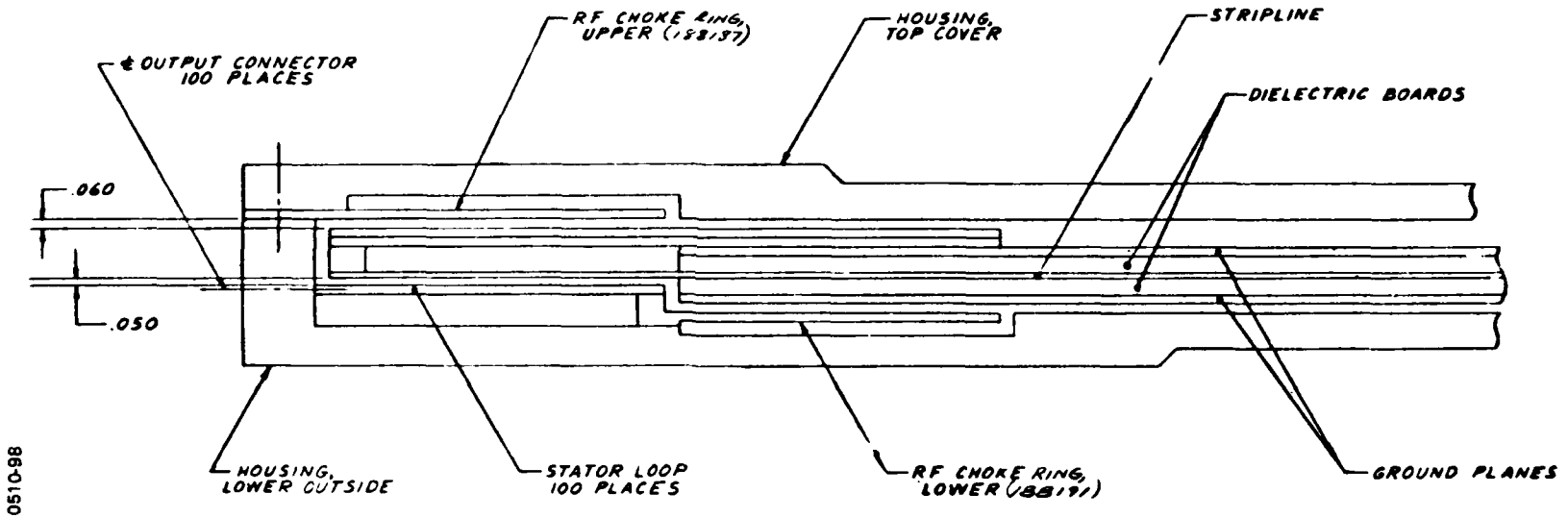

Detail of loop-coupling region

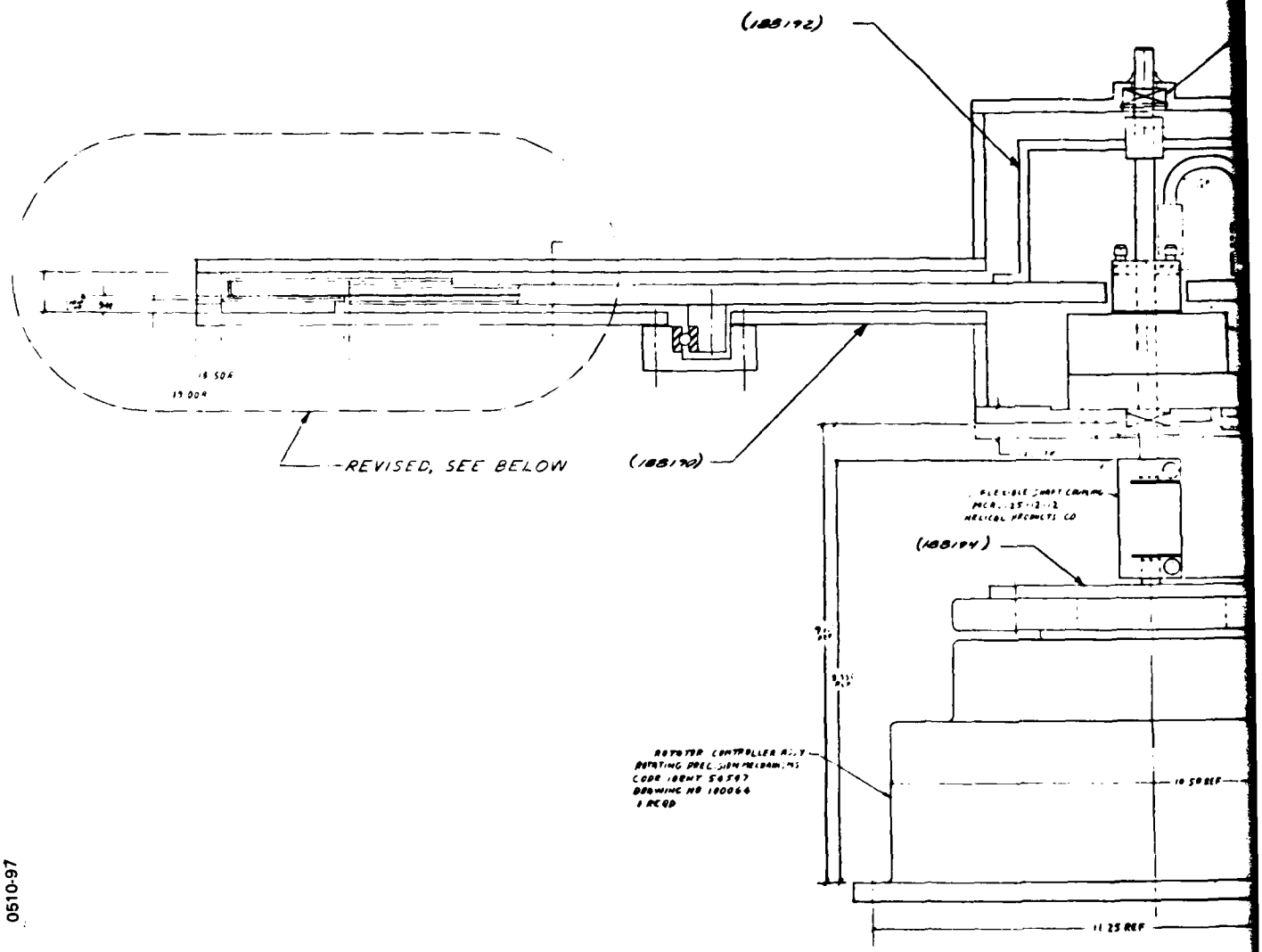

0510-97

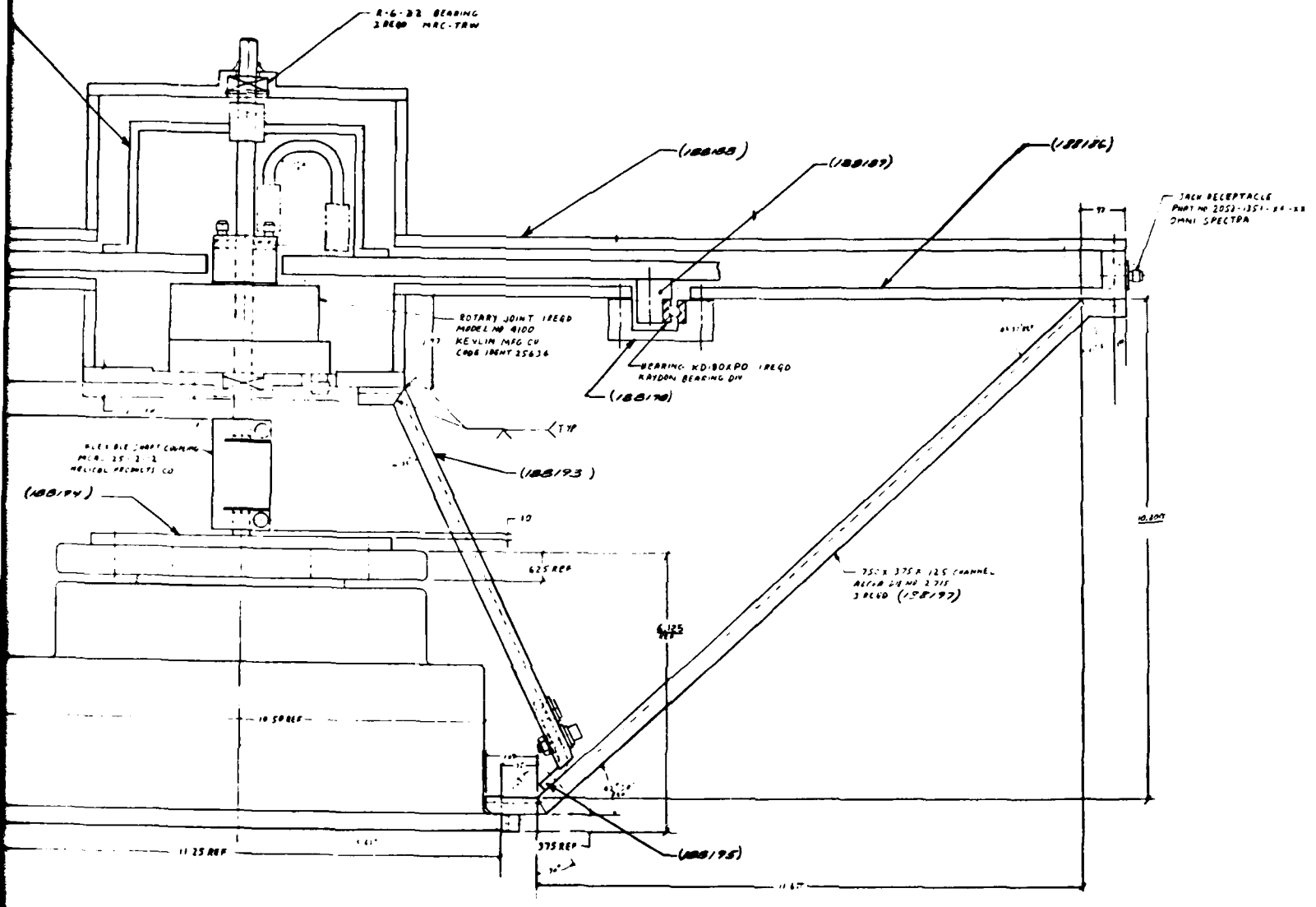

Layout drawing of experimental commutator feed

MISSION
of
Rome Air Development Center

RADC plans and executes research, development, test and selected acquisition programs in support of Command, Control Communications and Intelligence (C^3I) activities. Technical and engineering support within areas of technical competence is provided to ESD Program Offices (POs) and other ESD elements. The principal technical mission areas are communications, electromagnetic guidance and control, surveillance of ground and aerospace objects, intelligence data collection and handling, information system technology, ionospheric propagation, solid state sciences, microwave physics and electronic reliability, maintainability and compatibility.

Printed by
United States Air Force
Hanscom AFB, Mass. 01731


DATE
FILMED
8